BRANZ

Study Report

SR393 [2018]

Materials within geothermal environments

Zhengwei Li, Nick Marston and Kathryn Stokes

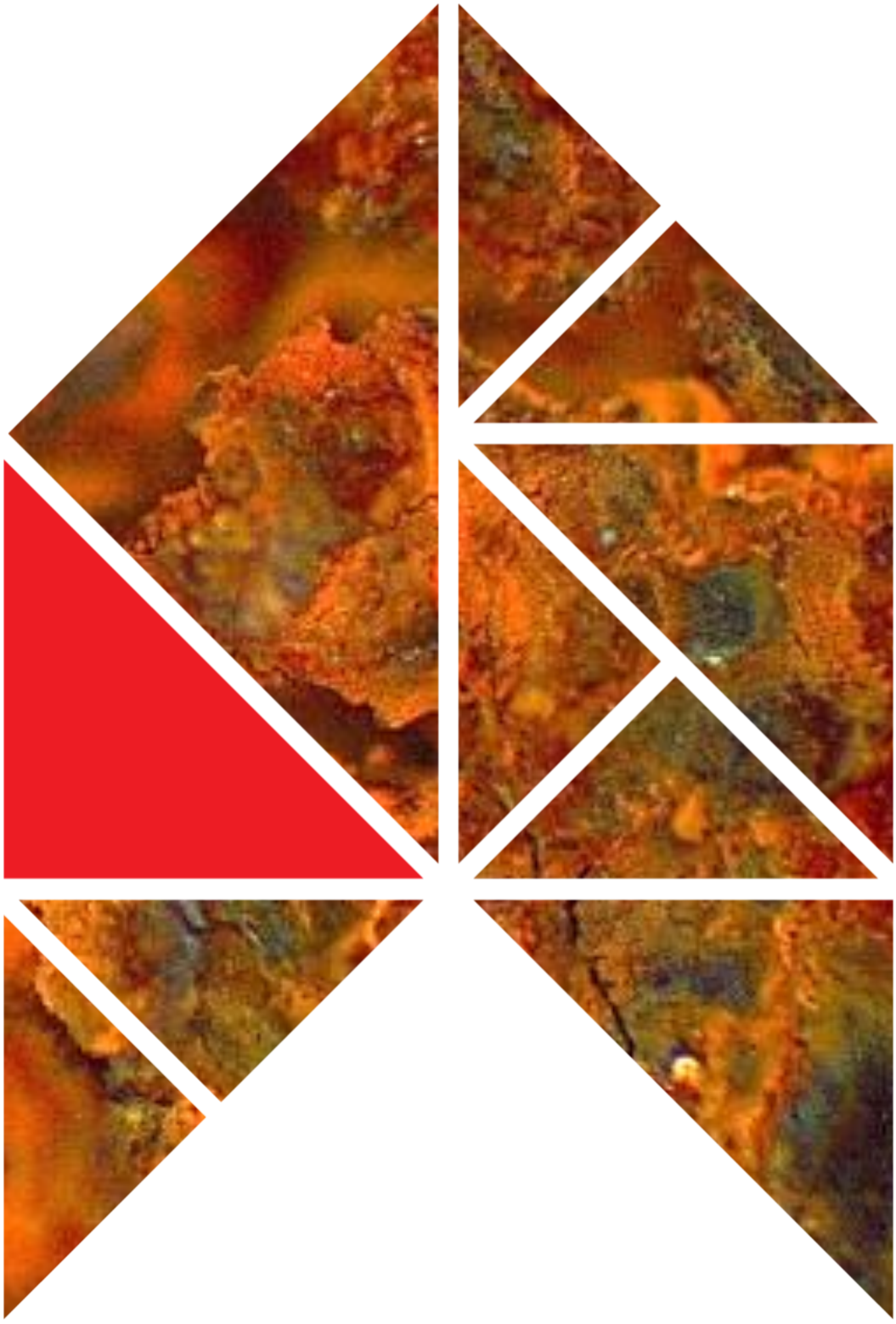

1222 Moonshine Rd
RD1, Porirua 5381
Private Bag 50 908
Porirua 5240
New Zealand
branz.nz

Funded from the Building Research Levy

The work reported here was funded by BRANZ from the Building Research Levy.

ISSN: 1179-6197

Preface

This study report was prepared during BRANZ's research into the performance and durability of several typical building and construction materials when exposed to geothermally influenced environments in Rotorua, New Zealand.

Acknowledgements

We would like to thank the Rotorua District Council, Bay of Plenty Regional Council, Scion and a number of private property owners in Rotorua for allowing installation of monitoring devices and exposure racks within their premises and for sharing some environmental monitoring data.

Figure 1 Geothermal systems in New Zealand was provided by the New Zealand Geothermal Association. Refer to http://nzgeothermal.org.nz/ for full details.

Figure 2 Geothermal systems in the Taupo Volcanic Zone (TVZ) was provided by Environment Waikato. Refer to https://www.waikatoregion.govt.nz/ for full details.

Materials within geothermal environments

BRANZ Study Report SR393

Authors

Zhengwei Li, Nick Marston and Kathryn Stokes

Reference

Li, Z., Marston, N. & Stokes, K. (2018). *Materials within geothermal environments*. BRANZ Study Report SR393. BRANZ Ltd, Judgeford, New Zealand.

Abstract

New Zealand has numerous geothermal systems, particularly in the central part of the North Island. Geothermal emissions with sulphur-containing gas species, such as hydrogen sulphide and sulphur dioxide, can be aggressive towards susceptible building and construction materials. These may include metals, timbers, paints and composites. Current information on how materials perform in geothermal environments is limited, which makes specific engineering design (SED), required by NZS 3604:2011 *Timber-framed buildings*, difficult.

This study summarises the results derived from BRANZ short-term field exposure testing in Rotorua – a population centre with known geothermal influences on the performance and durability of materials, buildings and infrastructure assets. It basically covers two experimental aspects – environmental monitoring and degradation analysis of several metals and timbers.

This study reveals that atmospheric corrosion of metals in geothermal environments can be very different from those in other New Zealand environments, such as marine, industrial and rural. These are shown as extremely high corrosion rates and unusual degradation kinetics. These behaviours are challenging environmental corrosivity classification using model metals according to ISO 9223:2012 *Corrosion of metals and alloys – Corrosivity of atmospheres – Classification, determination and estimation* and service-life estimation based on short-term performance monitoring data.

This study suggests it would be necessary to perform long-term, systematic monitoring and testing of performance and durability of representative building materials and protective coating systems, particularly in areas with high concentrations of geothermal sulphur-containing species. Data, information and knowledge derived will benefit the building and construction industry and strongly support its safe practice in geothermal environments.

Keywords

Atmospheric corrosion, geothermal, hydrogen sulphide, corrosion rate, corrosion kinetic, mild steel, zinc, copper, aluminium, stainless steel, Al-Zn alloy coating, wood

Contents

Figures

Tables

1. Introduction

New Zealand has numerous distinctive geothermal environments that are typically classified into (very) low, moderate and high-temperature systems (Figure 1). The Taupo Volcanic Zone (TVZ) in the central part of the North Island has a large number of high-temperature geothermal systems comprised mainly of geysers, springs, mud pools, steaming grounds, hydrothermal eruption craters and fumaroles (Figure 2).

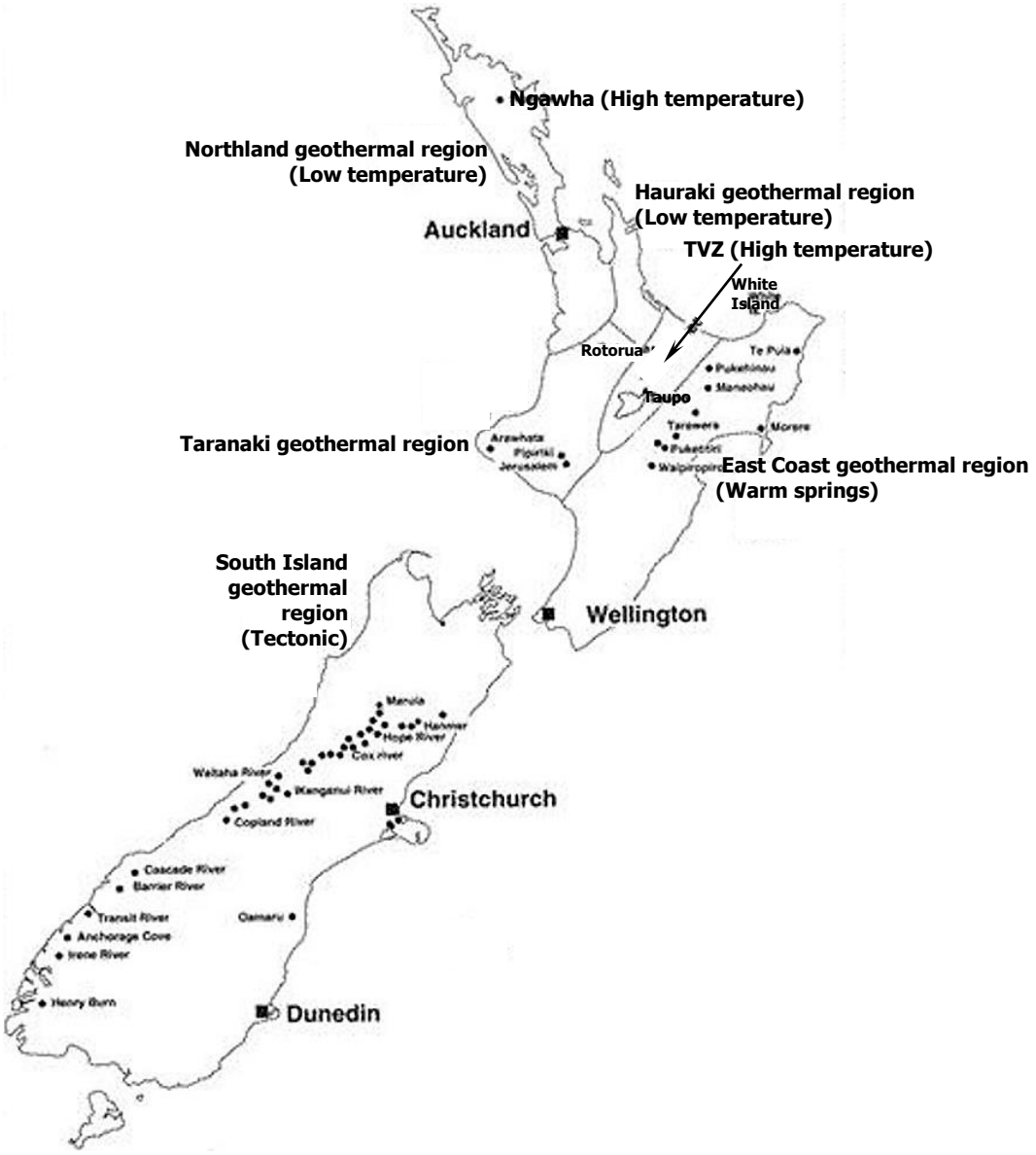

Figure 1. Geothermal systems in New Zealand (Source: New Zealand Geothermal Association). (Some notes were added to original figure).

Various gaseous species can be identified within geothermal environments. These include steam (water vapour), carbon dioxide (CO_2), sulphur dioxide (SO_2), hydrogen sulphide (H_2S), ammonia (NH_3), methane (CH_4), hydrogen chloride (HCl), hydrogen fluoride (HF), nitrogen (N_2), argon (Ar) and hydrogen (H_2) (Lichti et al., 1996; Lee et al., 2005; Luketina, 2007; Teschner et al., 2005; Scott, 2011; Ochieng et al., 2012).

Of these, sulphur-containing species are seen as the major contributing factor in poor material durability and performance. Airborne H_2S and/or SO_2 of high concentrations can play important roles in the corrosion processes of copper (Cu), iron (Fe), lead (Pb), silver (Ag) and zinc (Zn), leading to the formation of corrosion products with reduced protective capability (Salas et al., 2012). H_2S can also cause blackening of some paints with metal-based pigments or drying agents, especially basic lead carbonate pigment, $2PbCO_3 \cdot Pb(OH)_2$ (Wohlers & Feldstein, 1966). Several hours of exposure to H_2S at concentrations of about 50 $\mu g/m^3$ can give this effect, although it might be reversible if the exposure is only intermittent.

Discolouration of woods has been found in geothermal environments. Chronic exposure can also lead to severe deterioration of woods and wood structures, observed as the formation of deep and large cracks.

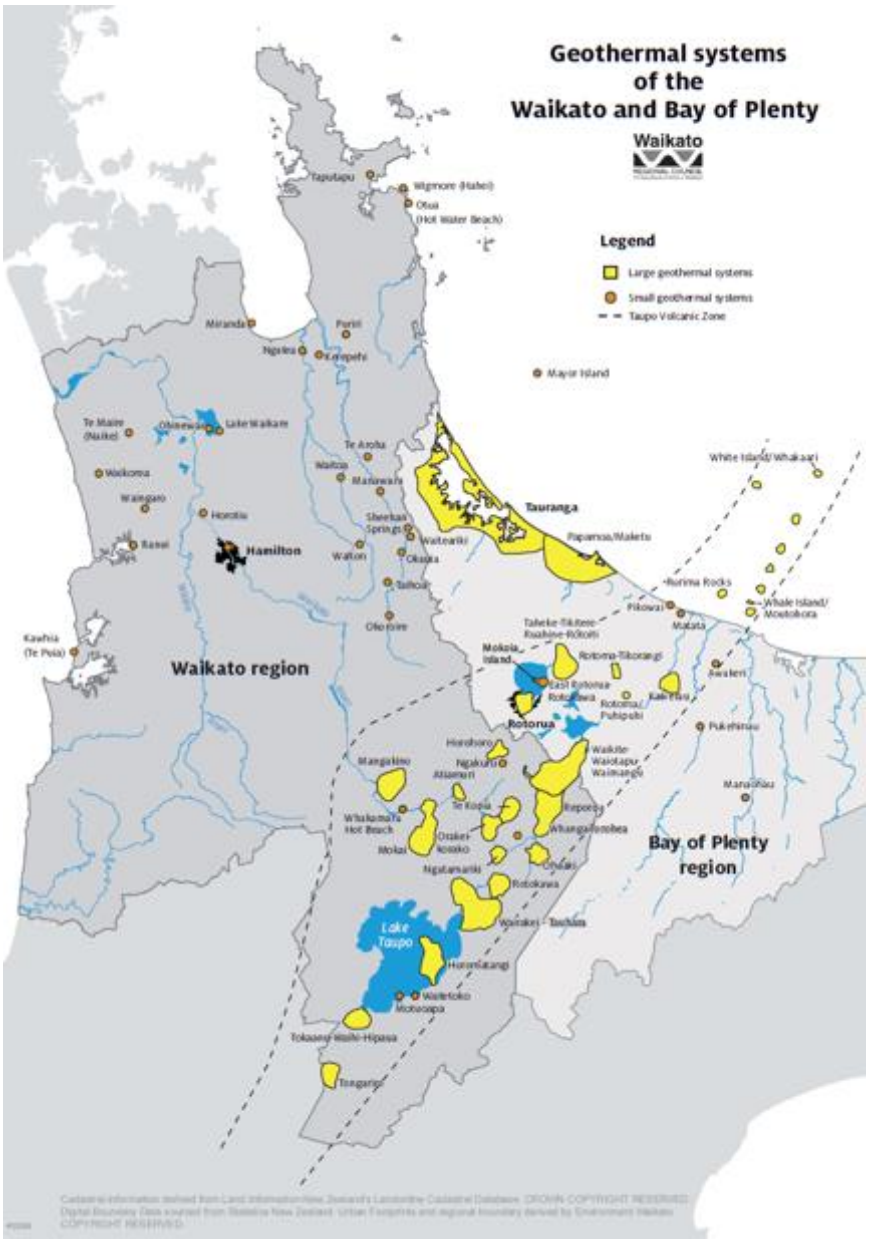

Figure 2. Geothermal systems in the Taupo Volcanic Zone (TVZ) (Source: Environment Waikato).

A unique aspect of New Zealand geothermal environments is that most of them have urban areas nearby. More than 58,000 people live in the Rotorua city, one of the major cities located within the TVZ. Material deterioration problems with buildings and infrastructure assets are common within these environments, resulting in huge costs for repair and maintenance. As such, NZS 3604:2011 *Timber-framed buildings* requires specific engineering design (SED) for building and construction within environments influenced by geothermal hot spots.

There are a limited number of international studies on the performance of building materials within geothermal environments. Most geothermal environments in other countries are sparsely populated and there is low demand for this knowledge (Hawthorn et al., 2007).

A survey of literature identified a limited number of studies in the New Zealand context:

- In the 1980s, BRANZ measured the atmospheric corrosion rates of mild steel and hot-dip galvanised zinc coating at 168 sites spread throughout New Zealand (Duncan & Cordner, 1991). Some exposure sites were within geothermally influenced regions such as TVZ. Extremely high mass losses were observed at some exposure sites. For example, mass losses of 4,800 g/m^2 and 141.6 g/m^2 were observed with mild steel and zinc coating, respectively, in the first year of exposure at the Lake Roto-a-Tamaheke site. However, at other sites within the TVZ, corrosion rates of mild steel or zinc were relatively low and comparable to those measured at other typical New Zealand atmospheric environments. This indicates that geothermal environmental conditions can be highly variable and, therefore, material performance can be highly changeable.
- In the 1990s, the then Industrial Research Ltd (IRL) and Japanese researchers evaluated the performance of 27 types of metallic materials when exposed to geothermal volcanic environments at White Island, New Zealand (Kurata et al., 1995). These included carbon steels, low alloy steels, stainless steels and nickel-based alloys. Most of these materials are not widely used within building and construction.

These studies delivered highly variable results and gave very little guidance to design, specification and maintenance of buildings in New Zealand geothermal environments, except for a general warning to be wary.

This study aimed to address this information shortage with three interconnected research components.

- A better understanding of geothermal environment characteristics by monitoring sulphur-containing species.
- An investigation into deterioration behaviours, kinetics and failure mechanisms of typical building materials as a function of geothermal discharges.
- An evaluation of interactions between different materials, particularly the impacts of one material on another when influenced by geothermal contaminants.

The findings will support the development of material specification schemes for design, construction and maintenance of new and existing buildings and infrastructure assets in New Zealand geothermal environments.

2. Experimental approach

2.1 Exposure sites

Rotorua city is a large population centre in the TVZ with many unique geothermal features and systems. Surface geothermal activities are mainly confined to three areas: Whakarewarewa/Arikikapakapa, Kuirau Park/Ohinemutu and Government Gardens/Ngapuna/Sulphur Bay (Gordon et al., 2005; Ratouis et al., 2014).

Six field exposure sites were established, roughly crossing the city from the west to the east (Figure 3). Three of them were on the south side of Malfroy Road (west city area). The remaining three were in the wastewater treatment plant (WWTP, south of Sulphur Bay – a large, mixed geothermal system), Ngapuna and Lynmore (east city area).

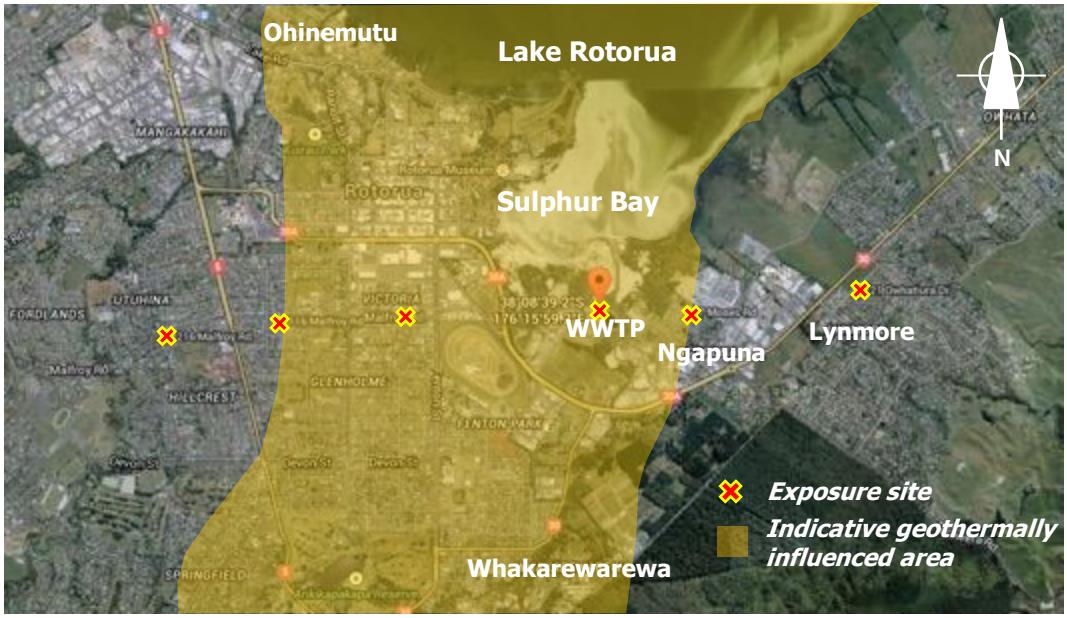

Figure 3. Some exposure sites established in Rotorua.

Sulphur Bay is in the southeastern corner of Lake Rotorua and stretches from Motutara Point to Ngapuna. Puarenga Stream flows into Sulphur Bay and features geothermal activity at its mouth – fumaroles, mudpools and steaming grounds. The south boundary of Sulphur Bay with the wastewater treatment plant features scrubland and other plants.

This arrangement was designed to investigate the concentration and distribution of sulphur-containing species in the city region and their influences on local atmospheric corrosivity and material deterioration.

Another four field exposure sites were established within Scion campus at Whakarewarewa. One site was located within the enclosure of a small-sized geothermal spring (~1.5–2 m in diameter). The other three were grouped together to investigate the effects of distance and also height from an active, small gas-emitting fumarole (~0.5 m in diameter) on material deterioration. One of these three sites was approximately 5 m away from this geothermal source, the second was approximately 50 m east and the third was approximately 60 m southwest.

The exposure site arrangement with geothermal spring, fumarole and Sulphur Bay (wastewater treatment plant) also provided an opportunity to explore the influences of geothermal features on material deterioration.

For comparison, two exposure sites were established in the Wellington region (Figure 4). One was within the BRANZ campus at Judgeford, Porirua. This site is in a sheltered semi-rural environment, located approximately 5 km from the nearest salt water, a tidal estuary, and further protected from the open sea by gently rolling hills. It lies within Zone C (or C3 according to ISO 9223:2012) according to the atmospheric corrosivity map shown in the NZS 3604:2011 based on severity of exposure to marine aerosols. However, it is considered a fairly benign example of this classification based upon atmospheric corrosion testing with standardised mild steel and zinc coupons.

Figure 4. Exposure sites established in Wellington region.

The other site was on the beach-front of Oteranga Bay, located at map coordinates 41.30°S and 174.62°W (west coast of Wellington). It is only a few metres away from the breaking surf and can be exposed to extremely strong winds in some seasons. It is considered a typical sea spray zone, i.e. a (very) severe marine environment. Previous

BRANZ studies revealed very high salt deposition and corrosion rates with mild steel and hot-dip galvanised steel coupons (Holcroft, 1998; Haberecht & Kane, 1999).

2.2 Materials

Seven metals were selected to investigate material deterioration: mild steel, weathering steel (AS/NZS 1594-HW350), austenitic stainless steel (AISI 304), aluminium (Al), zinc (Zn), copper (Cu) and aluminium-zinc alloy coating (55%Al-Zn). Their nominal chemical compositions are given in Table 1.

Table 1. Chemical composition of metals used in the study.

Metal	Element (wt.%)							
Mild steel	C	N	Al	Si	P	S	Ti	V
	0.18	0.003	0.007	0.04	0.027	0.014	0.005	0.002
	Cr	Mn	Ni	Cu	Mo	Sn	Nb	Fe
	0.03	0.69	0.02	0.03	<0.001	<0.001	<0.001	Bal.
Weathering steel	C		Cr		Al		Si	Mn
	0.10		0.78		0.039		0.49	0.83
	P		S		Ni		Cu	
	0.086		0.017		0.19		0.28	
Stainless steel (AISI 304)	C		Cr		Ni		Si	Mn
	0.03		18		8.14		0.48	1.23
	P		S					
	0.044		0.012					
Aluminium	Si		Fe		Cu		Mn	Al
	0.15		0.48		<0.01		<0.01	Bal.
Copper	P		S		Si		Cu	
	0.001		0.001		<0.002		Bal.	
Zinc	Al	Cu		Ti		Zn		
	0.004	0.136		0.089		Bal.		
Al-Zn alloy coating	Al	Zn		Si				
	55	43.5		1.5				

The testing coupons had a dimension of ~150 × 100 × 1–3 mm. The surface of mild steel and weathering steel coupons was grit blasted to SA2.5 grade before exposure. The surface of aluminium, copper, zinc and stainless steel was finished with 800 grit silicon carbide paper.

Galvanic corrosion risks in geothermal environments were also investigated. Galvanic pairs were prepared using aluminium, copper, stainless steel, zinc and 55%Al-Zn alloy coating plates. Metallic samples had a dimension of ~40 × 40 mm. Their surfaces were ground down to 800 grit with SiC papers, except the 55%Al-Zn alloy coating samples.

Pairs were held together using nylon bolts and washers through a hole in the centre. One sample was turned 45° relative to the other for assembly. This sample arrangement is different from the configuration recommended by ASTM G149-97 *Standard practice for conducting the washer test for atmospheric galvanic corrosion*.

Wood was included in this field exposure test to investigate the discolouration phenomena commonly observed in geothermal environments. The samples included untreated and treated *Pinus radiata*. The treatments were based on copper-bearing preservatives – chromated copper arsenate, copper azole, alkaline copper quaternary and micronised copper azole to H3.2 and H4 levels. Wood samples with a dimension of ~20 × 20 × 100 mm were cut from originally treated long wood blocks. The longest dimension was in parallel to the grain (longitudinal direction) of the wood structure. The four major surfaces were finished with 800 grit sandpaper to remove any precipitated preservation chemicals on original surfaces and to obtain a reasonably smooth and uniform surface for exposure.

2.3 Exposure racks

Exposure racks were fabricated with aluminium extrusions chosen on the basis of their good corrosion performance in various atmospheric environments and weight advantages over steel. To minimise cross-contamination, supporting arms on the rack were arranged with at least 50 mm gaps between coupons.

Small exposure racks carrying a small number of testing coupons (six metal coupons in total) were directly fixed to strong timber posts with a finished height of about 2 m from the ground. Large-sized racks were fixed onto galvanised steel tripods, which were levelled and stabilised through bolt connections to heavy concrete blocks. All testing coupons on the racks were oriented north at an angle of 45°. A typically finished large exposure rack can be seen in Figure 5.

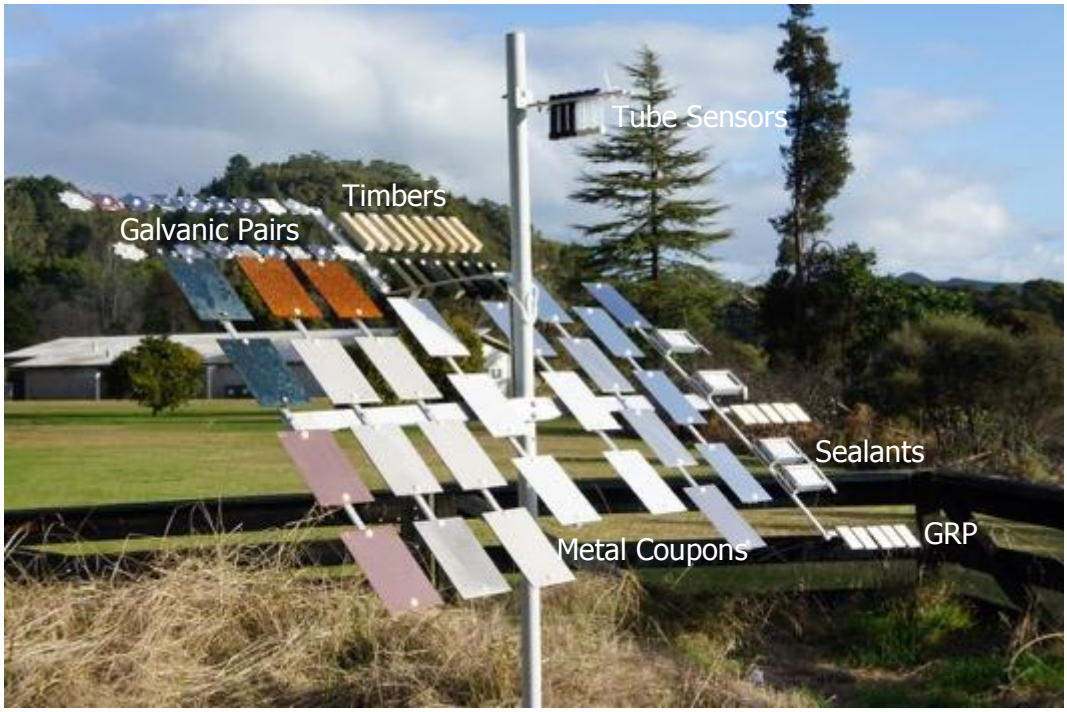

Figure 5. A typical large exposure rack.

Nylon bolts, nuts and washers were used to fix metal coupons onto the racks to avoid potential galvanic corrosion risks between testing material and aluminium. Washers of 12 mm thick were also used to increase the gaps between the back of some of the coupons and the aluminium supporting arms. This was designed to minimise water ponding and dirt accumulation in these sheltered areas.

2.4 Environmental monitoring

Atmospheric environmental data including ambient temperature, humidity, rainfall and wind speed was downloaded directly from the National Climate Database, CliFlo, NIWA. The meteorological station operated by MetService within Rotorua Airport is approximately 6 km northeast of Rotorua city.

Passive tube sensors (DIF 200 RTU and DIF 600 RTU) were installed about 2 m from the ground to measure the concentrations of airborne hydrogen sulphide (H_2S) and/or sulphur dioxide (SO_2) at exposure sites. The typical monitoring period was 3–4 weeks. These sensors were supplied and analysed by Ormantine USA Ltd. With this technique, airborne H_2S and/or SO_2 were chemically adsorbed and transformed into a stable compound in the tube. They were then quantitatively determined by UV/visible spectrophotometry and/or ion chromatography with reference to calibration curves derived from the analysis of standard solutions (ISO and UKAS accredited methods).

2.5 Sample evaluation

Metallic samples were regularly retrieved for laboratory analysis including corrosion rate measurement, surface morphological characterisation and corrosion product phase composition identification.

Time-dependent atmospheric corrosion behaviours and kinetics were monitored with mild steel and zinc samples exposed at the wastewater treatment plant site and in an area close to an active, small fumarole within Scion campus. Mild steel coupons were removed after 1, 3, 6 and 12 months. Zinc coupons were removed after 3, 6, 9 and 12 months.

To measure metal corrosion rates, corrosion products remaining on sample surfaces were cleaned thoroughly following the procedures recommended by ASTM G1 – 03(2017)e1 *Standard practice for preparing, cleaning, and evaluating corrosion test specimens* to determine corrosion rates:

- Aluminium: nitric acid (HNO_3, specific gravity: 1.42, 69%) at 20–25°C.
- Copper: 0.1 L/L sulphuric acid (H_2SO_4, specific gravity: 1.84, 98%) at 20–25°C.
- Mild steel and weathering steel: 0.5 L/L hydrochloric acid (HCl, specific gravity: 1.19, 38%) + 3.5 g/L hexamethylenetetramine ($C_6H_{12}N_4$) at 20–25°C.
- Stainless steel: 0.1 L/L nitric acid (HNO_3, specific gravity: 1.42, 69%) at 60°C.
- Zinc: 100 g/L ammonium chloride (NH_4Cl) at 70°C.

The chemically cleaned samples were rinsed with flowing water, dried with hot air and re-weighed to determine their mass losses due to atmospheric exposure. Several clean, unexposed metal samples were also immersed into these chemical solutions for the same period as the cleaning process. Their mass losses were recorded for corrosion rate measurement correction.

The characterisation of surface and cross-sectional morphologies of exposed samples was carried out with optical microscopy (Olympus) and scanning electron microscopy (JEOL JSM-6610LA) with an energy dispersive X-ray spectroscopy attachment (EDS). EDS is a chemical microanalysis technique commonly used in conjunction with scanning electron microscopy (SEM). This technique detects X-rays emitted from the sample during bombardment by an electron beam to characterise the elemental composition of the analysed volume. EDS can be operated in spot, line and area modes. Specifically, elemental mapping was used in this study to reveal the distribution of the specified elements across the area scanned.

To characterise crystalline phase composition of corrosion products, X-ray diffraction (XRD) measurements were carried out with a PANalytical X'Pert PRO diffractometer equipped with a Cu-Kα radiation. The generator setting was 45 kV and 40 mA. In this study, a typical scan was performed from 20° to 80° (2θ).

3. Environmental monitoring results

Three geothermal environmental monitoring stages were completed within the period December 2014 to December 2017. The BRANZ campus at Judgeford, with no obvious source of H_2S and/or SO_2, was used as the reference environment.

- First monitoring: 19 December 2014 to 09 January 2015, H_2S tube sensor.
- Second monitoring: 21 June 2015 to 14 July 2015, H_2S and SO_2 tube sensors.
- Third monitoring: 19 December 2015 to 12 January 2016, H_2S tube sensor.

The average concentrations of H_2S for a 3-week exposure are shown in Figure 6.

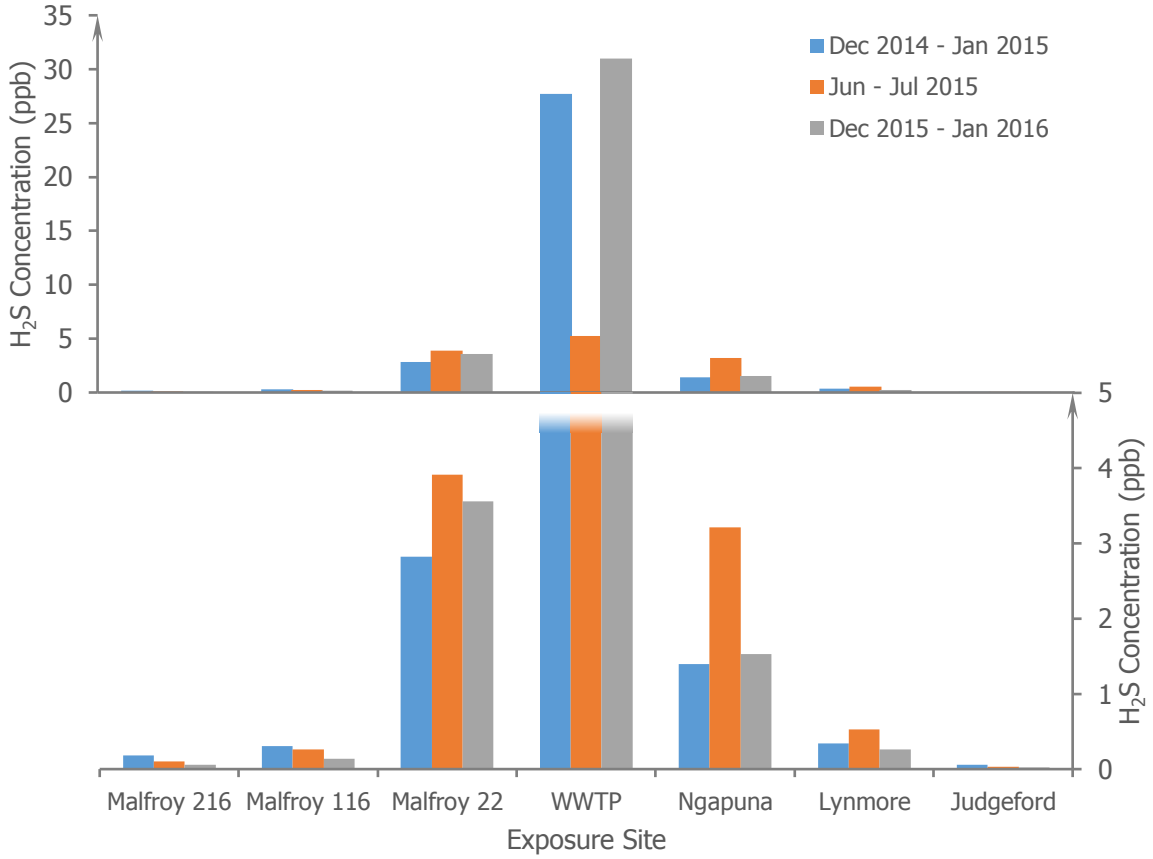

Figure 6. Average H_2S concentration during a 3-week exposure.

H_2S concentrations in the west and east areas were much lower than that in the central part of Rotorua city. The highest concentration (30.98 ppb) was observed at the wastewater treatment plant site close to Sulphur Bay (started from December 2015). This concentration was ~500 times higher than that measured at the far west location during the same testing period. In addition, H_2S concentration in the east area was slightly higher than that in the west area.

Other researchers used either passive samplers to monitor H_2S concentrations in Rotorua (Horwell et al., 2005) or Chemcassette® tape (Hinz, 2011). Those measurements showed that the central Rotorua city area experienced high H_2S concentrations. Meanwhile, the west and east areas had low H_2S concentrations. Thus, previous and current measurements consistently showed the similar location-

dependent H_2S concentration. It was noted that these monitoring studies showed somewhat different H_2S concentrations although they were performed in similar areas. This was attributed to the use of different monitoring equipment, technique and period.

The west area of Rotorua had low H_2S concentrations that were still approximately 3 times higher than that measured at Judgeford – a rural area with limited marine, industrial and traffic influences. This indicates that geothermal sources can affect fairly large areas.

H_2S concentrations measured at locations ~50–60 m away from a fumarole were ~5–10 times lower than that close to the source (Figure 7). However, their concentrations were still at least 3 times higher than those measured in west and east areas of Rotorua city or more than 25 times higher than those measured at Judgeford.

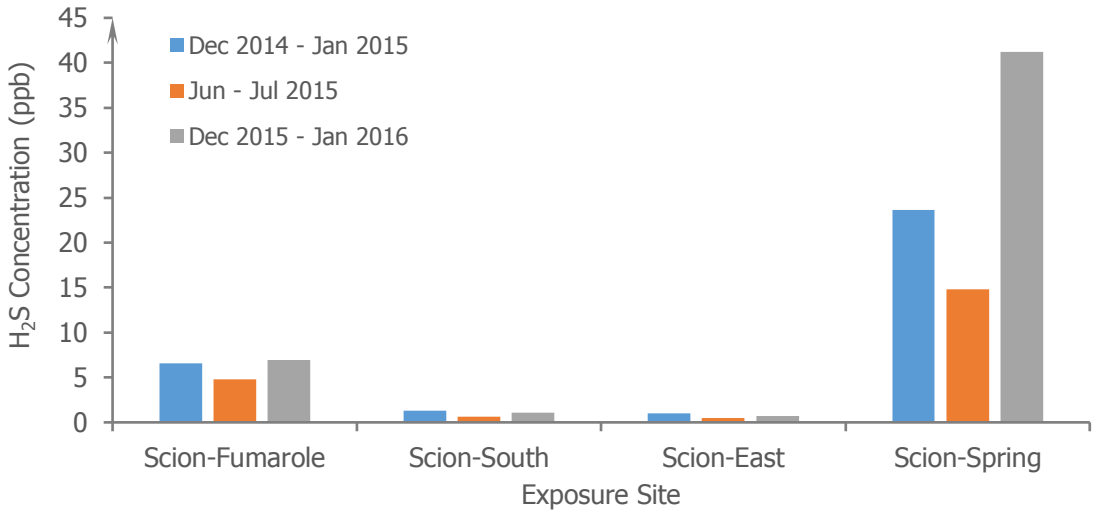

Figure 7. Average H_2S concentration during a 3-week exposure.

The geothermal spring within Scion campus had the potential to discharge emissions with much higher H_2S concentrations than the small fumarole. Its H_2S concentrations were even higher than those measured at the wastewater treatment plant located at the south of Sulphur Bay, a large area with various geothermal features. Actually, the highest H_2S concentration (41.2 ppb) within those three monitoring periods was measured at this geothermal spring.

The average 3-week H_2S concentrations varied even at one specific exposure site, relative to the monitoring timing (Figure 6). For example, the H_2S concentration at the wastewater treatment plant site was 5.2 ppb during June–July 2015, ~5–6 times lower than those measured during December 2014 to January 2015 and December 2015 to January 2016. This pattern was also observed at other sites.

The emission capability of a geothermal feature may change with time. For example, rainfall can affect shallow unconfined ground water levels within geothermal systems, physically modifying emission rates of gas species.

Meanwhile, climatic conditions may affect the concentration of airborne sulphur-containing species. Wind in particular could have impacts on their distribution and, therefore, the areas affected. Airborne sulphur-containing species could also be

(partially) absorbed by rainwater, decreasing their concentration in air. Therefore, concentration differences observed in these monitoring periods might be partly explained by the climatic difference between these monitoring periods.

Figures 8–10 show the weather conditions during the three monitoring periods.

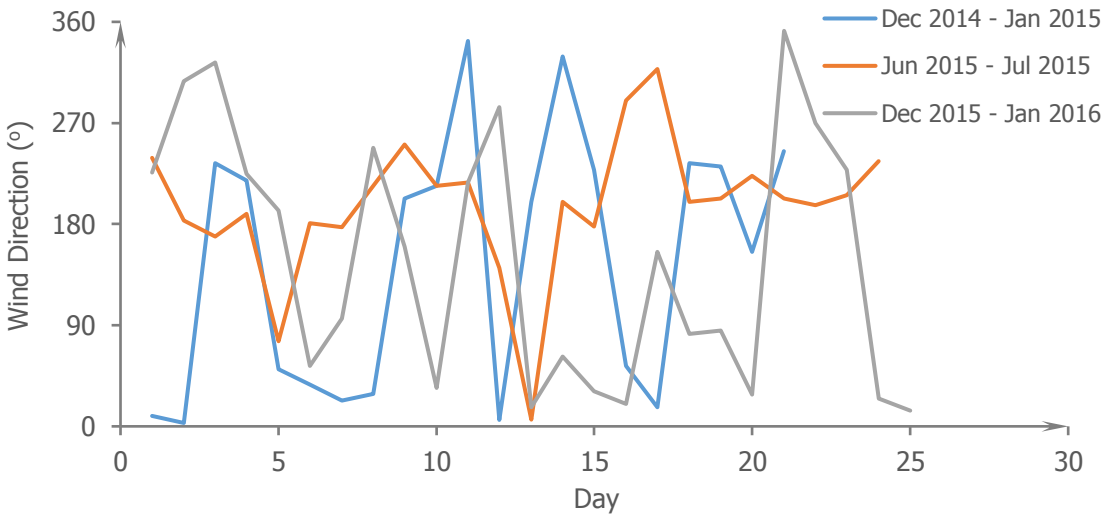

Figure 8. Wind direction during the monitoring periods (north: 0°, east: 90°, south: 180°, west: 270°).

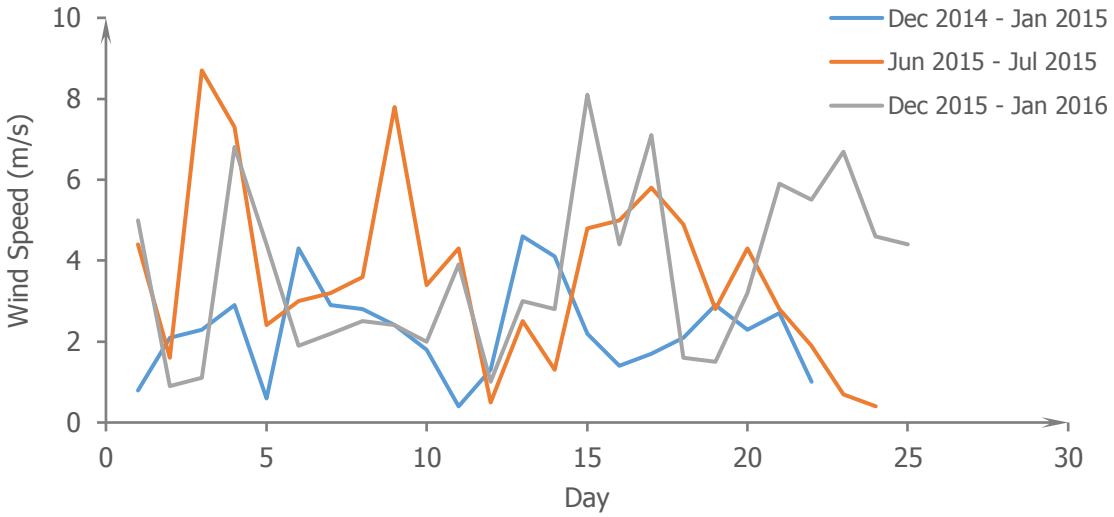

Figure 9. Wind speed during the monitoring periods.

The prevailing wind was from the southwest direction in June–July 2015. During the two summer periods, the prevailing wind was from the southwest and northeast. The rainfall quantities were 24.6 mm, 59.4 mm and 72.6 mm for December 2014 to January 2015, June–July 2015 and December 2015 to January 2016, respectively.

The prevailing wind direction could explain two phenomena revealed in Figure 6:

- Geothermal features are located mainly in the central part of Rotorua city. The prevailing wind from the southwest could carry sulphur-containing species to the northeast and east regions, leading to higher H_2S concentrations in the west area.

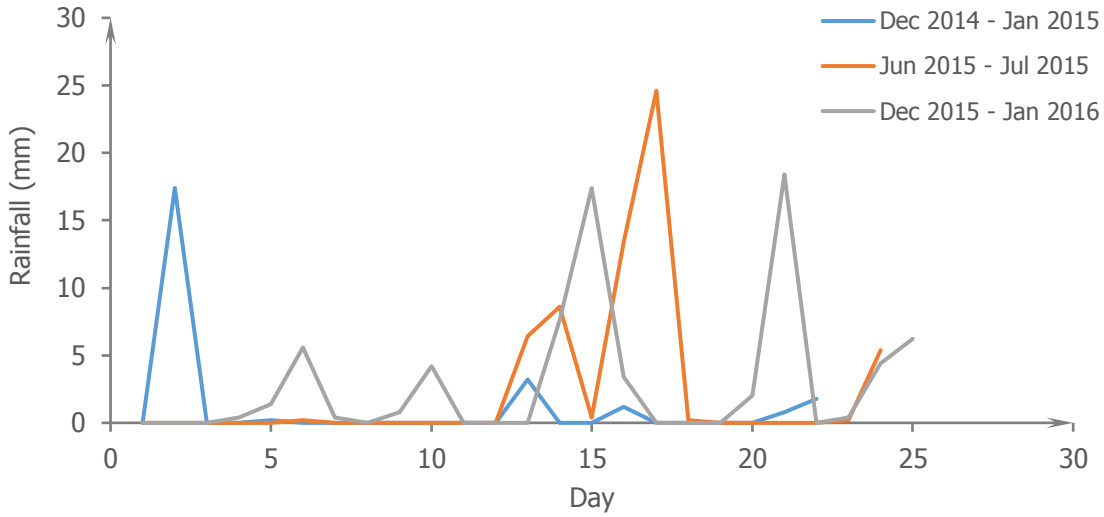

Figure 10. Rainfall during the monitoring periods.

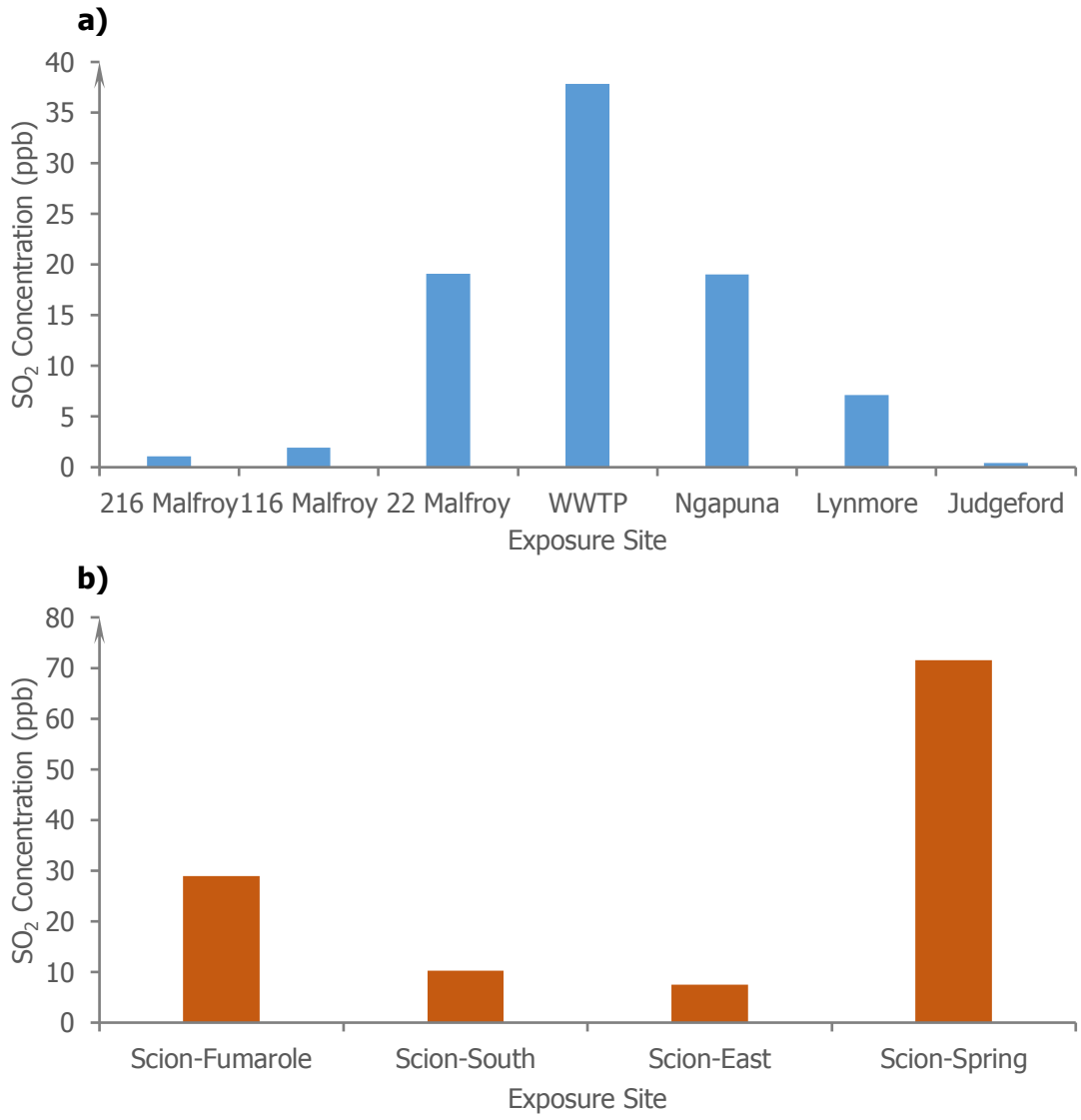

Figure 11. Average SO_2 concentration during a 3-week exposure.

- During June–July 2015, the southwest wind could blow gaseous emissions from Sulphur Bay away from the wastewater treatment plant site, leading to lower H_2S concentrations. In the summer periods, wind from the northeast direction could bring emissions to the site and, therefore, higher H_2S concentrations.

The December 2015 to January 2016 period had H_2S concentrations similar to the December 2014 to January 2015 period. Rainfall in the December 2015 to January 2016 period was much higher than the December 2014 to January 2015 period. Meanwhile, the prevailing wind directions in these two periods were quite similar. This could not be explained by the rainwater absorption effect proposed by some studies (Olafsdottir et al., 2014). Other factors or mechanisms may contribute.

The concentration of airborne SO_2 also showed a distinct correlation with the measurement location in Rotorua city (Figure 11a). The wastewater treatment plant site had the highest concentration (37.8 ppb). Meanwhile, the west area had lower SO_2 concentration than the east area.

SO_2 concentrations measured at the two locations ~50–60 m away from a small fumarole were ~3–4 times lower than that close to the source (Figure 11b). This concentration decrease with distance was smaller than that of H_2S. The concentrations at these two locations were ~4–10 times higher than those measured in the west area of Rotorua city, slightly higher than that measured in the east area, and ~19–26 times higher than that at Judgeford.

The geothermal spring within Scion campus also had the highest SO_2 concentration among all measurement sites (71.6 ppb). This value was approximately 2 times higher than that measured at the wastewater treatment plant.

Airborne concentration of SO_2 was much higher than that of H_2S at the same site. It is currently not known if the detected SO_2 is directly released from a geothermal feature or is an oxidation product of H_2S in the atmosphere under favourable transformation conditions (Cox & Sandalls, 1974; Spedding & Cope, 1984). Some monitoring results indicated that H_2S and SO_2 were present simultaneously in the gaseous discharges of some geothermal features in the TVZ (Luketina, 2007).

4. Corrosion of mild steel, zinc and copper

Three 1-year exposure tests were performed from December 2014 to December 2015, from June 2015 to June 2016 and from December 2015 to December 2016. To determine the atmospheric corrosivity category of a geothermal environment, the first-year metal corrosion rates were measured according to international and national standards including:

- ISO 9223:2012 *Corrosion of metals and alloys – Corrosivity of atmospheres – Classification, determination and estimation*.
- AS/NZS 2312:2014 *Guide to the protection of structural steel against atmospheric corrosion by the use of protective coatings*.

4.1 Location effects

4.1.1 Corrosion rate

The first-year atmospheric corrosion rates of mild steel, zinc and copper at the six sites across Rotorua city are presented in Figures 12–14.

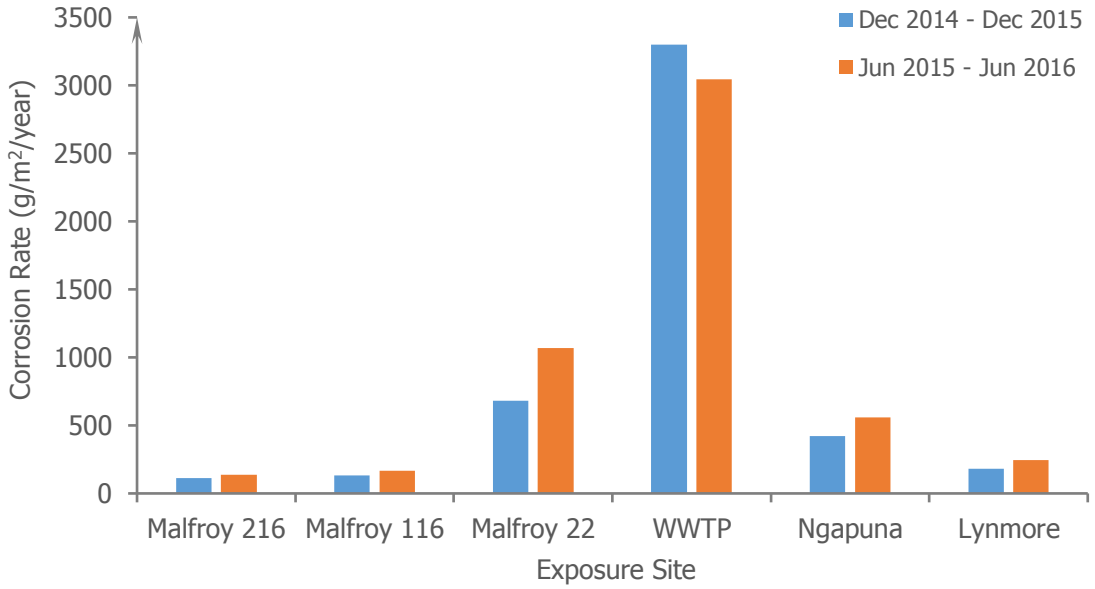

Figure 12. First-year corrosion rate of mild steel at six exposure sites in Rotorua.

An obvious dependence of corrosion rate on exposure site location was found with these three metals. Corrosion rates lower than 200 g/m^2/year (lower limit of ISO 9223:2012 C3 or NZS 3604:2011 Zone C) were measured with mild steel at only two sites in the west areas – 216 and 116 Malfroy Road (Figure 12). Metal corrosion was significantly increased at the other four sites. Not surprisingly, the highest corrosion rates were observed at the wastewater treatment plant site – 3,302 g/m^2/year, 84.2 g/m^2/year and 495 g/m^2/year for mild steel, zinc and copper, respectively.

The starting season was found to have an effect on metal corrosion. At most exposure sites, there was a trend that a higher corrosion rate was measured when the exposure was commenced from June (the beginning of winter/wet season in New Zealand). With

the two starting seasons chosen for this study, the most significant difference is rainfall.

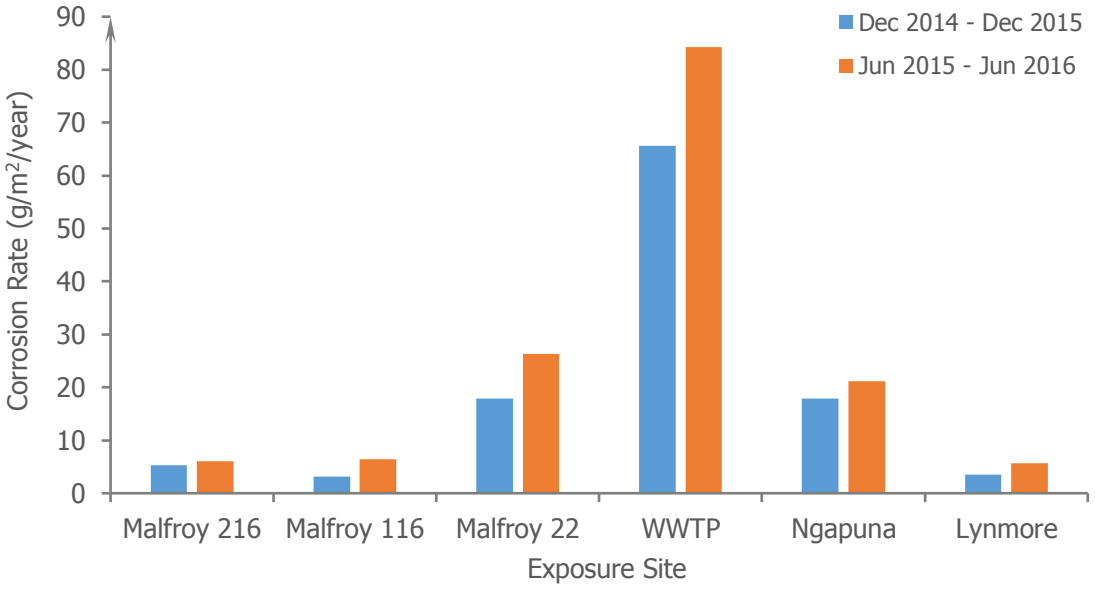

Figure 13. First-year corrosion rates of zinc at six exposure sites in Rotorua.

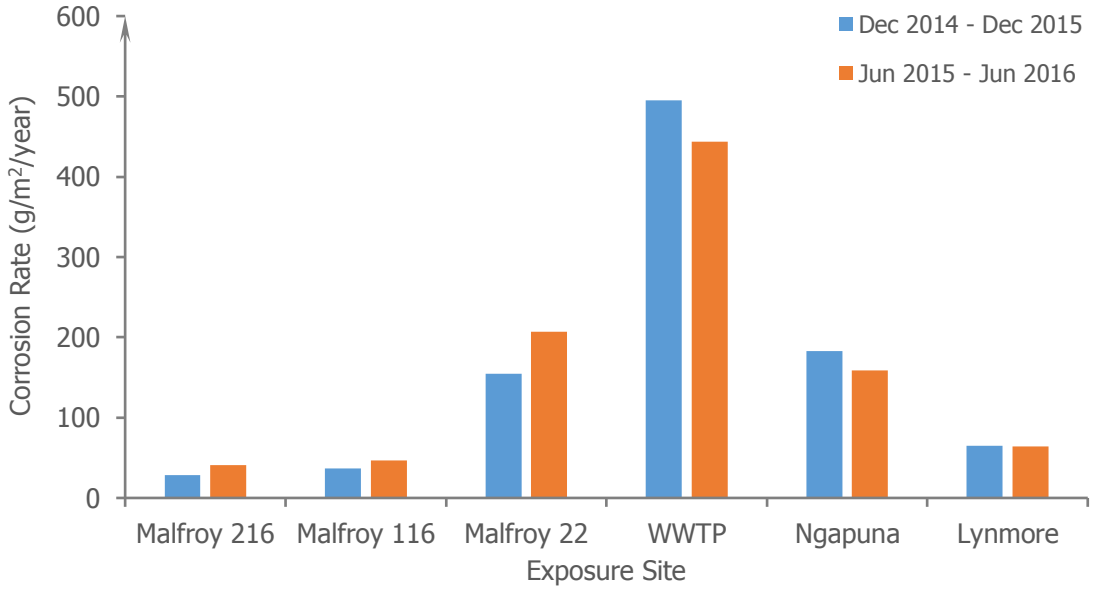

Figure 14. First-year corrosion rates of copper at six exposure sites in Rotorua.

Rainfall can affect the atmospheric corrosion of metal in many ways. During New Zealand winters, abundant rain can cause environmental humidity to stay above the critical relative humidity to initialise corrosion. Meanwhile, rain retained in pockets or crevices of the growing corrosion products can maintain moisture in these areas for longer periods. These sustain and/or accelerate corrosion (Cole & Ganther, 2006; Cole & Paterson, 2007).

Rainwater retained on the sample surface may provide an ideal medium for the dissolution of airborne contaminants such as sulphur-containing species in geothermal environments. This contaminated water layer can have a higher capability to attack

susceptible metals. Washing the sample surface with flowing rainwater could also partially remove loose corrosion products, more easily exposing the underlying metal substrate to corrosive environments.

4.1.2 Morphology

The difference in corrosion rates measured at different exposure sites was strongly supported by the variation in sample surface morphologies. At the wastewater treatment plant site, a thick corrosion product layer was formed on the mild steel sample surface, leading to a significant increase of total sample thickness from 3 mm to ~5–6 mm after a 1-year exposure. This thick corrosion product layer (~1–2 mm thick) on each side could readily detach from the sample surface (Figure 15).

Physical defects such as pores, cracks and fracture features were observed on the exposed underlying surface (Figure 16b). By comparison, the corrosion products formed on the mild steel samples exposed in the west and east areas were compact with fewer physical defects (Figures 16a & c). Spallation or detachment of corrosion products was not observed on these samples.

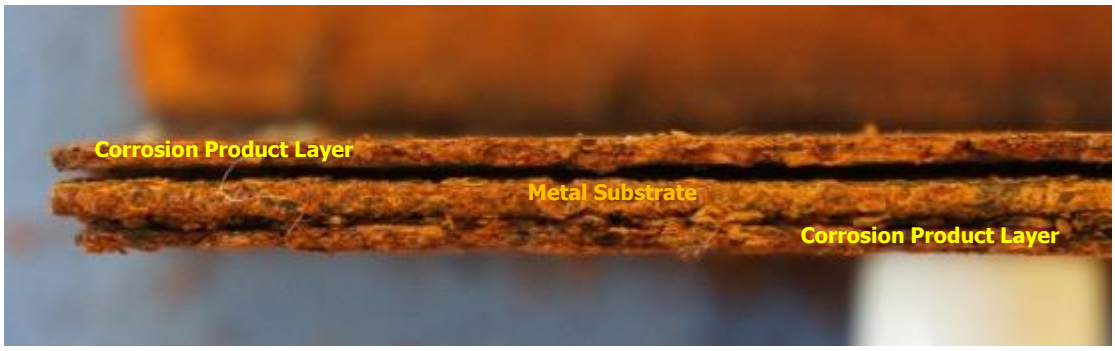

Figure 15. Corrosion products remaining on the mild steel sample exposed at the wastewater treatment plant site for 1 year.

The corrosion products on zinc samples exposed in the west and east areas (216 Malfroy Road and Lynmore) grew roughly along the fine grounding marks to form a uniform, dense and thin layer (Figures 17a & c). This corrosion product with a limited number of defects can provide relatively good protection to the underlying substrate and grow slowly, leading to low corrosion rates (Figure 13).

By contrast, the surface of zinc sample exposed at the wastewater treatment plant site was rough and had a large number of clusters growing from underlying pit-like features. These clusters connected to form a network-like structure on the top of a relatively dense layer of fine particles (Figure 17b).

It should be noted that the surface morphology observed with a microscope after this 1-year exposure may not represent the complete surface features of the corroding zinc sample. A field visit found that white powder-like corrosion products had formed on both skyward and groundward surfaces. However, these corrosion products were not able to stay on the skyward surface permanently once formed. They had low adherence to the underlying substrate and could be removed partially by flowing rainwater. Therefore, samples retrieved for lab analysis may or may not have these powder-like corrosion products on their skyward surfaces.

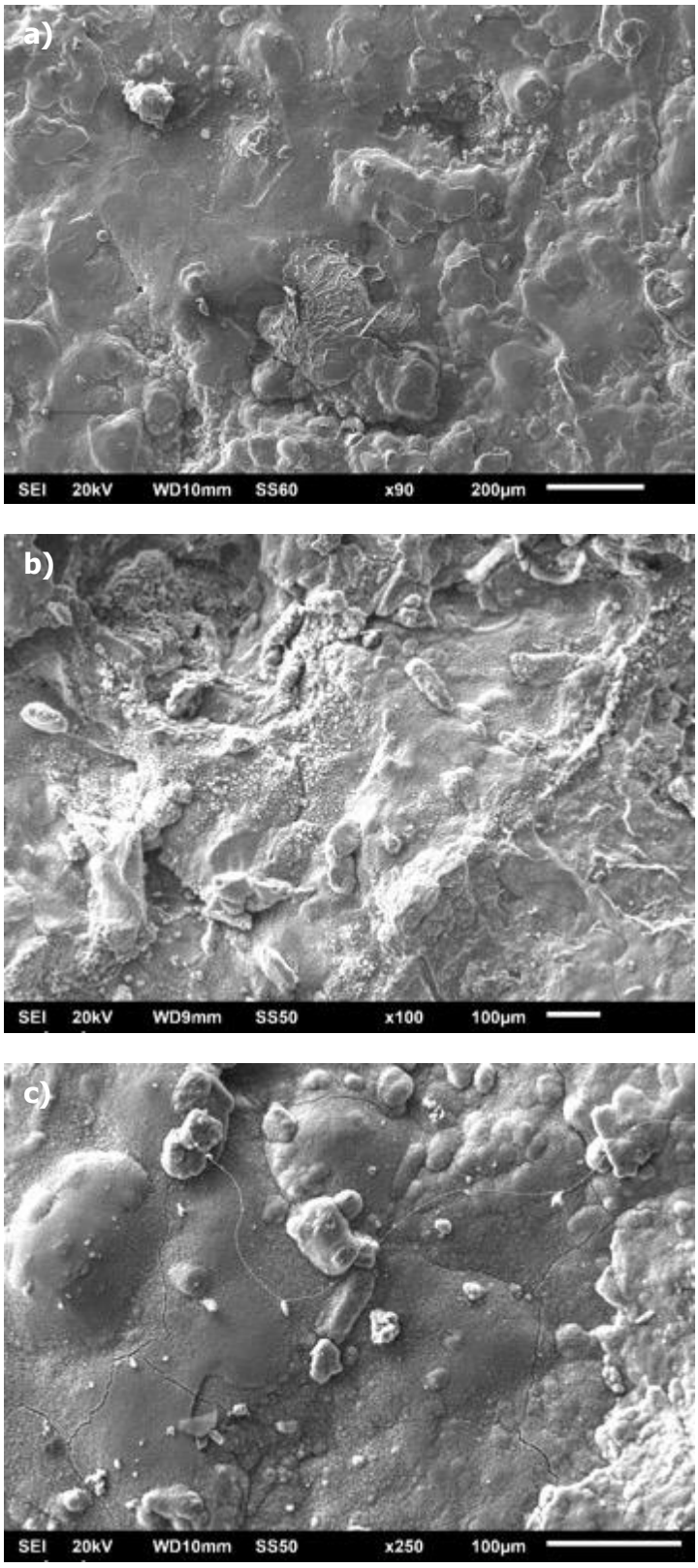

Figure 16. Surface morphology of mild steel exposed at (a) 216 Malfroy Road (west area of Rotorua), (b) wastewater treatment plant (south of Sulphur Bay) and (c) Lynmore (east area of Rotorua) for 1 year.

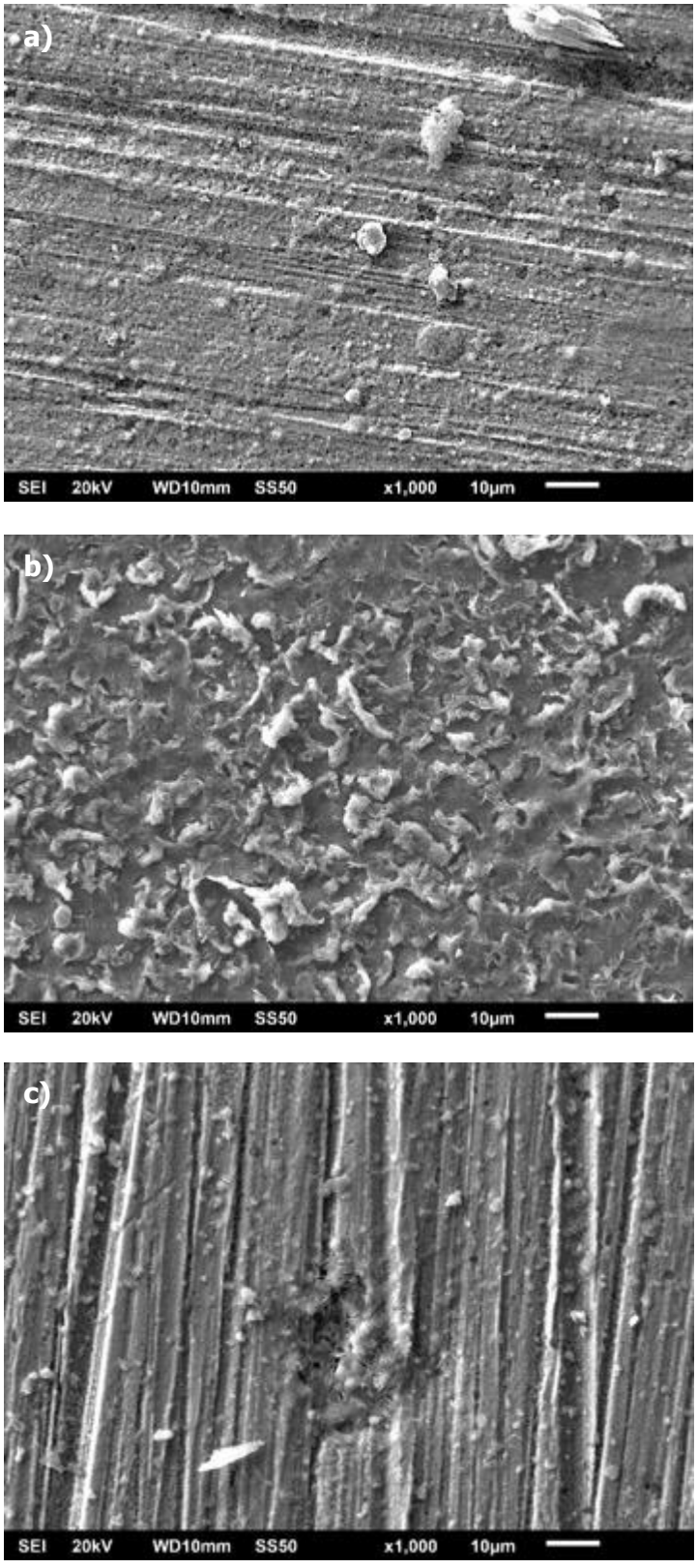

Figure 17. Surface morphology of zinc exposed at (a) 216 Malfroy Road (west area of Rotorua), (b) wastewater treatment plant (south of Sulphur Bay) and (c) Lynmore (east area of Rotorua) for 1 year.

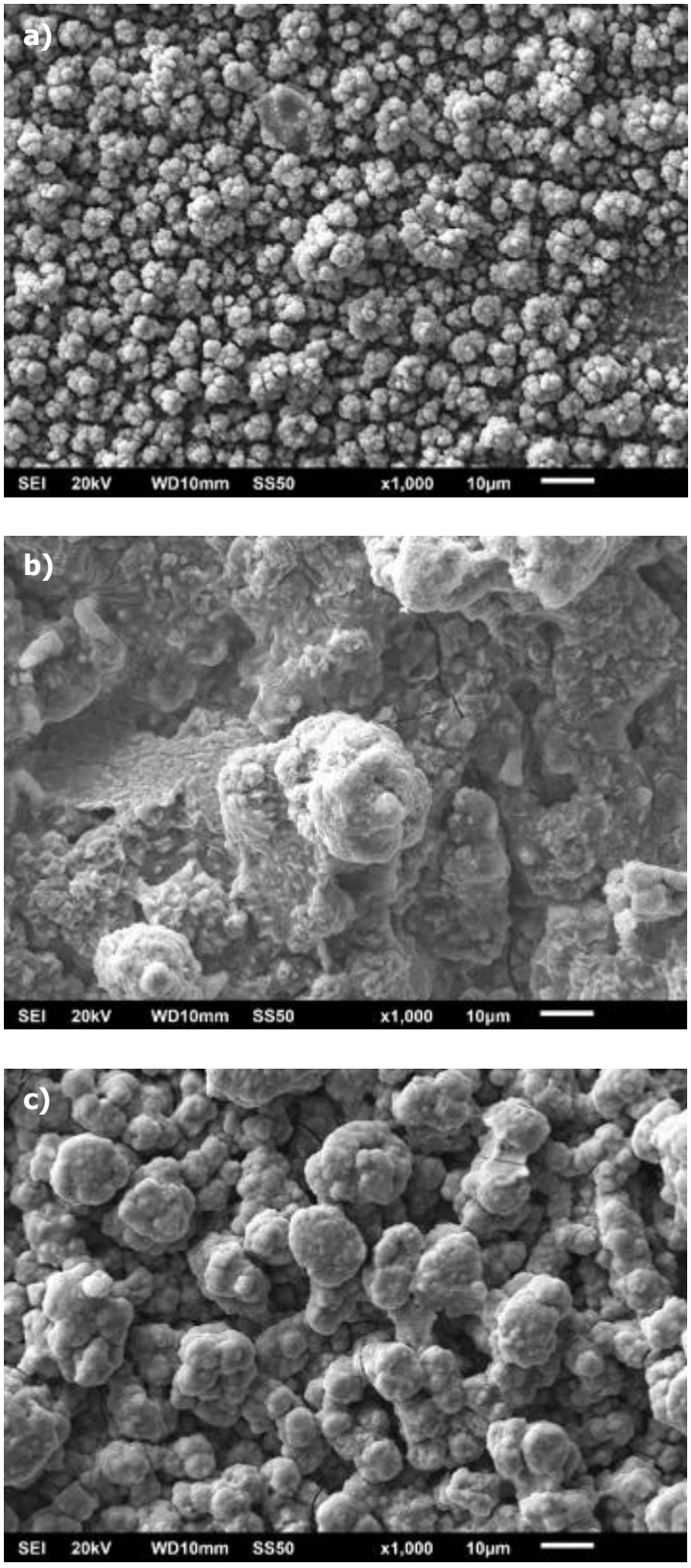

Figure 18. Surface morphology of copper exposed at (a) 216 Malfroy Road (west area of Rotorua), (b) wastewater treatment plant (south of Sulphur Bay) and (c) Lynmore (east area of Rotorua) for 1 year.

The copper samples exposed at the wastewater treatment plant site had a corrosion rate ranging from 443 g/m^2/year to 495 g/m^2/year. This extremely high corrosion rate was a direct result of the rapid interactions of copper and sulphur-containing species and poor protection offered by the corrosion products with a large number of defects. Corrosion products on copper samples started to crack and detach partially as flakes after approximately 1 month of exposure at this site, exposing fresh copper substrate to this highly corrosive environment. Microscopic characterisation also revealed a rough surface with a large number of nodules and deep etch-like pit features after a 1-year exposure (Figure 18b). This indicated that the attack to metal was extremely non-uniform and a complete corrosion product layer was unlikely to be present to provide a good protection to the underlying substrate.

Copper samples exposed in the west and east areas were covered with clusters of small particles (Figures 18a & c). Though not compact and dense, a certain degree of protection could still be expected.

The corrosion product layer on the copper sample exposed in the east area was thicker and had larger clusters or particles than that on the copper exposed in the west area. A comparison between Figure 18a and Figure 18c indicated that a small difference in concentration of airborne sulphur-containing species would be enough to make a large difference in copper deterioration.

4.1.3 Comparison with reference sample

Geothermal environments are unique and quite different from other New Zealand natural environments with marine, industrial or rural influences. To investigate these potential influences, metal coupons were also exposed at two reference sites in Wellington – one rural (BRANZ Judgeford campus) and the other severe marine (Oteranga Bay).

At Judgeford site, during the periods of December 2014 to December 2015 and June 2015 to June 2016, the corrosion rates were 162 g/m^2/year and 174 g/m^2/year for mild steel, 8.3 g/m^2/year and 6.8 g/m^2/year for zinc and 14.0 g/m^2/year and 15.6 g/m^2/year for copper respectively.

At Oteranga Bay site, during the period of June 2015 to June 2016, the corrosion rates were 650 g/m^2/year for mild steel, 33.1 g/m^2/year for zinc and 65.7 g/m^2/year for copper.

A comparison between the first-year metal corrosion rates measured at these exposure sites showed the following:

- The mild steel corrosion rate at Judgeford was slightly higher than those at 216 and 116 Malfroy Road, similar to that at Lynmore, but lower than those at the other three sites in Rotorua. The surface morphology of this sample was similar to those of samples exposed in the west and east areas of Rotorua (Figure 16 and Figure 19a). The corrosion product layer was reasonably uniform and dense, acting as a reasonably good barrier against the corrosive environment. One distinct feature of the corrosion product layer on the mild steel exposed at Judgeford was that corrosion was developing rapidly along grain boundaries, resulting in the formation of a network with cracks (Figure 19a).
- The mild steel corrosion rate at Oteranga Bay was higher than that at Ngapuna but lower than those at 22 Malfroy Road and the wastewater treatment plant site.

Specifically, the corrosion rate measured at Oteranga Bay was ~5 times lower than that at the wastewater treatment plant site. Corrosion products formed on the mild steel sample at Oteranga Bay tended to detach partially, leading to an uneven thickness reduction and a very rough surface.

- As discussed above, corrosion products remaining on the mild steel samples exposed at the wastewater treatment plant site were growing into extremely thick layers. Due to the huge volume expansion and large stresses, these corrosion products detached from the substrate as a complete piece after extended exposures. However, the corrosion products remaining on the surface were still thick with a large number of physical defects, such as long cracks.
- The zinc corrosion rate measured at Judgeford was lower than those measured at three exposure sites close to or in the central city of Rotorua but slightly higher than those measured at the other three sites in the west and east areas (216 and 116 Malfroy Road and Lynmore). The corrosion rate at the wastewater treatment plant site was ~8–12 times higher than that at Judgeford.
- Zinc corrosion products on the sample exposed at Judgeford were relatively dense and covering the whole surface uniformly, providing good protection to the underlying substrate (Figure 19b). This corrosion product layer might be slightly thicker than those formed on the zinc samples exposed in the west and east areas of Rotorua since there was no reflection of original grinding marks (Figure 17a and c). This is consistent with the corrosion rate measurement. Clusters of chloride-containing particles were observed occasionally on this sample surface. Chloride-containing sea salt particles are detrimental to corrosion resistance of zinc. However, no significant increase in corrosion rate was observed at Judgeford where salt deposition was low due to limited marine influences.
- The zinc corrosion rate measured at Oteranga Bay was only lower than that measured at the wastewater treatment plant site. The sample surface was rough with erosion-like features and cracks (Figure 20b). This was a direct result of accelerated surface attack induced by high salt deposition and mechanical impacts of strong winds.
- The copper corrosion rate measured at Judgeford was lower than those at all six exposure sites in Rotorua. The corrosion product layer on the copper sample exposed at Judgeford was dense and uniform and composed of particles of ~100–200 nm and occasionally some large cubic particles (~3–5 μm) of unknown phase composition (Figure 19c). This morphology is different from that of copper samples exposed in the west and east areas of Rotorua (Figure 18a and c), indicating that very low concentrations of sulphur-containing species in air could still significantly affect copper corrosion.
- The copper corrosion rate measured at Oteranga Bay was similar to that measured at Lynmore but lower than those measured at sites close to or within the central Rotorua city areas. The copper sample exposed at Oteranga Bay had a rough surface on which small particles and clusters were observed on a dense sublayer with long and deep cracks (Figure 20c). This surface morphology was quite different from that of copper samples exposed to strong geothermal environments. These sample surfaces featured a large number of nodules, clusters of particles and deep pits (Figure 18b).

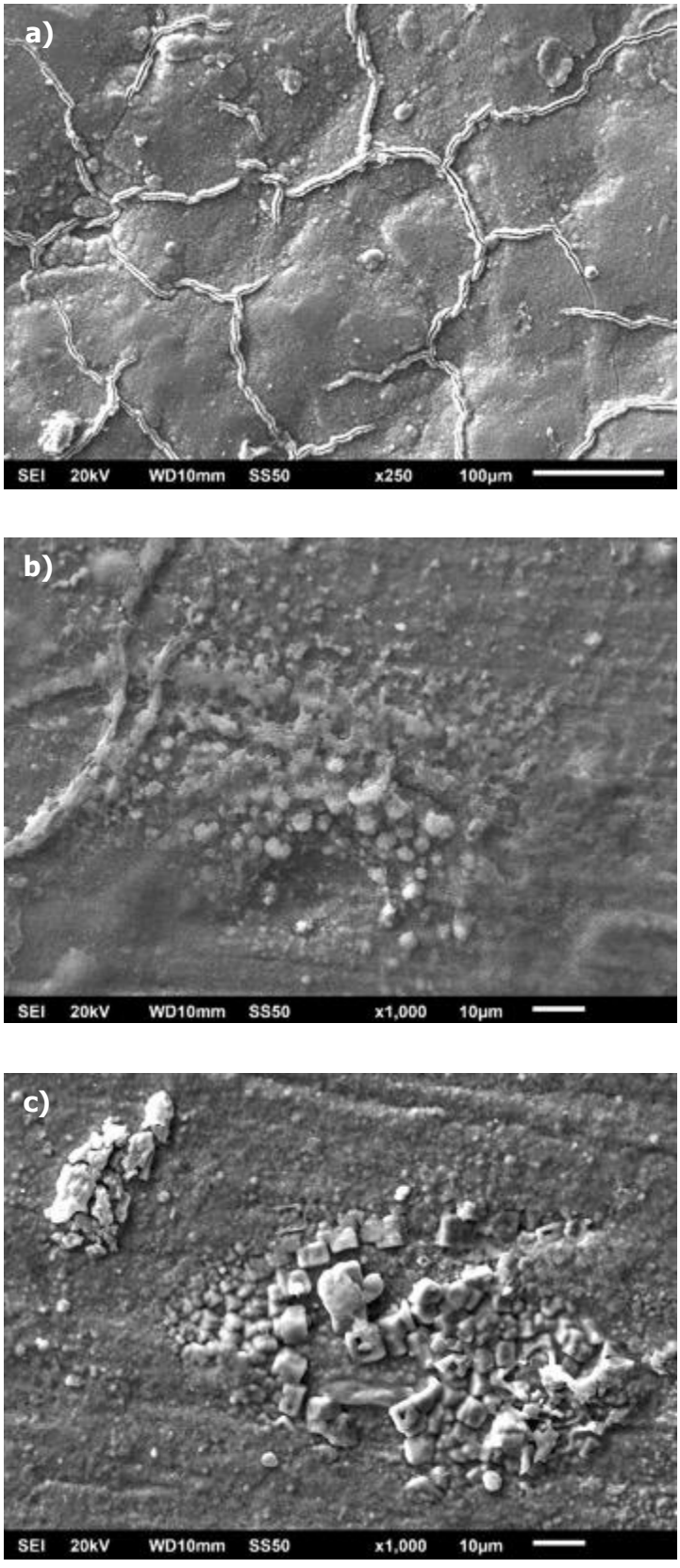

Figure 19. Surface morphology of (a) mild steel, (b) zinc and (c) copper exposed at Judgeford for 1 year.

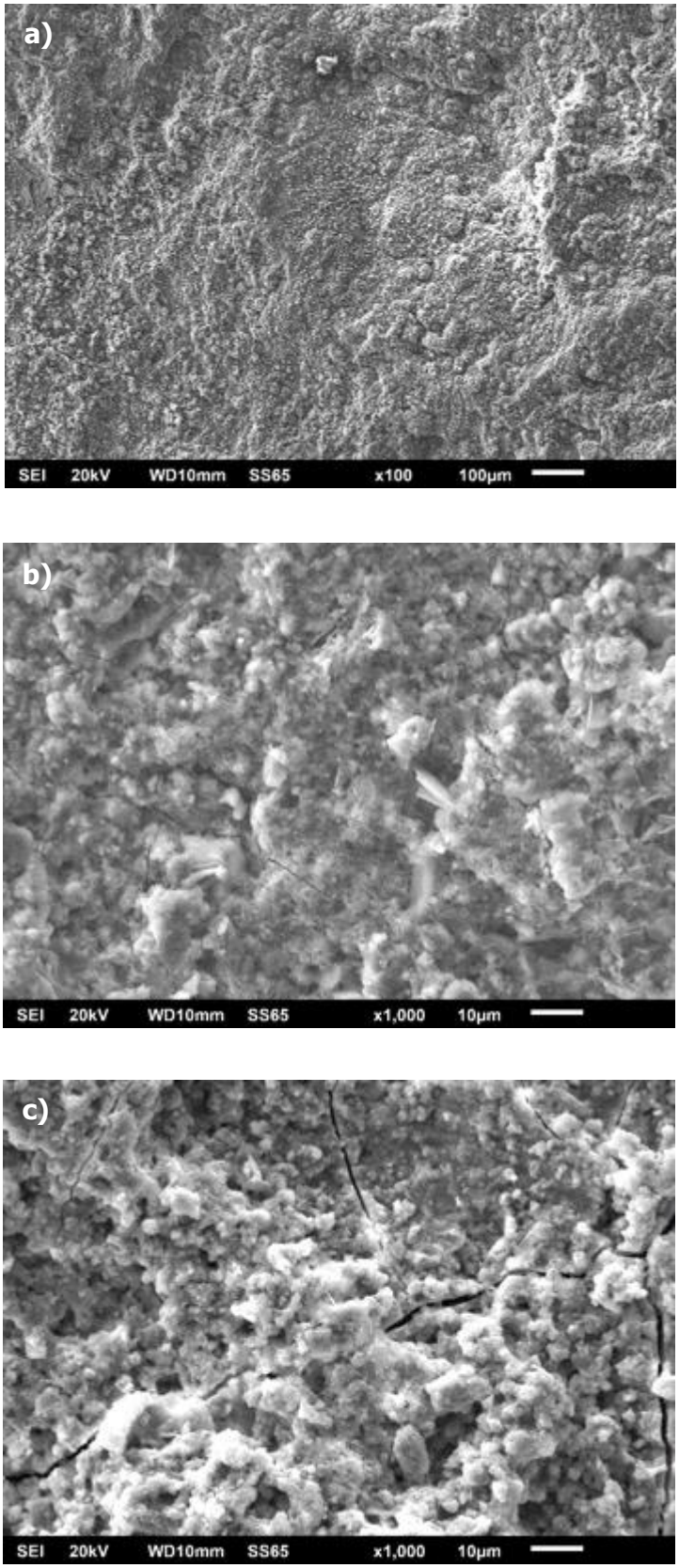

Figure 20. Surface morphology of (a) mild steel, (b) zinc and (c) copper exposed at Oteranga Bay for 1 year.

4.2 Distance effects

NZS 3604:2011 defines geothermal hot spots as being within 50 m of a bore, mud pool, steam vent or other sources. This distance was used to investigate the effects of distance on metal atmospheric corrosion in geothermal environments. As described in section 2.1, one exposure site was ~5 m away from a fumarole in Scion campus, the second ~50 m east and the third ~60 m southwest.

4.2.1 Corrosion rate

The first-year metal corrosion rates were measured after three exposure periods – December 2014 to December 2015, June 2015 to June 2016 and December 2015 to December 2016.

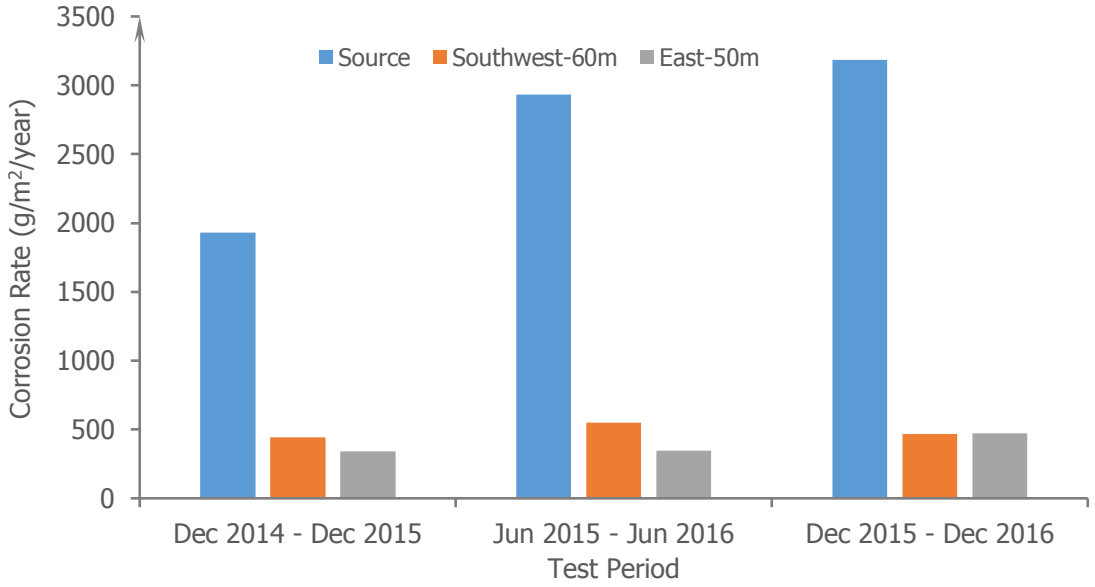

Figure 21. First-year mild steel corrosion rates at three locations around a fumarole.

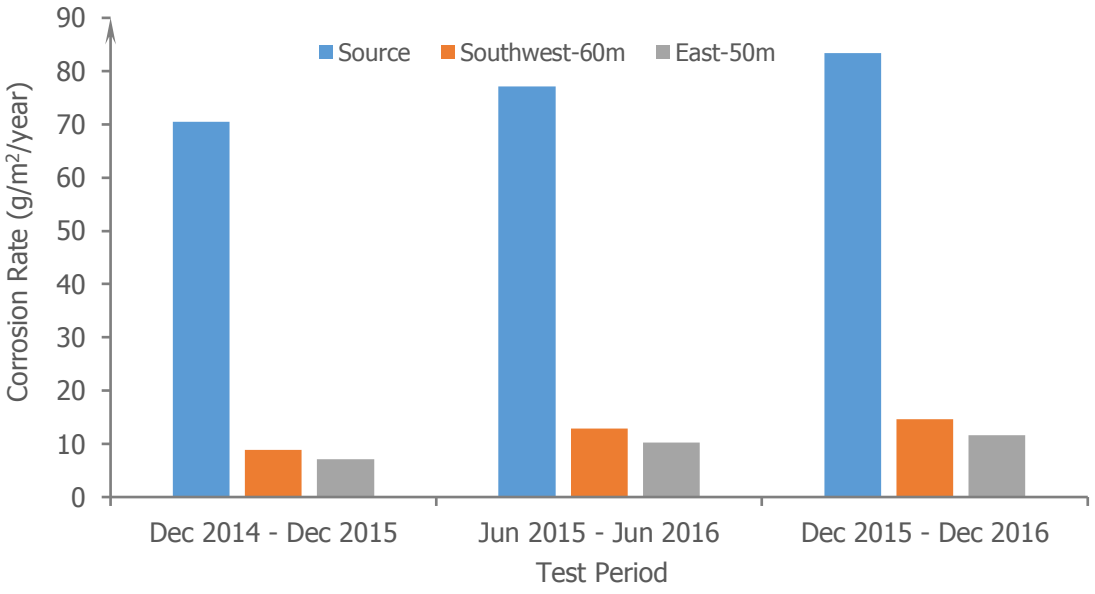

Figure 22. First-year zinc corrosion rates at three locations around a fumarole.

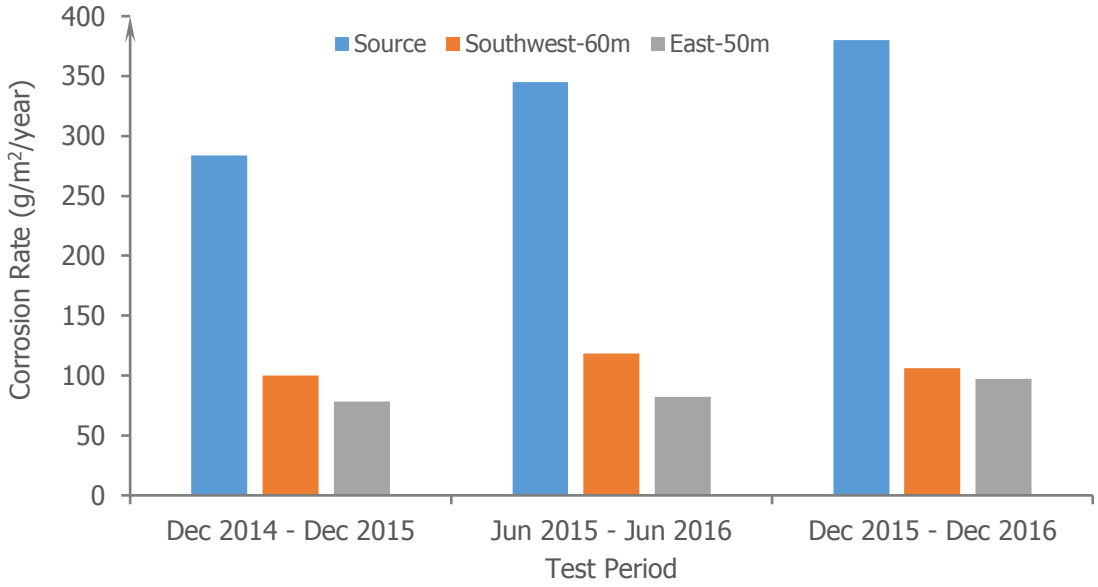

Figure 23. First-year copper corrosion rates at three locations around a fumarole.

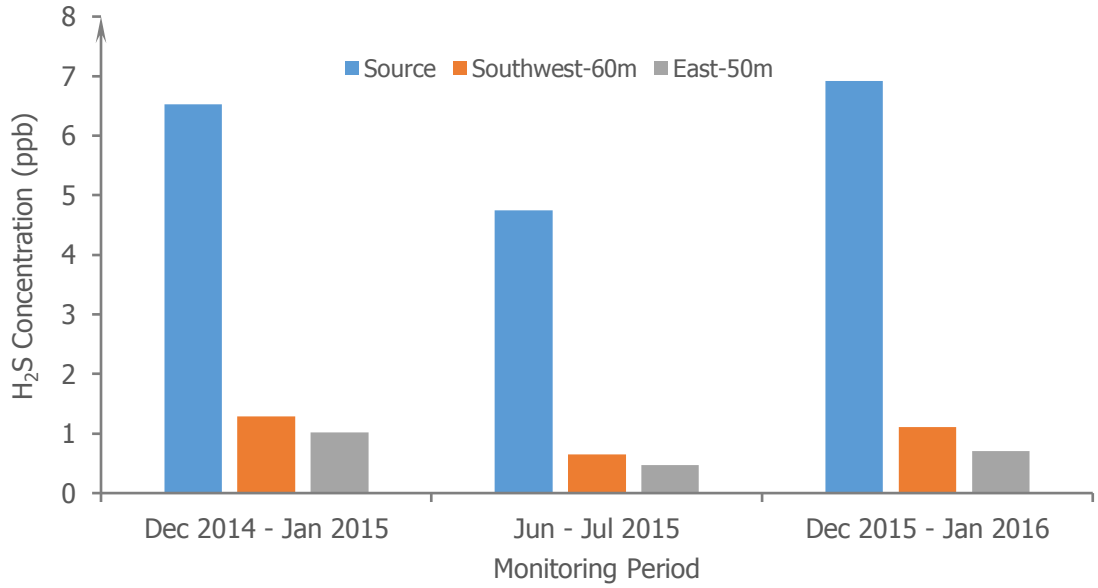

Figure 24. Average H_2S concentrations at three locations around a fumarole.

As shown in Figures 21–23, a separation of approximately 50–60 m, either to the southwest or east of this fumarole, significantly decreased the corrosion rates of all three metals tested. The decrease was 4–9, 6–10 and 3–4 times for mild steel, zinc and copper, respectively.

This is likely related to the concentration decrease of airborne sulphur-containing species (H_2S and/or SO_2). As shown in Figure 24, H_2S concentrations measured at the southwest and east locations approximately 50–60 m away from this fumarole was 5–10 times lower than that at the source. Similarly, SO_2 concentrations measured at these two locations were approximately 3–4 times lower than that at the source (Figure 11b).

4.2.2 Morphology

Surface morphological characterisation confirmed that ~50–60 m separation could lead to the formation of corrosion product layers with a better protection capability. As shown in Figure 25, mild steel samples exposed at a location ~5 m away from this fumarole were suffering severe corrosive attack. Cracking and spallation of corrosion products were easily found (Figure 25a). By contrast, corrosion products formed on mild steel samples exposed ~50–60 m away showed no sign of significant detachment or spallation although some cracks were still observed (Figure 25b).

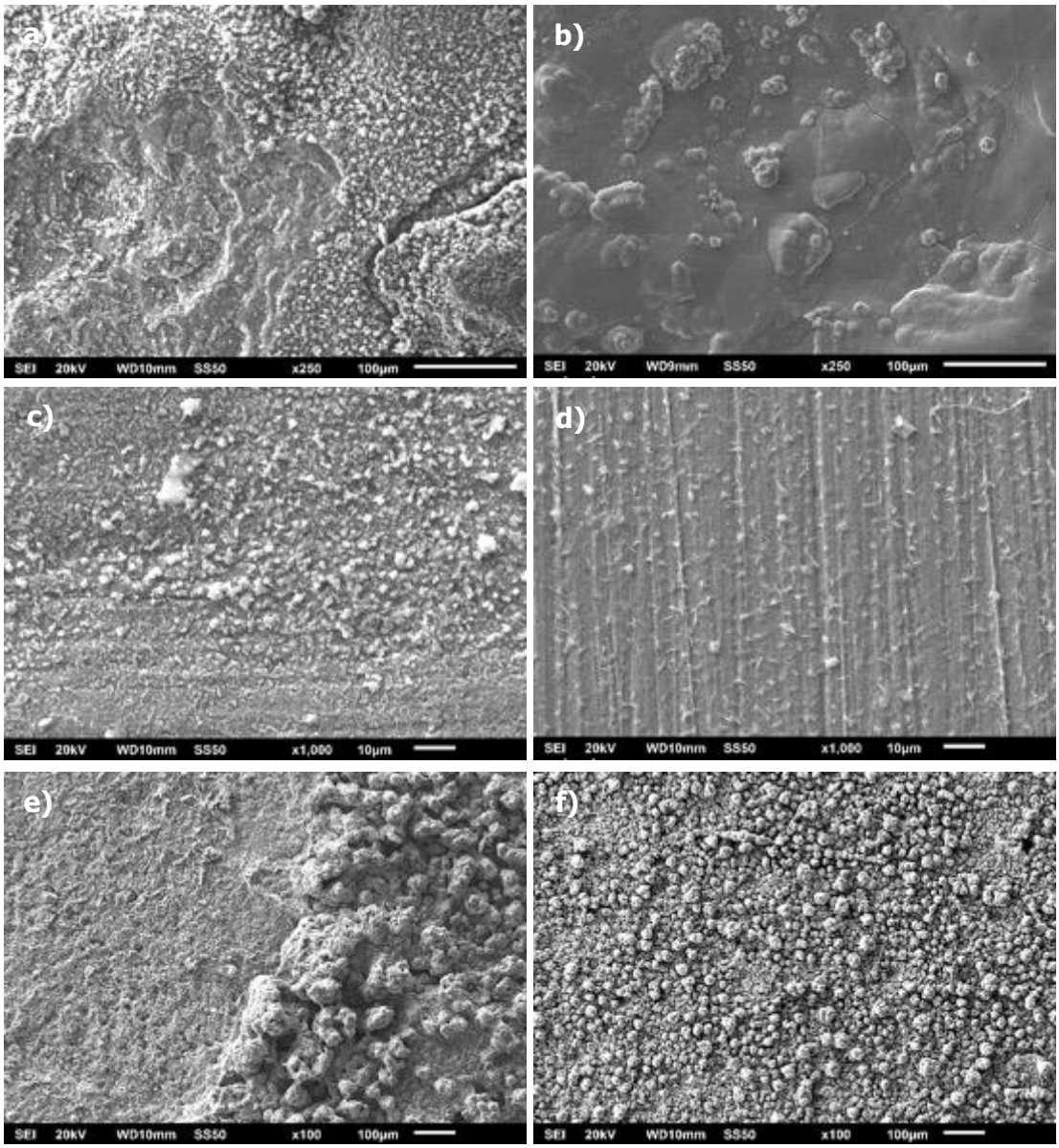

Figure 25. Surface morphology of metal coupons at three locations around a fumarole. (a, c, e) ~5 m and (b, d, f) ~50 m east. (a & b) mild steel, (c & d) zinc and (e & f) copper.

The corrosion product layer on the zinc sample exposed ~50–60 m away from this fumarole was uniform and dense and showed the reflection of original grinding lines on the surface (Figure 25d). This layer was thinner than that on the zinc sample ~5 m

away from this fumarole and could provide better protection, evidenced by lower corrosion rates.

Corrosion products formed on copper close to this fumarole detached and spalled partly during exposure, leading to a very rough surface (left section of Figure 25e). Meanwhile, a large number of discrete corrosion product nodules and/or clusters were found on the sample surface (right section of Figure 25e). By contrast, spallation and/or detachment was not observed on the copper samples exposed ~50–60 m away. The corrosion product layer was composed of clusters of small particles (Figure 25f). Some fine powder-like materials could be wiped off with a finger from the surface. This surface morphology was somewhat similar to that of copper after short exposure to H_2S of 1 ppm (Tran et al., 2003).

Based on corrosion rate measurement and morphological characterisation, it is arguable that a ~50–60 m separation from an active geothermal feature could put the local atmospheric environment into relatively benign corrosivity categories.

Table 2. Corrosivity category determined according to ISO9223:2012.

Metal	Location	Corrosivity category		
		Dec 2014 – Dec 2015	**Jun 2015 – Jun 2016**	**Dec 2015 – Dec 2016**
Steel	Source	CX – Extreme	CX – Extreme	CX – Extreme
	Southwest-60 m	C4 – High	C4 – High	C4 – High
	East-50 m	C3 – Medium	C3 – Medium	C4 – High
Copper	Source	>CX – Extreme*	>CX – Extreme*	>CX – Extreme*
	Southwest-60 m	>CX – Extreme*	>CX – Extreme*	>CX – Extreme*
	East-50 m	CX – Extreme	CX – Extreme	>CX – Extreme*
Zinc	Source	CX – Extreme	CX – Extreme	CX – Extreme
	Southwest-60 m	C3 – Medium	C3 – Medium	C3 – Medium
	East-50 m	C3 – Medium	C3 – Medium	C3 – Medium

* When the first-year corrosion rate of copper is used for atmospheric corrosivity category classification, the ISO 9223:2012 CX category indicates the corrosion rate will be in the range of 50–90 g/m^2/year. In this study, the first-year corrosion rate of copper can be ~5 times higher than the upper limit, 90 g/m^2/year.

The corrosion rate of mild steel exposed at ~60 m southwest of a small fumarole was measured to be 443–551 g/m^2/year, based on which a ISO 9223:2012 C4 (High) corrosivity category can be assigned (Table 2). Further, if copper corrosion rate was used, the corrosivity of the environment ~50–60 m away from this fumarole was confidently classified into CX (Extreme), the highest category defined by ISO 9223:2012. It should be noted that copper corrosion rates measured at these locations were much higher than the upper limit of copper corrosion rate in ISO 9223:2012 CX (Extreme) category – 90 g/m^2/year.

Extremely high metal corrosion rates were measured at the wastewater treatment plant site which is ~200 m south of Sulphur Bay with a number of active geothermal features. The first-year corrosion rates were 3,044–3,443 g/m^2/year, 65.6–88.6 g/m^2/year and 443–517 g/m^2/year for mild steel, zinc and copper, respectively. In the

1980s, BRANZ measured the first-year corrosion rate of mild steel as 2,293 g/m^2/year at a site approximately 400 m southwest of Sulphur Bay. All these measurements indicated that the area ~200–400 m south or southwest from Sulphur Bay was extremely corrosive and the atmospheric environment could be classified as ISO 9223:2012 CX (Extreme).

Environmental corrosivity categories determined by using the first-year corrosion rate of different model metals can be somewhat different. For example, the atmospheric corrosivity category of Oteranga Bay can be determined to be C5 (Very high), C5 (Very high) and CX (Extreme) based on the first-year corrosion rates of mild steel, zinc and copper, respectively. However, results shown in Table 2 showed a much larger difference in atmospheric corrosivity category using those three model metals in geothermal environments. This difference could be misleading and sometimes risky in practice.

The method recommended by ISO 9223:2012 might not be appropriate for atmospheric corrosivity classification of geothermal environments. This is because those model metals have quite different interactions with sulphur-containing species. For example, this study found that copper was more prone to geothermal attack when compared with mild steel and zinc.

4.3 Height effects

Gaseous emissions including H_2S and/or SO_2 are major airborne pollutants contributing to material degradation in geothermal environments. H_2S with a density of ~1.363 kg/m^3 is slightly denser than air, therefore tending to concentrate in areas close to the ground. This creates an H_2S concentration gradient at height, possibly exerting influences on performance of materials at different heights.

The height effects were investigated with mild steel coupons installed at three different heights from ground – 1 m, 2 m and 3 m in this study. These coupons were exposed at a location ~5 m away from a fumarole and installed at three angles relative to the ground – 0° (horizontal), 45° and 90° (vertical). The skyward surface of the 45° inclined samples and one surface of the 90° inclined samples were facing north. The exposure was started in December 2015 and completed after 1 year. H_2S concentrations at these three heights were monitored with passive tube sensors in the first 3 weeks of this exposure.

The first-year mild steel corrosion rates are reported in Figure 26. An increase of exposure height from 1 m to 3 m significantly decreased the mild steel corrosion rate. For example, the corrosion rate of the vertically installed mild steel coupon at 3 m was ~5 times lower than that of the coupon installed at 1 m. Meanwhile, the H_2S concentration at 3 m was ~22 times lower than that at 1 m height.

The correlations between corrosion rate and height and H_2S concentration and height were explored with mathematical fitting.

Mild steel corrosion:

$$y = -733.5x^2 + 1428.5x + 3262;\ R^2 = 1$$

H_2S concentration:

$$y = 52.963x^{-2.814};\ R^2 = 0.9977$$

Although both metal corrosion and airborne H_2S concentration decrease with height, their decreasing behaviours were not the same (Figure 27). H_2S concentration tended to decrease more rapidly with height increase.

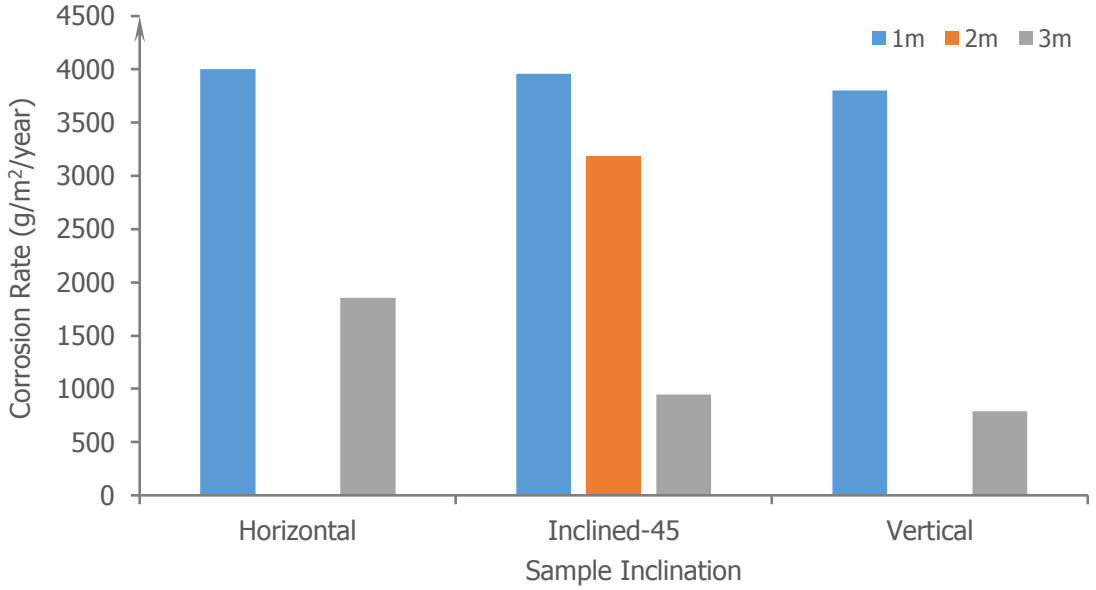

Figure 26. First-year corrosion rates of mild steel coupons at three heights.

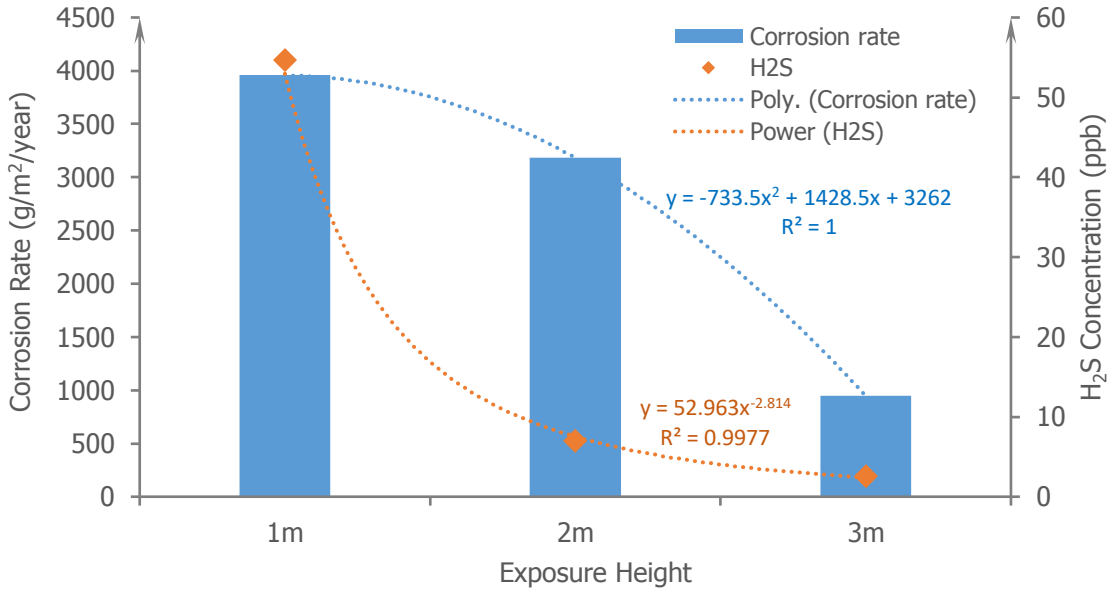

Figure 27. Correlation between mild steel corrosion rate, H_2S concentration and exposure height (mild steel coupon installed at an angle of 45° and faced north).

The coupon inclination angle affected metal corrosion rate at the same installation height and an increase of inclination angle from 0° to 90° decreased corrosion rate. Specifically, this decrease was more obvious with the samples installed at 3 m high.

Horizontal samples tend to have a higher time-of-wetness (ToW) than those samples at an inclination angle of 45° or 90° due to a higher probability of water/moisture being retained on their top surfaces for longer periods. A surface that is wet for longer

periods could have a larger chance to dissolve more gaseous or solid species that promote corrosion.

At 1 m above the ground, H_2S concentration in air was very high as measured. Under this condition, H_2S concentration on the sample surface (dry) or in the surface moisture layer (wet) would be high enough to maintain rigorous attack to metal, despite the sample surface being inclined at different angles. At a height of 3 m, H_2S concentration is much lower and its contribution to corrosion would be achieved mainly through dissolution into the surface water/moisture layer. Retention of the surface water/moisture layer will then be critical to sustain corrosion. A horizontal surface tends to hold a water/moisture layer for longer periods during which more airborne H_2S could be dissolved, contributing to more severe corrosion in extended exposures.

4.4 Geothermal feature effects

Three geothermal systems were used to investigate the effects of geothermal feature on metal corrosion. These include a fumarole (~0.5 m in diameter), a spring (~1.5–2 m in diameter) and Sulphur Bay (a mixed, large geothermal system; the exposure site was within the wastewater treatment plant ~200–300 m south of Sulphur Bay).

Figures 28–30 show the first-year corrosion rates of mild steel, zinc and copper exposed to these three geothermal features. The following corrosion rate orders were roughly derived based on corrosion rate measurements done in three testing periods:

- Mild steel: mixed geothermal system (Sulphur Bay, WWTP) ≥ spring (Whakarewarewa, Scion) ≥ fumarole (Whakarewarewa, Scion).
- Zinc: mixed geothermal system (Sulphur Bay, WWTP) ≥ fumarole (Whakarewarewa, Scion) ≥ spring (Whakarewarewa, Scion).
- Copper: mixed geothermal system (Sulphur Bay, WWTP) > fumarole (Whakarewarewa, Scion) > spring (Whakarewarewa, Scion).

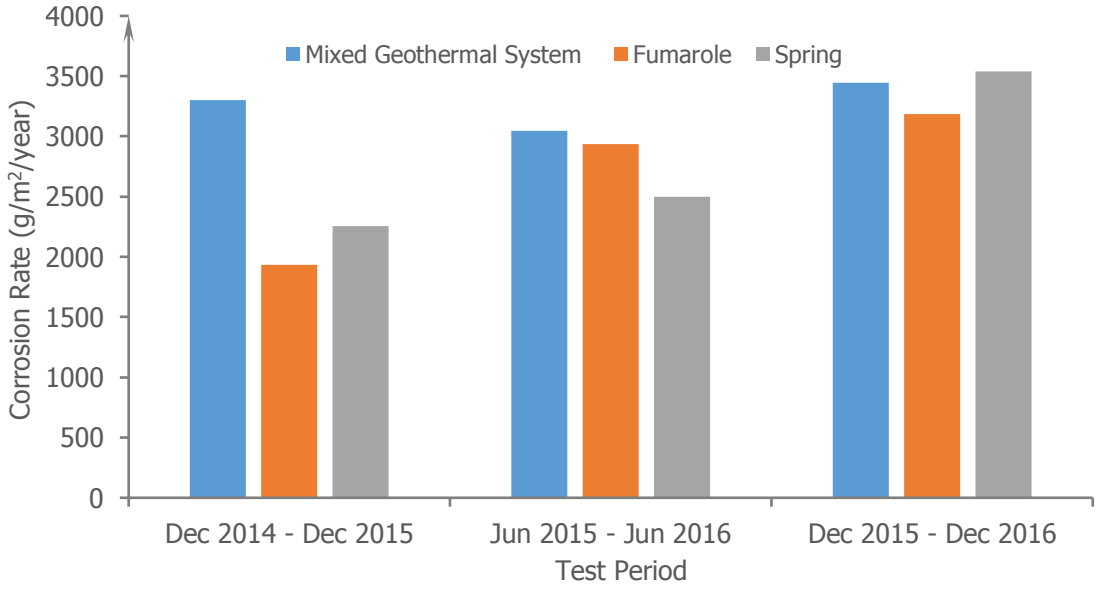

Figure 28. First-year corrosion rates of mild steel coupons exposed to three geothermal features.

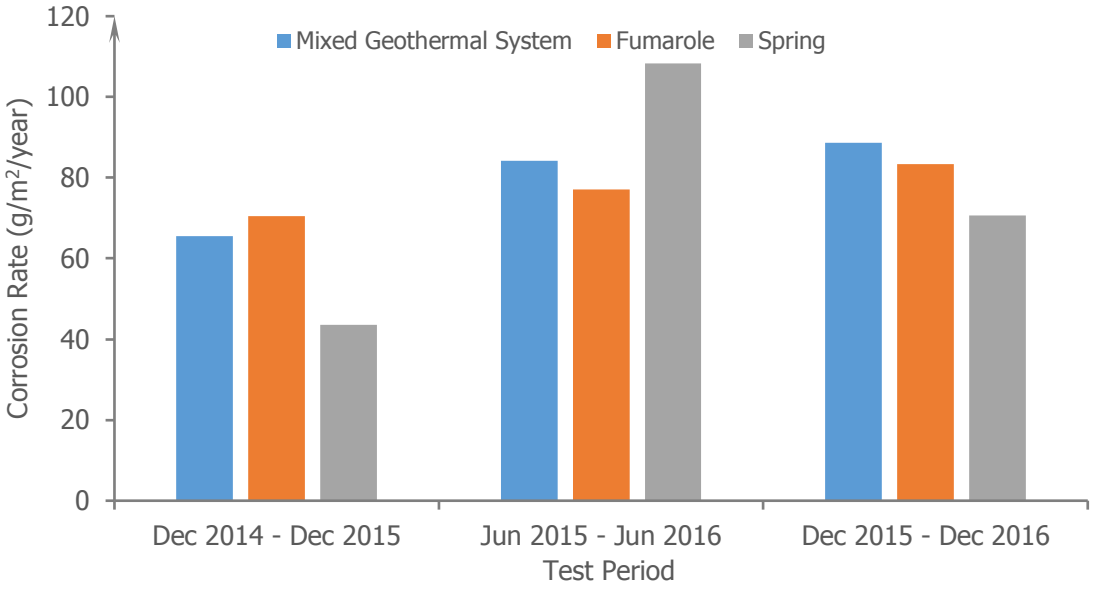

Figure 29. First-year corrosion rates of zinc coupons exposed to three geothermal features.

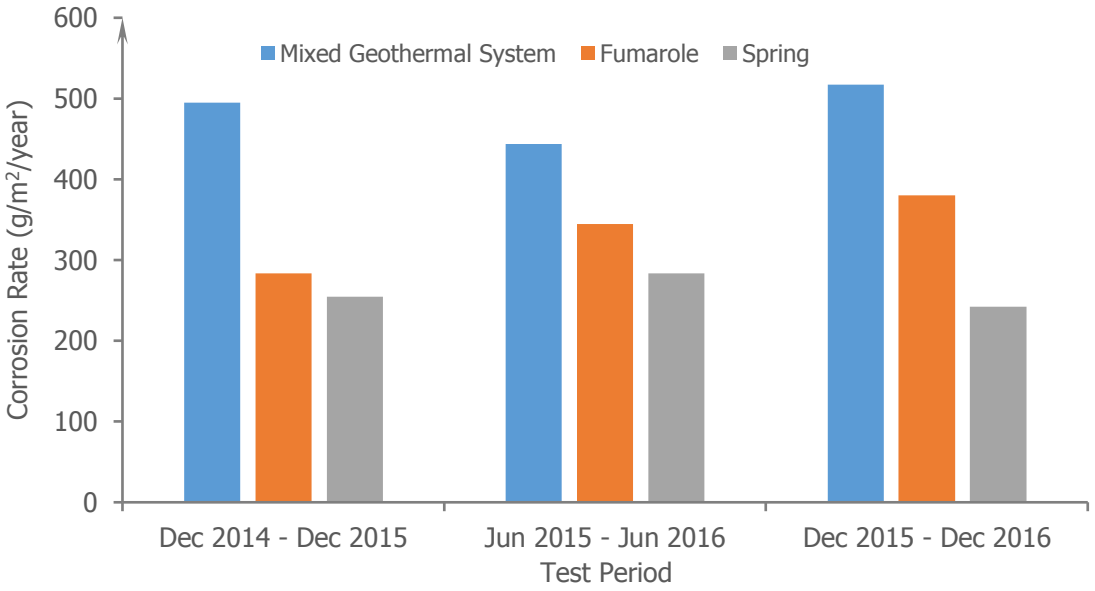

Figure 30. First-year corrosion rates of copper coupons exposed to three geothermal features.

Three runs of 3-week monitoring of airborne H_2S concentrations were performed at these three exposure sites and the results are presented in Figure 31.

The fumarole within Scion campus had the lowest H_2S concentration among these three geothermal features (~3–6 times lower). The H_2S concentration measured close to this fumarole was reasonably stable in these testing periods.

At the wastewater treatment plant site, the H_2S concentration was its lowest, 5.2 ppb, during the June–July 2015 monitoring period. As discussed previously, this was due mainly to the prevailing wind from the southwest, which would blow the geothermal emission away from this site.

The H_2S concentration measured at the geothermal spring also showed a large variation in these three monitoring periods. It was high during the summer period and low during winter, probably related to activity variation of this geothermal feature and seasonal change in climatic factors.

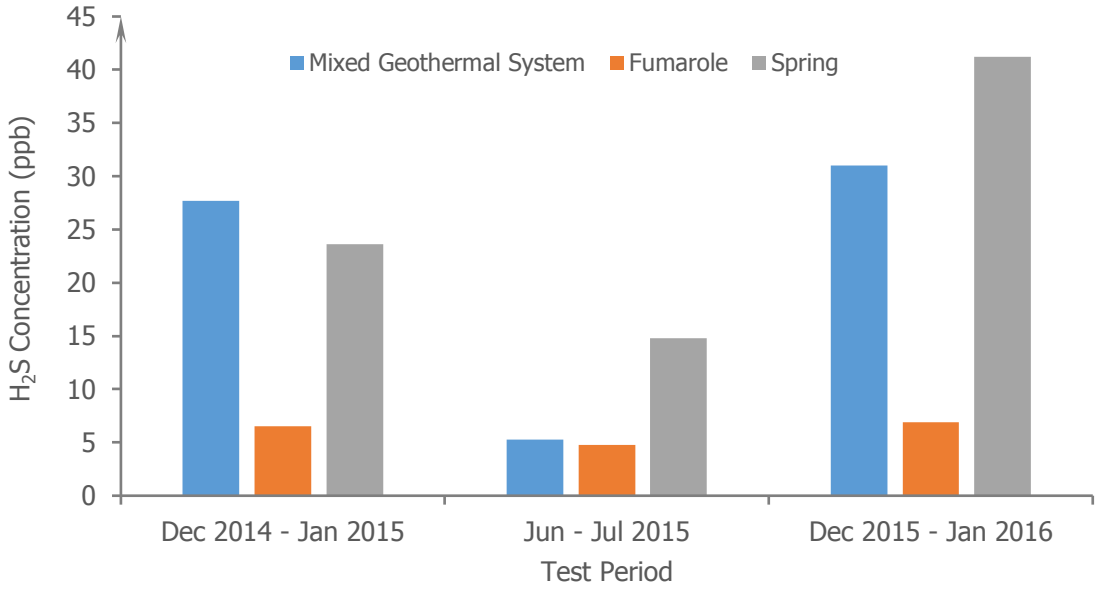

Figure 31. H_2S concentration measured at three geothermal features during a 3-week exposure.

The following general trend of airborne H_2S concentration with geothermal feature could be given:

spring (Whakarewarewa, Scion) > mixed geothermal system (Sulphur Bay, WWTP) > fumarole (Whakarewarewa, Scion).

This was somewhat different from the finding derived from corrosion rate measurements. These three atmospheric environments were consistently classified into ISO 9223:2012 category CX (Extreme) (Table 2).

This study found that the fumarole always had the lowest H_2S concentration, but its surrounding atmospheric environment was still very corrosive to mild steel, zinc and copper.

Why would this happen?

It is postulated that H_2S might not be the only species contributing to metal corrosion in these geothermal environments. Actually, SO_2 was detected and this species is aggressive towards many metals, e.g. Al and Zn (Manning, 1988; Yamashita et al., 1994; Blücher et al., 2005).

However, the fumarole had the lowest SO_2 concentration (Figure 11). A complete compositional analysis of gaseous species discharged from these geothermal features would be helpful to determine if other factors or species were contributing to metal corrosion in these specific geothermal environments.

H_2S and/or SO_2 are corrosive. However, different metals may still have different interactions with them and therefore show different resistance to their attack.

It is also highly likely that there are lower and/or upper limits for these sulphur-containing species, below or above which, metal corrosion might be very limited or levelled off.

Local climatic conditions such as wind speed/direction and rainfall can exert significant influences on atmospheric corrosion, particularly with the involvement of airborne corrosive pollutants. However, this study did not monitor all these climatic factors due to instrumental constraints.

4.5 Time dependence

4.5.1 1-year exposure

Time-dependent corrosion kinetics were studied with mild steel and zinc exposed at the wastewater treatment plant site (~200 m south of Sulphur Bay) and at a location ~5 m away from a fumarole within Scion campus. The exposure periods were 1 year from December 2014 to December 2015 and 2 years from June 2015 to June 2017.

Corrosion kinetics and rates were also measured with a 1-year exposure at Judgeford (rural) and Oteranga Bay (severe marine) in the Wellington region.

4.5.1.1 Corrosion rate

Atmospheric corrosion of mild steel normally decreased with time in a variety of New Zealand natural environments as shown in Figures 32–33 (Kane, 1996; Landolfo et al., 2010; Ma et al., 2010; de la Fuente et al., 2011; Morcillo et al., 2011). For example, when exposed in an area with industrial (fertiliser) emissions, mild steel corrosion rates were measured to be 767 g/m^2/year, 460 g/m^2/year and 289 g/m^2/year, after 3 months, 6 months and 12 months of exposure, respectively.

A common explanation of this corrosion behaviour is that corrosion products formed and remained on the sample surface could, more or less, act as a chemical/physical barrier against the corrosive environment. This could slow down mass transfer and provide a certain degree of protection to the underlying metal substrate.

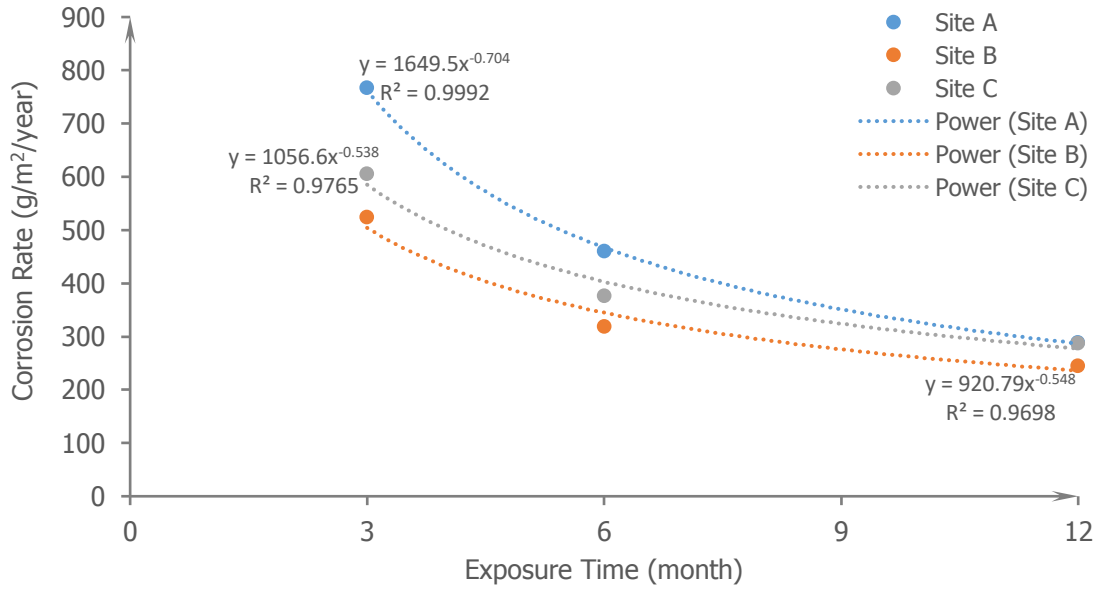

Figure 32. Corrosion behaviour of mild steel exposed in industrial (fertiliser) areas.

This type of time-dependent corrosion behaviour was not observed with mild steel and zinc exposed to geothermal environments with high concentrations of sulphur-containing species (H_2S and/or SO_2) in this study.

As shown in Figure 34a, the corrosion rate of mild steel exposed at the wastewater treatment plant site increased from 2,677 g/m^2/year to 3,719 g/m^2/year in the first 3 months – a ~39% increase. After 6 months, the corrosion rate reached its maximum – 4,019 g/m^2/year. It then started to decrease. However, the corrosion rate measured after 12 months of exposure – 3,302 g/m^2/year – was still ~23% higher than that measured after 1 month of exposure.

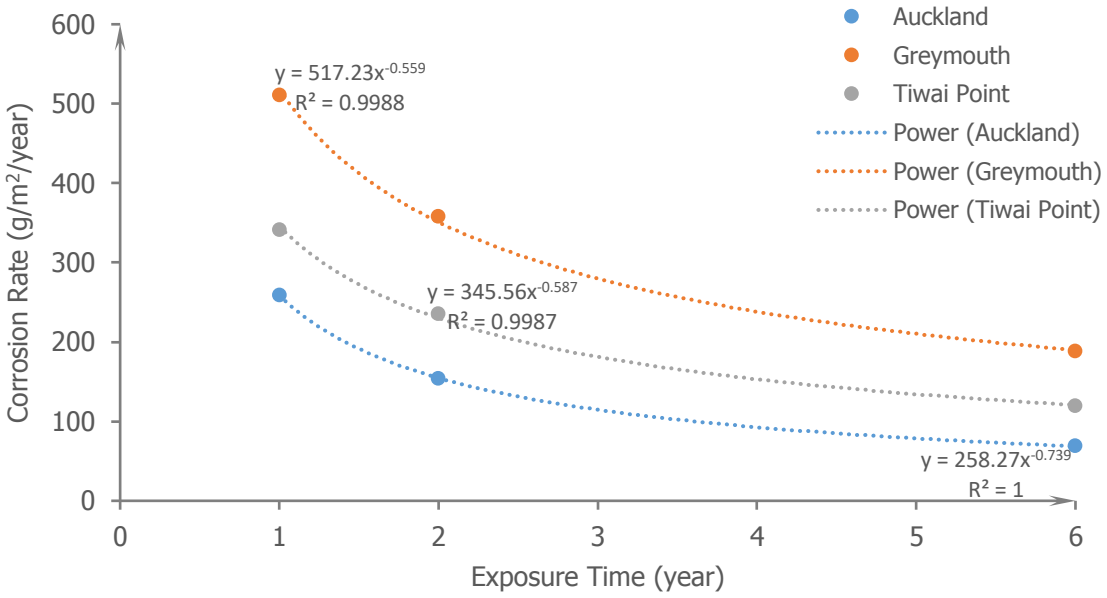

Figure 33. Corrosion behaviour of mild steel exposed to different environments in New Zealand. Auckland: urban, Greymouth: marine, Tiwai Point: marine and industrial (aluminium smelter).

A similar time-dependent corrosion behaviour was observed with mild steel exposed at a location ~5 m away from a fumarole (Figure 34a).

Atmospheric corrosion of zinc also showed a two-stage behaviour (Figure 34b). Its corrosion rate increased in the first 6–9 months and then decreased. Specifically, the corrosion rate of zinc coupon exposed at the wastewater treatment plant site increased significantly from 46.8 g/m^2/year to 161.2 g/m^2/year in the first 9 months of exposure, i.e. an increase of more than 3 times.

This unusual time-dependent corrosion behaviour indicates that corrosion products formed on mild steel and zinc surfaces in the initial stage did not provide any protection to the underlying substrate. Instead, their presence was, to some extent, promoting corrosion.

Why would this happen?

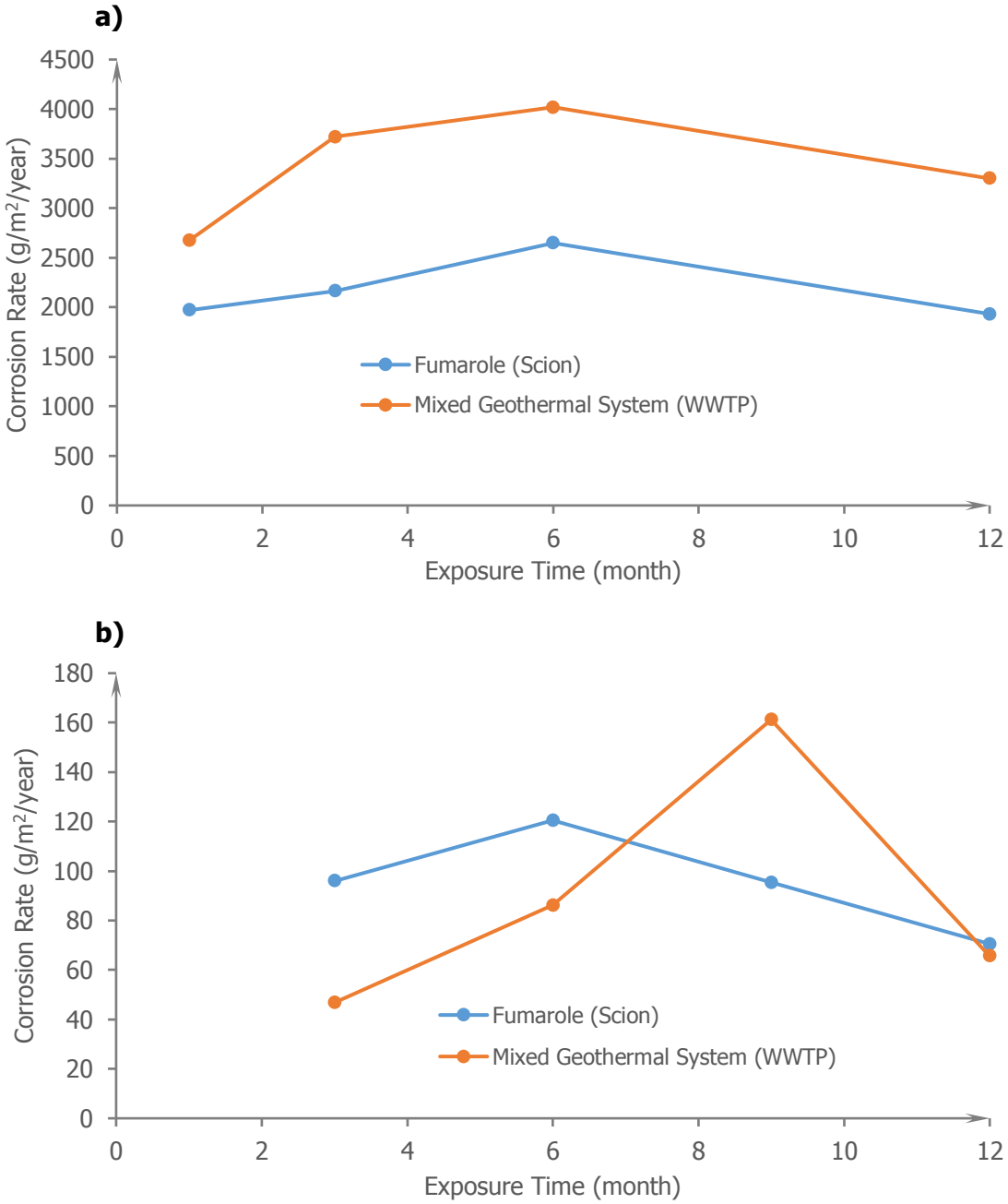

Figure 34. Corrosion behaviour of mild steel (a) and zinc (b) exposed to strong geothermal environments (December 2014 to December 2015).

4.5.1.2 Morphology

As shown in Figure 35a, the top surface of the mild steel sample after a 1-month exposure at the wastewater treatment plant site was covered with clusters of porous corrosion products and open-mouthed bubbles. These morphological features could significantly increase the effective surface area to collect and retain more corrosive contaminants – gaseous and/or solid – from the air and moisture for longer periods, promoting corrosion in extended exposure.

Cracks present in the corrosion product layer could also provide easy paths for inward transportation of water/moisture and pollutants. Therefore, the underlying metal substrate would be partially exposed and under attack continuously.

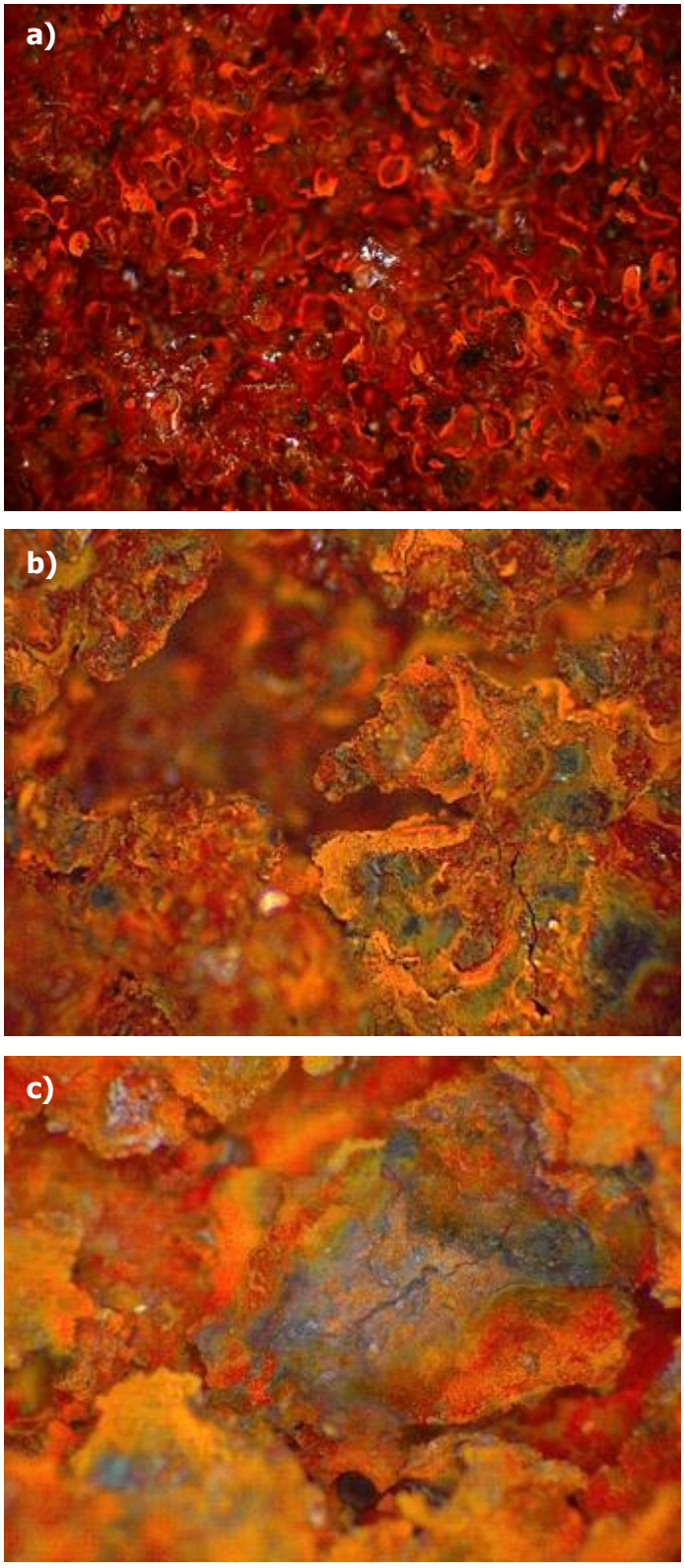

Figure 35. Surface morphology (32×) of mild steel sample after (a) 1 month, (b) 3 months and (c) 6 months of exposure at the wastewater treatment plant site.

After 3–6 months of exposure, the corrosion product layer was growing thicker, with a larger number of physical defects such as cracks, pores and cavities, particularly in its deep sections (Figure 35b & c). The presence of these defects was detrimental to the formation of a corrosion product layer with good protection capability.

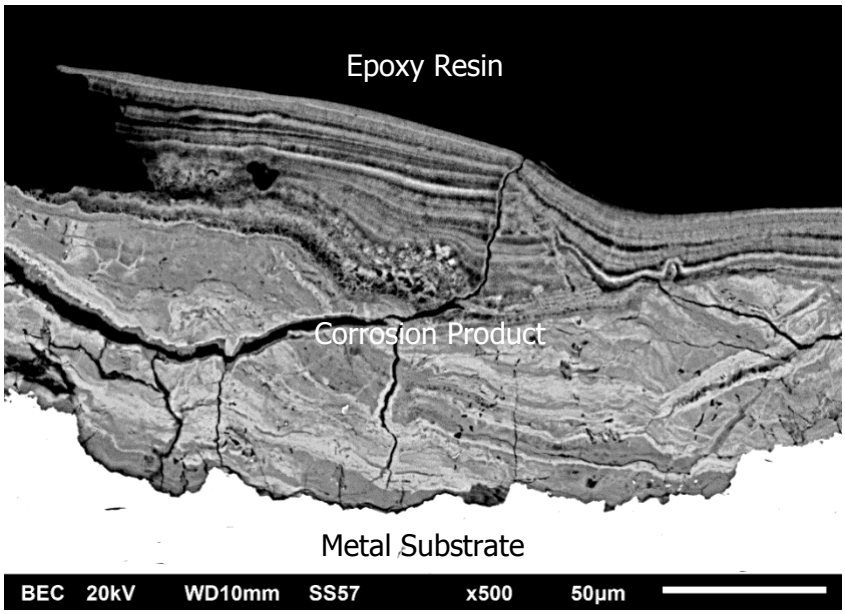

Figure 36. Cross-sectional morphology of mild steel sample after a 1-year exposure at the wastewater treatment plant site.

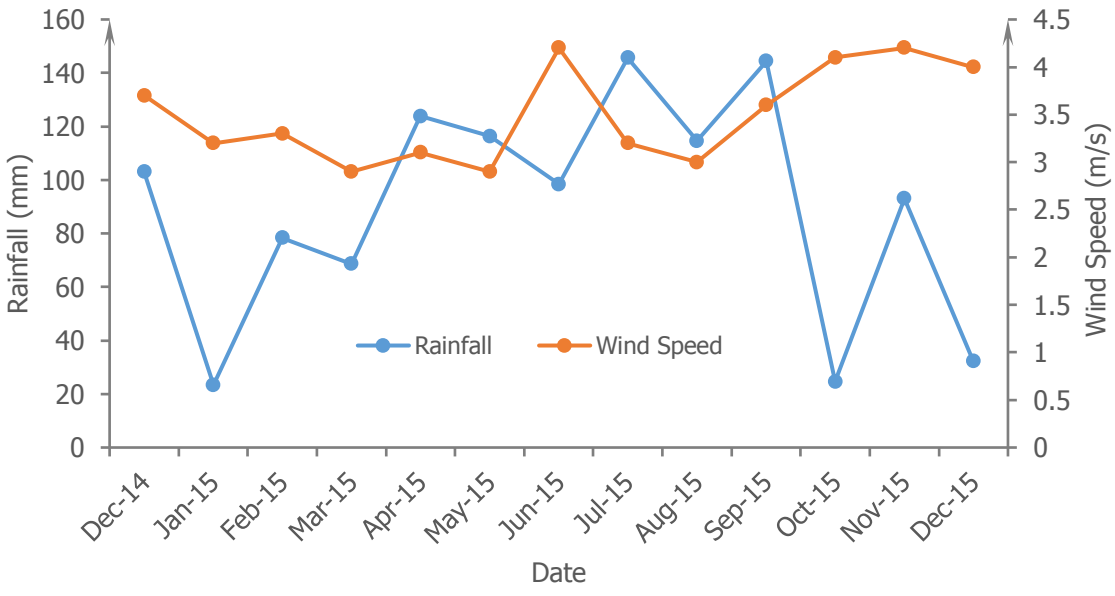

Figure 37. Rainfall and wind speed data from December 2014 to December 2015.

A part of this corrosion product layer tended to detach as a complete layer (~1 mm) from the mild steel surface. A sub-layer (~50–120 µm thick) could then be seen in the interfacial area and could provide some protection to the underlying metal substrate. However, it might not be able to slow down corrosion significantly in extended exposures since it still had a large number of cracks and pores that could provide fast channels for inward transfer of corrosive media (Figure 36).

Climatic monitoring showed that during the first 2–3 months of this exposure, rainfall was relatively low although it kept increasing. Meanwhile, average monthly wind speed was relatively low – ~3 m/s – and stable (Figure 37). These atmospheric conditions could favour a steady presence of H_2S in air with high concentrations (Olafsdottir et al., 2014), maintaining rigorous attack to metal within a relatively long period.

Zinc has reasonably good performance in environments without significant airborne pollution. Corrosion products formed are normally adherent and compact, protecting the underlying substrate with a barrier effect. They are rich with zinc carbonate ($ZnCO_3$) through reactions between zinc hydroxide ($Zn(OH)_2$), zinc oxide (ZnO) and carbon dioxide (CO_2) in air. In marine environments, zinc hydroxy chloride ($Zn_5(OH)_8Cl_2{\cdot}H_2O$) can form due to the involvement of airborne sea salt particles such as NaCl and $MgCl_2$ (Guttman, 1968; Friel, 1986; de la Fuente et al., 2007).

Some studies claim that zinc performs reasonably well when exposed to environments with H_2S since the main corrosion product, ZnS, was insoluble (Total Materia, 2002).

Hot-dip galvanised zinc coatings were not performing well in geothermal environments with high H_2S concentrations (10–30 ppm) (Gao et al., 1997). After 6.5 months, red iron-rich corrosion products were formed extensively on the entire surface with some flaking thick rust layers on some small sections. The zinc coating at these sections was completely consumed according to microscopic observation.

This study also found that zinc had high corrosion rates and a two-stage corrosion kinetic when exposed to strong geothermal environments (Figure 34b).

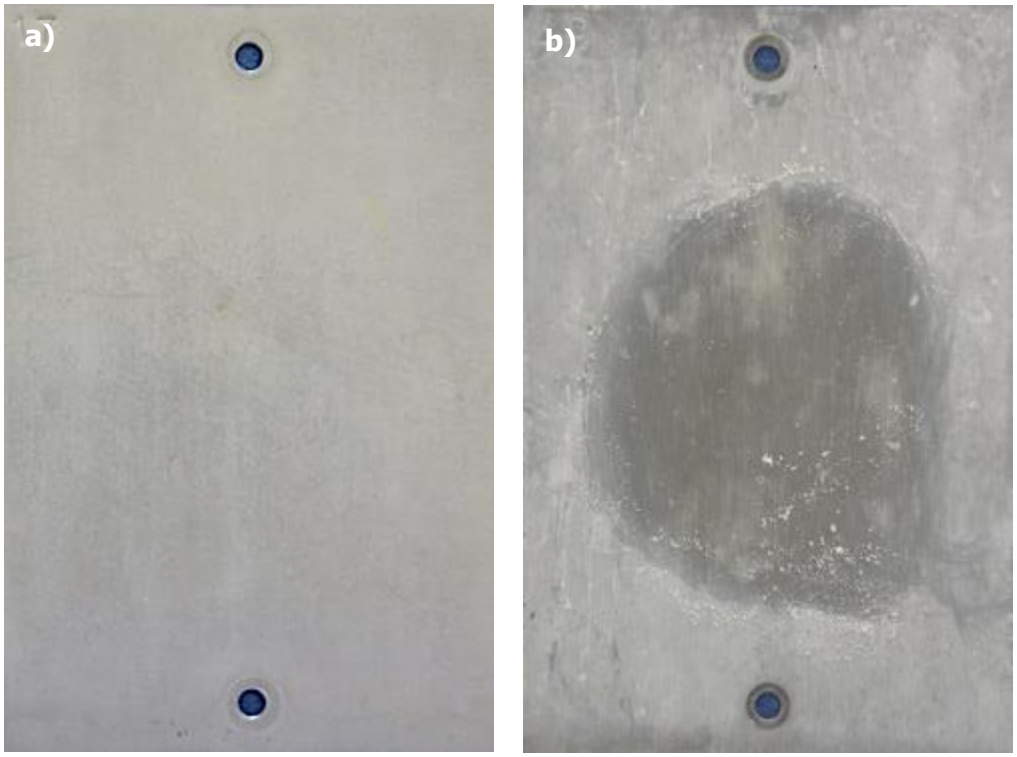

Figure 38. Surface morphology of zinc exposed at the wastewater treatment plant site for (a) 3 months and (b) 12 months.

As shown in Figure 38, the zinc sample surface was covered with a grey-white layer after 3 months of exposure. This layer, more easily observed on the groundward

surface, could be partially removed by wiping with paper or a finger, indicating that the corrosion products were not adherent or compact and could be washed away periodically by rainwater during exposure.

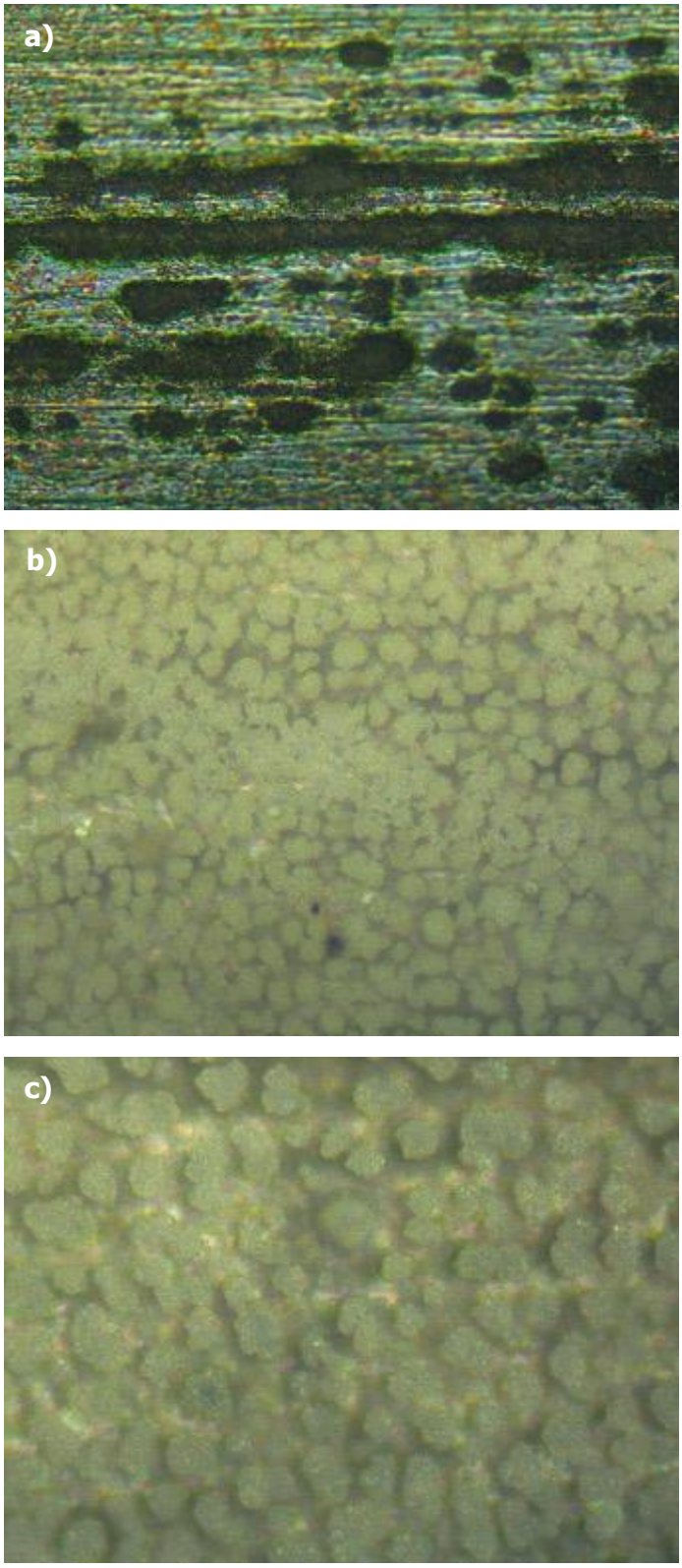

Figure 39. Optical surface morphology (400×) of zinc after (a) 3 months, (b) 6 months and (c) 9 months of exposure at the wastewater treatment plant site.

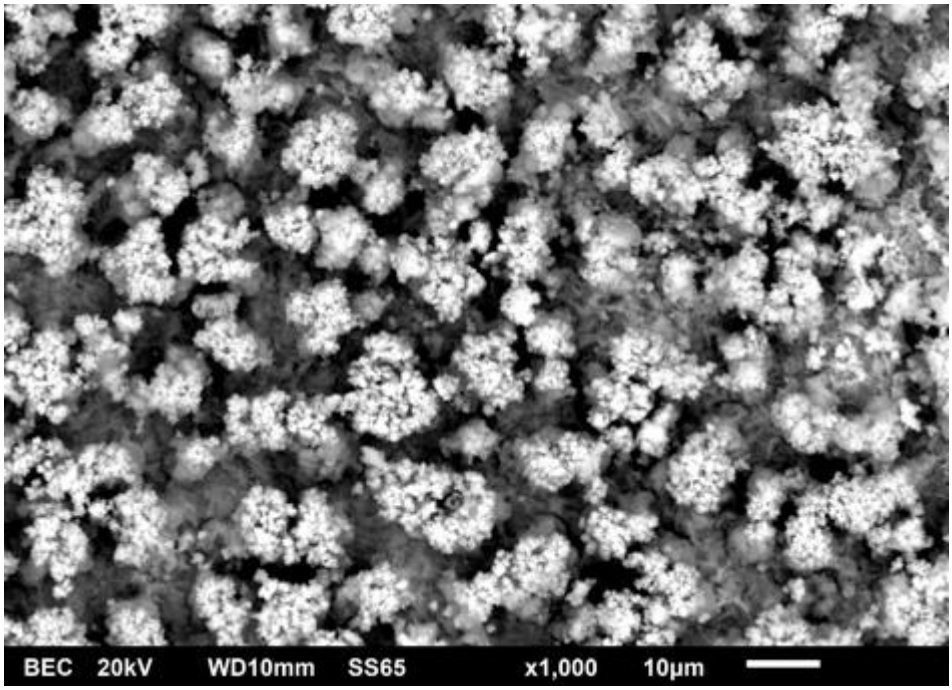

Figure 40. SEM surface morphology of zinc after a 1-year exposure at the wastewater treatment plant site.

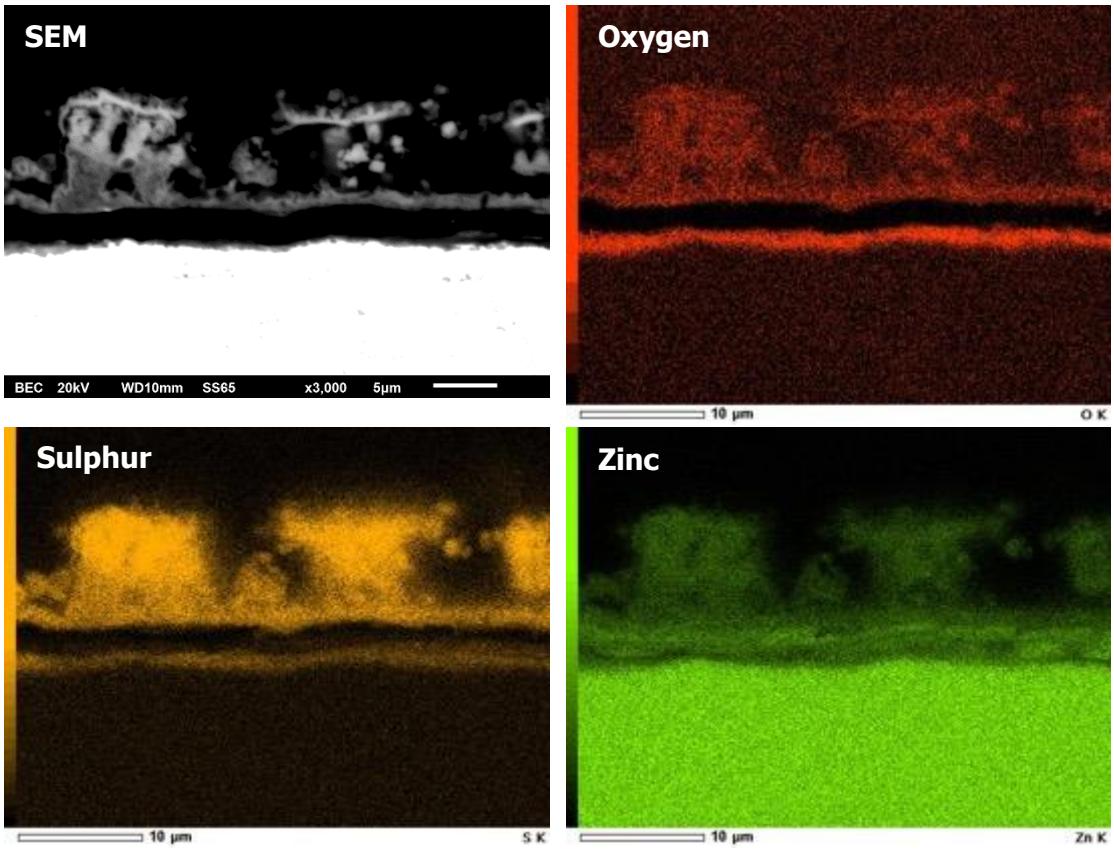

Figure 41. EDS elemental mapping performed on a polished cross-sectional zinc sample after a 1-year exposure at the wastewater treatment plant site.

Microscopic characterisation found that corrosion products seen as discrete particles were mainly formed along the fine grinding lines on the original zinc surface during the initial exposure stage (Figure 39a). The surface distribution density of these particles increased gradually with exposure time. A large number of smaller particles were also formed slowly under these larger discrete particles, leading to the formation of another corrosion product layer after about 6–9 months of exposure. This layer was more uniform than the top layer (Figure 40) and might be able to provide better protection to the underlying zinc substrate.

This surface morphological development could partially explain the corrosion kinetics shown in Figure 34b. However, the overall protection capability of this corrosion product layer was still limited, evidenced by a high first-year corrosion rate of ~70 g/m^2/year.

To better understand the protection capability of the corrosion products, energy dispersive X-ray spectroscopy (EDS) elemental mapping was performed on a polished cross-section of the zinc sample exposed at the wastewater treatment plant site for 1 year.

As shown in Figure 41, sulphur was rich in the discrete particles or clusters on the top part of the corrosion product layer. Oxygen was also detected within these particles, indicating a possible mixture of zinc sulphide, zinc oxide or zinc sulphate. Further, oxygen was rich in the interfacial area where sulphur was only detected with a low quantity, indicating the possible formation of a thin zinc oxide rich layer on the underlying zinc substrate. This continuous oxide-rich layer might be able to act as a barrier against the highly corrosive environment if it can be maintained and continue to grow in extended exposures.

These observations showed that zinc sulphide formed on zinc exposed to strong geothermal environments tended to develop into discrete particles and/or clusters, therefore a uniform, sulphide-rich layer could not develop. These particles and/or clusters also had weak connection to the underlying corrosion products and/or metal substrate and therefore could be removed, by rainwater, for example, providing limited protection to the interfacial oxide-rich thin layer or underlying zinc substrate.

4.5.2 2-year exposure

Due to the uncertainty of morphological development and corrosion process observed after a 1-year exposure, corrosion kinetics were studied in a 2-year exposure, from June 2015 to June 2017. The first-year corrosion rates of mild steel and zinc exposed at Judgeford and Oteranga Bay were also measured with field exposures started from June, i.e. wintertime with high rainfall for comparison purposes.

Mild steel corrosion rate continued to increase in the first year of exposure, particularly for the samples exposed at the wastewater treatment plant site (Figure 42a). This is somewhat different from the behaviour observed in the 1-year exposure started from December 2014. After 1 year, the corrosion rate had a small decrease, 17–24%. Therefore, the overall corrosion kinetics showed an accelerating and/or oscillating behaviour, leading to a degree of uncertainty over the estimation of corrosion behaviour in extended exposures.

By comparison, the mild steel corrosion rate decreased with time at Judgeford and the first-year corrosion rate was only ~26% of the first-month corrosion rate.

The corrosion behaviour of zinc in this 2-year exposure was different from that observed in the 1-year exposure started from December 2014 (Figure 42b). The time-dependent corrosion behaviours for the samples exposed to two strong geothermal environments were similar: decreasing – increasing – stabilising.

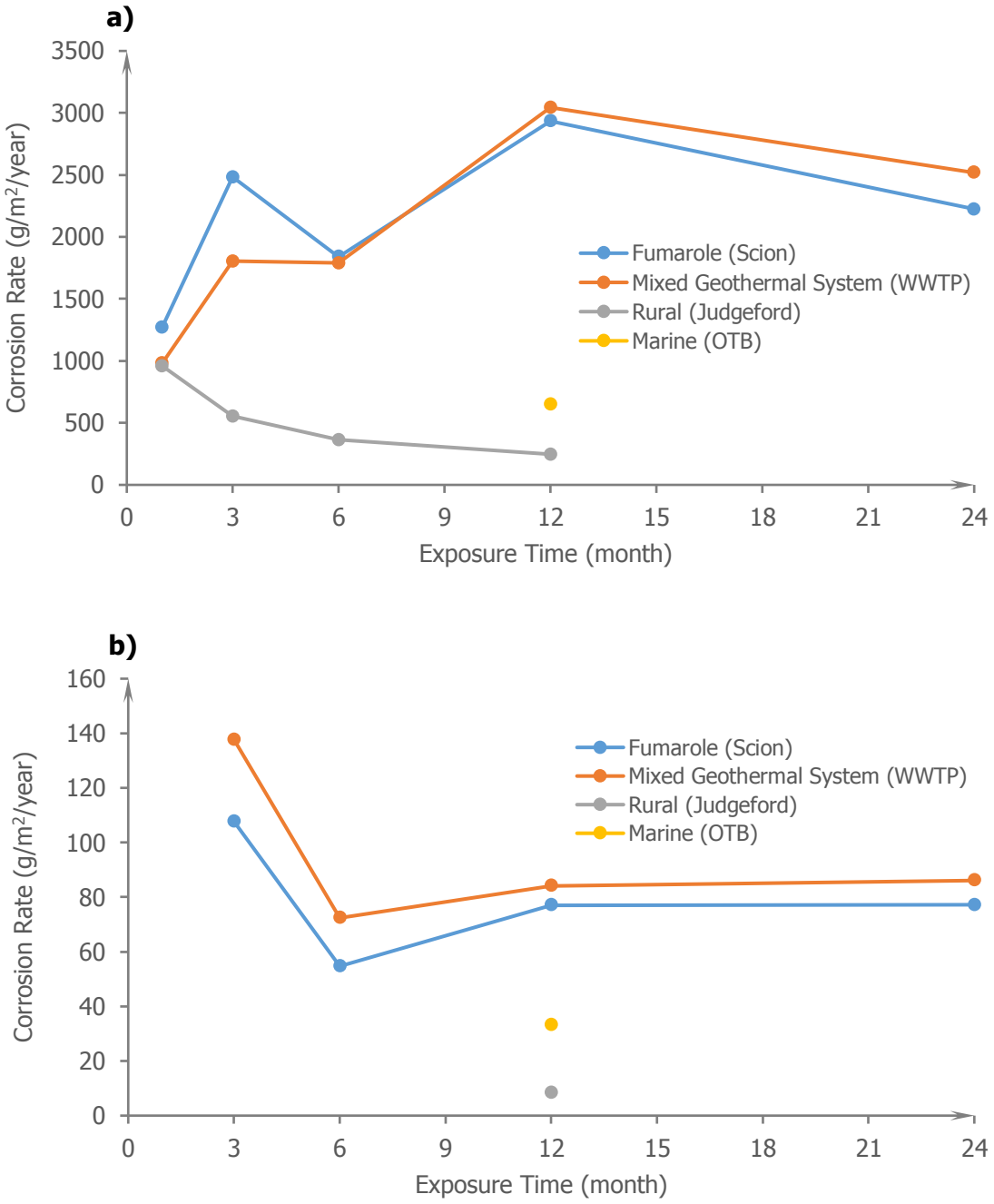

Figure 42. Corrosion behaviours of mild steel (a) and zinc (b) exposed to strong geothermal environments (June 2015 to June 2017).

Discrete particles and/or clusters were formed on the zinc sample surface after this 2-year exposure (Figure 43) and they were not highly protective as discussed before. Although the corrosion kinetics levelled off in the second year of exposure, its long-term behaviour was uncertain.

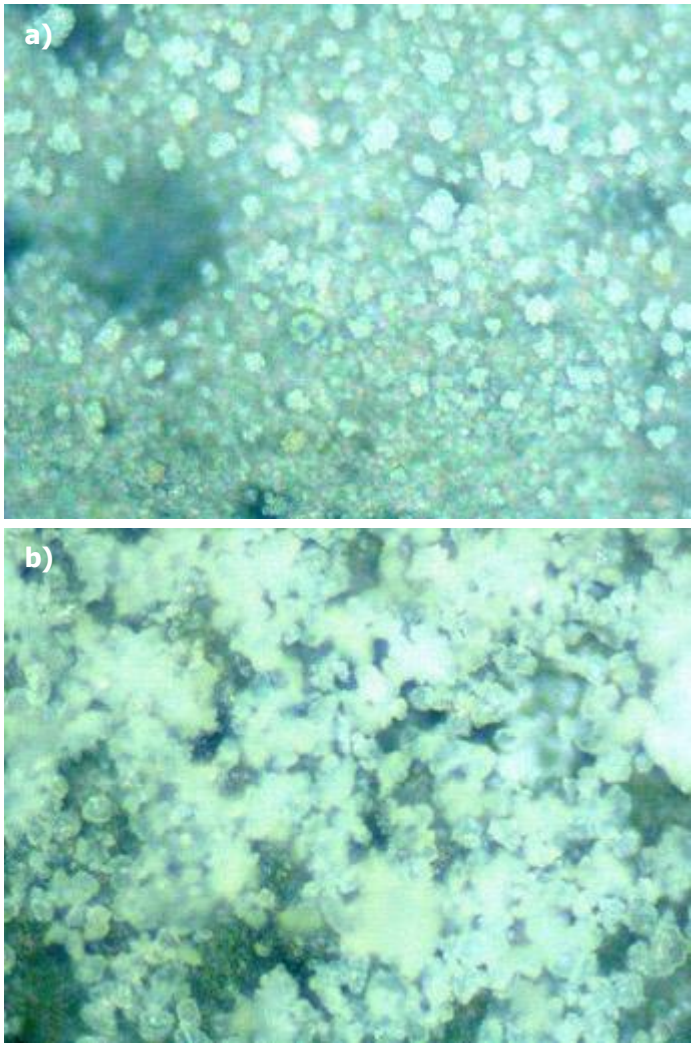

Figure 43. Morphology (400×) of zinc after a 2-year exposure at (a) a location ~5 m away from a fumarole in Scion campus and (b) the wastewater treatment plant site.

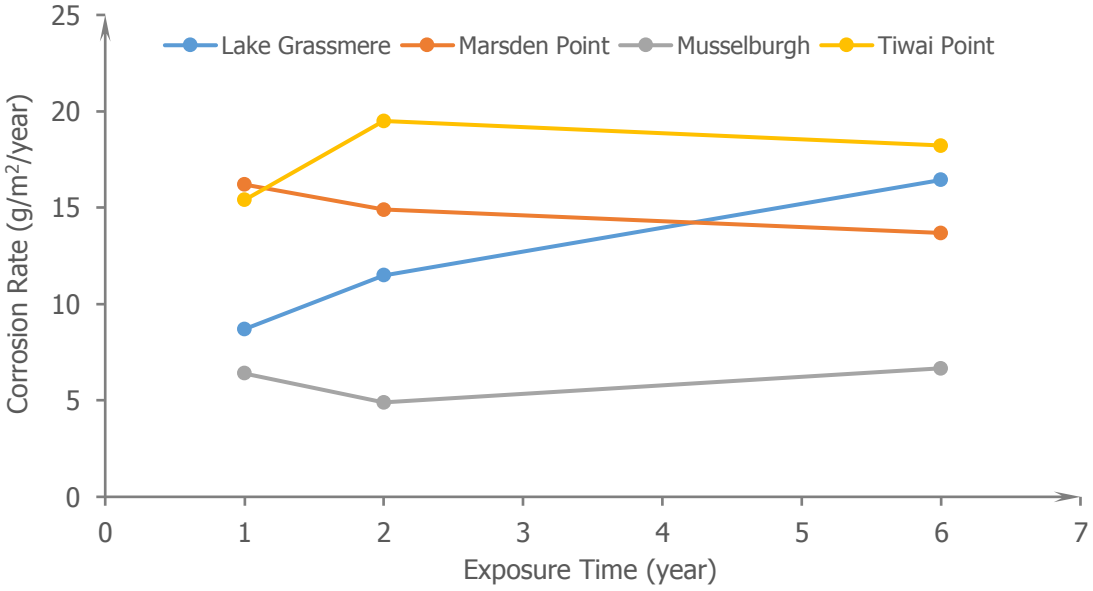

Figure 44. Corrosion of hot-dip galvanised zinc coating in different environments.

A variety of time-dependent corrosion behaviours had been observed with zinc samples exposed at different New Zealand natural environments (Figure 44) (Kane, 1997; Holcroft, 1998; Haberecht & Kane, 1999).

Zinc corrosion rates in these environments were much lower than those measured in strong geothermal environments. Great attention must be paid to monitor the corrosion behaviour of zinc in extended exposures to geothermal environments to better estimate its service life and to minimise premature failure.

4.6 Metal corrosion sensitivity to geothermal emission

The corrosion rate measurements discussed in above sections showed that different metals had quite different performance in geothermal environments. Copper was more prone to geothermal environmental attack than mild steel and zinc, evidenced by its high corrosion rates measured in the west and east areas of Rotorua city where (very) low H_2S concentrations were detected.

The corrosion rates measured at Judgeford were used as a reference to investigate the sensitivity of different metals to geothermal environmental attack. Airborne H_2S concentration at Judgeford was extremely low (0.03–0.06 ppb), consistent with the absence of geothermal features or agricultural biogas systems. This concentration was about 3–8 times lower than that measured at the two sites in the west area of Rotorua and ~6–18 times lower than that measured at the Lynmore site (east area).

Corrosion rate ratios were calculated with mild steel, zinc and copper (Table 3). In geothermal environments with low H_2S concentrations, there was no increase of mild steel and zinc corrosion rates. However, there was an increase of copper corrosion rate, and the ratios were quite similar to the H_2S concentration ratios.

Table 3. Metal corrosion sensitivity to geothermal H_2S emission.

Exposure site comparison	H_2S concentration ratio	Corrosion rate ratio		
	Dec 2014 – Jan 2015	Mild steel	Zn	Cu
216 Malfroy Rd (west) vs Judgeford	3	0.7	0.6	2.1
Lynmore (east) vs Judgeford	5.7	1.1	0.4	4.6

It is postulated that a threshold H_2S concentration might exist, above which significantly accelerated attack could be expected for mild steel and zinc. Based on current results, this concentration could be around 1.0 ppb. The threshold for copper might be much lower, possibly less than 0.1 ppb. It should be noted that this concentration was measured with a passive H_2S diffusion tube sensor within a 3-week exposure period.

5. Corrosion rate and H_2S concentration

Atmospheric corrosion of metals is governed by complicated interactions between climate, atmospheric pollutant (gas and solid) and material. In clean and benign environments, humidity and/or rainwater are the main factors contributing to corrosion as they create a favourable environment to initialise and maintain corrosion processes of a chemical or electrochemical nature.

In heavily contaminated atmospheres, such as marine and industrial, metal corrosion can be accelerated by the presence of chloride-containing particles or sulphur-containing species. These contaminants can interact with climatic factors to create more aggressive, micro-scale environments on the metal surface. These may include higher time-of-wetness (ToW), lower pH, formation of other more corrosive species through chemical or electrochemical reactions and negative changes in composition, microstructure and/or phase structure of corrosion products.

Sulphur-containing species, particularly H_2S, were present with high concentrations at some exposure sites in this study. As reported in section 3, airborne H_2S concentrations in the west and east areas of Rotorua were much lower than those in or close to the central city. The location dependence of corrosion rate and H_2S concentration are very similar – a high H_2S concentration always corresponds to a high metal corrosion rate, implying that H_2S may play an important role in corrosion of metals exposed to geothermal environments (Arzola & Genesca, 2005).

5.1 Mild steel

H_2S concentration was plotted against the first-year corrosion rate of mild steel exposed at the six sites in Rotorua, including 216, 116 and 22 Malfroy Road, the wastewater treatment plant, Ngapuna and Lynmore. Data collected from other exposure sites was not included in consideration of the influences of geothermal features on material deterioration behaviours and kinetics, as discussed in section 4.4.

The first trial was performed with H_2S concentrations collected from December 2014 to January 2015 and mild steel corrosion rates measured from December 2014 to December 2015. Two types of trend lines were produced with high coefficient of determination (R^2) values, linear and power.

Linear trend lines were produced with two slightly different data groups (Figure 45). One group included the five sites with low H_2S concentrations (i.e. the wastewater treatment plant site with a H_2S concentration of 27.7 ppb was excluded). This is because a turning point was identified when H_2S concentration increased sharply from 2.82 ppb to 27.7 ppb. An equation correlating H_2S concentration (x, in ppb) and mild steel corrosion rate (y, in g/m^2/year) was produced as

$$y = 217.18x + 86.249 \text{ (Eq.1)}$$

with an R^2 value of 0.9902. The other group used data from all six exposure sites and an equation was produced as

$$y = 113.15x + 187.37 \text{ (Eq.2)}$$

with an R^2 value of 0.9926.

The power fitting used all data points to produce an equation of

$$y = 339.03x^{0.6819} \text{ (Eq.3)}$$

with an R^2 value of 0.9951 (Figure 46).

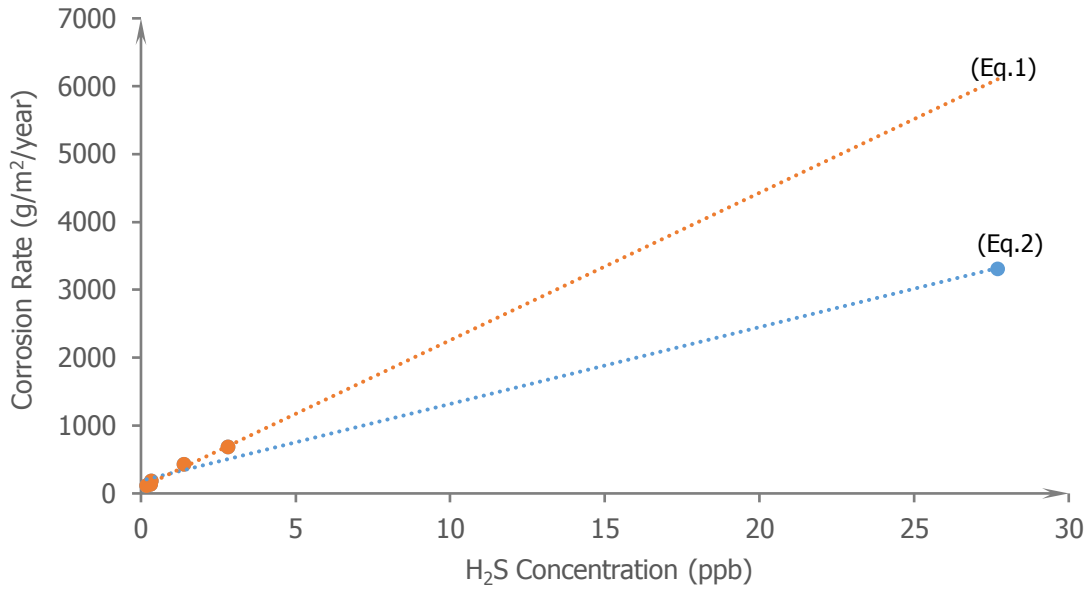

Figure 45. Linear fitting of H_2S concentration and first-year corrosion rate of mild steel.

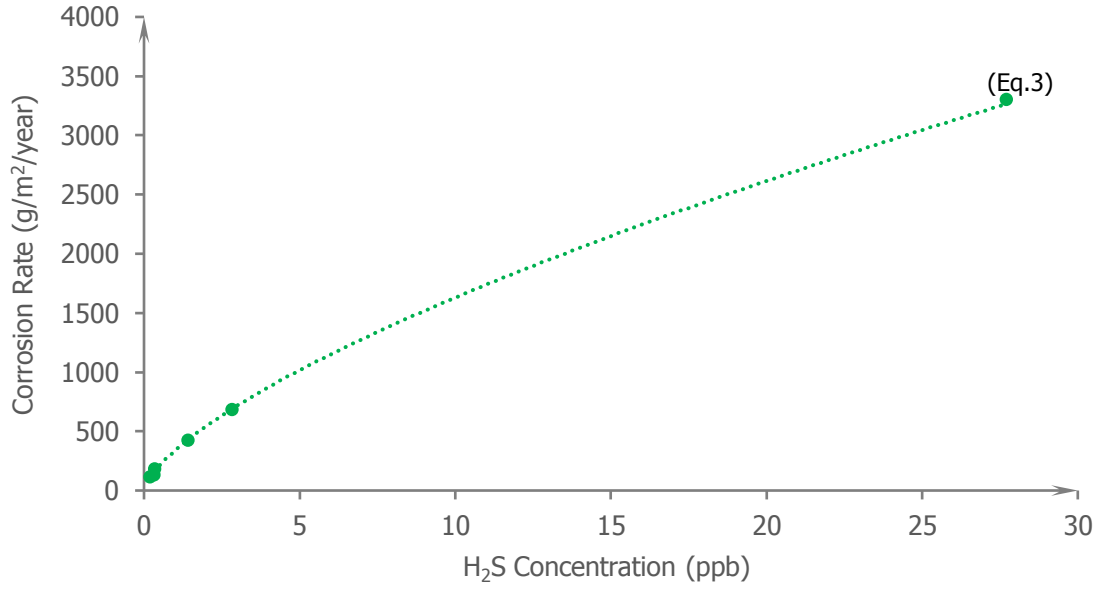

Figure 46. Power fitting of H_2S concentration and first-year corrosion rate of mild steel.

The second trial was performed with H_2S concentrations collected from June to July 2015 and mild steel corrosion rates measured from June 2015 to June 2016. The best fit was achieved by using an exponential trend line with all data points with an R^2 value of 0.963.

$$y = 143.42e^{0.5347x}$$ (Eq.4)

This trendline was quite different from those derived with the data collected from December 2014 to December 2015 (Figure 47).

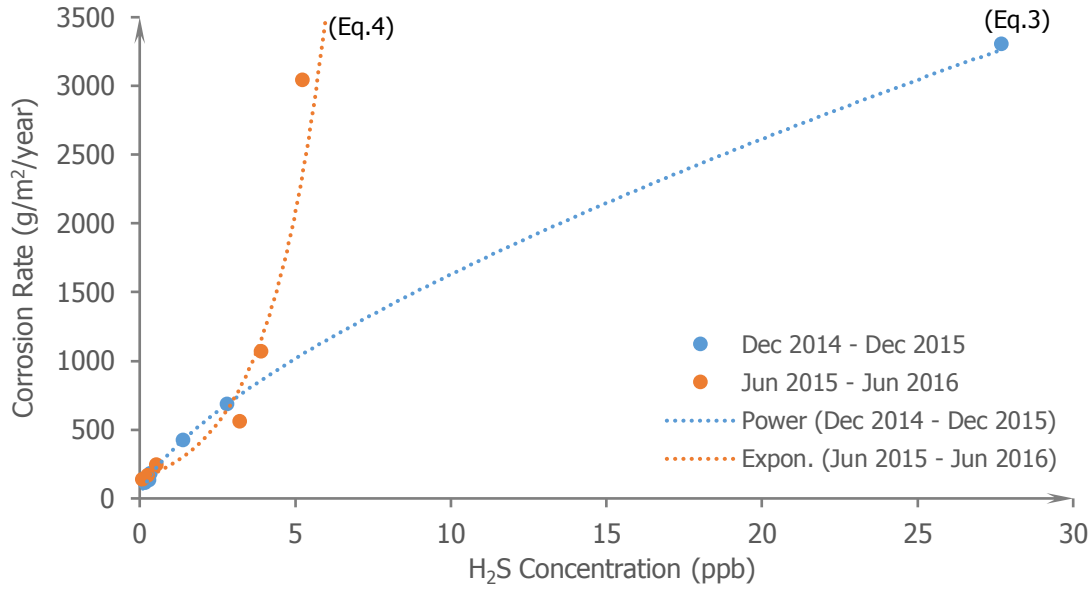

Figure 47. Comparison of trials using H_2S concentration and first-year mild steel corrosion rate collected from different exposure periods.

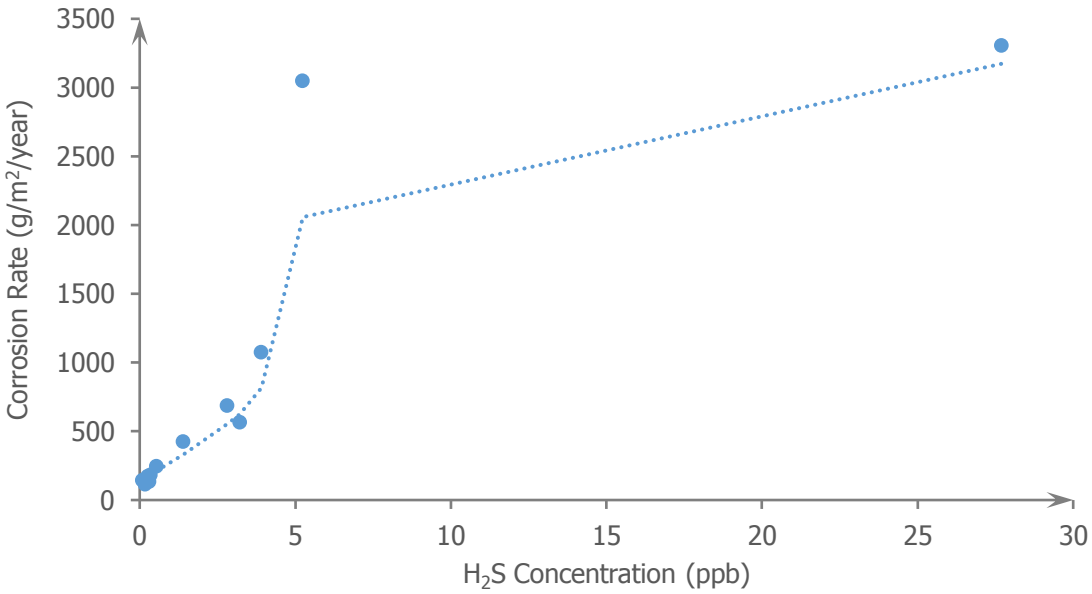

Figure 48. Fitting using H_2S concentration and first-year mild steel corrosion rate data collected from two exposure periods.

These fitting trials showed that H_2S concentration correlated with mild steel atmospheric corrosion rate. However, the following must be considered.

- In areas with low H_2S concentrations, the mass loss induced by direct H_2S attack might be small. As discussed before, there might be a lower limit of H_2S concentration below which mild steel corrosion will be accelerated. By contrast,

climatic factors (such as time-of-wetness and rainfall) may have large influences and contribution to atmospheric corrosion and mass loss in these areas.

- Figure 47 shows that the correlations between airborne H_2S concentration and first-year corrosion rate of mild steel are different for different exposure periods. This indicated that H_2S-induced attack might dominate metal corrosion in a certain concentration range. However, the potential influences of climatic factors on concentration, distribution and deposition of H_2S on a metal surface must be considered for correlation analysis.
- When the two datasets collected from two different exposure periods were combined for fitting, an upper H_2S concentration limit (~5 ppb) might exist, above which the mild steel corrosion rate would not increase further (Figure 48). However, the two high H2S concentrations were all measured at the wastewater treatment plant. The lower one, 5.2 ppb, measured during June–July 2015 was related to the prevailing wind from the southwest direction. Starting season plays a very important role in atmospheric corrosion and affects corrosion behaviour and kinetics significantly (Syed, 2006; Parekh et al., 2012). Therefore, this upper limit might not be true since those two datasets might not be comparable.
- H_2S concentration data used in these fitting trials was measured in the first 3 weeks of field exposure and metal corrosion rates were derived after 1 year of exposure. Airborne H_2S concentration in geothermal environments is highly variable at daily, monthly and/or yearly scales (Hinz, 2011; Iremonger, 2012). It is arguable that H_2S concentrations in the initial exposure stage might have limited impacts on metal corrosion in extended exposures.

5.2 Zinc

In Figure 49, the concentration of airborne H_2S measured during the period December 2014 to January 2015 was plotted against the first-year corrosion rate (December 2014 to December 2015) of zinc at six exposure sites crossing Rotorua city.

Two types of trendline were obtained with high R^2 values, linear and power.

Linear fitting:

$$y = 2.1327x + 7.259 \text{ (Eq.5)}$$

$$R^2 = 0.955$$

Power fitting:

$$y = 9.6446x^{0.6007} \text{ (Eq.6)}$$

$$R^2 = 0.906$$

Very similar to the results derived with mild steel (Figure 47), the correlation between H_2S concentration and first-year corrosion rate of zinc measured during June 2015 to June 2016 was different from the above. An exponential relationship appeared to be the best though the fitting for data points of high H_2S concentrations showed a relatively large deviation (Figure 50).

$$y = 5.0358e^{0.4865x} \text{ (Eq.7)}$$

$$R^2 = 0.9669$$

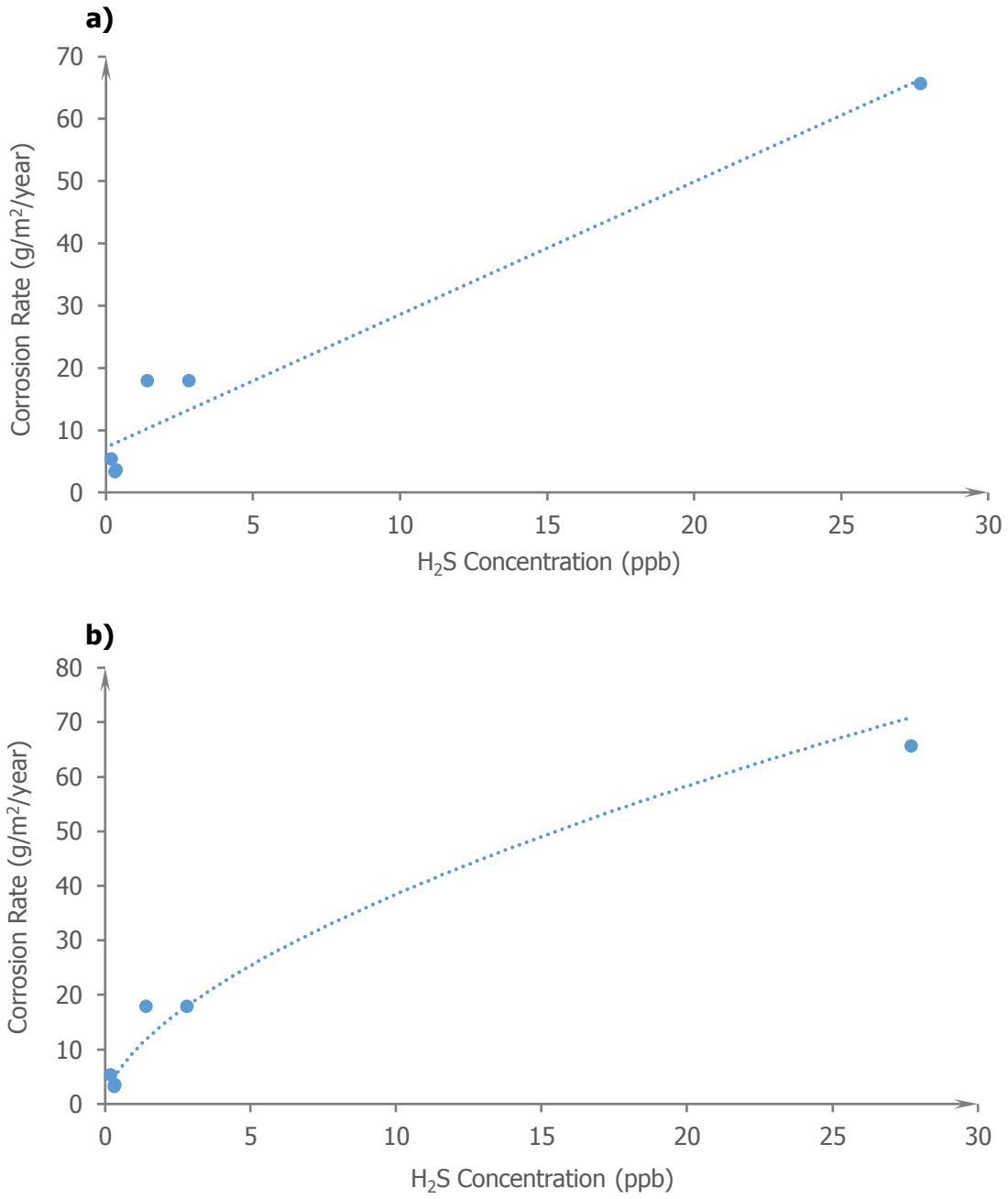

Figure 49. Correlations between H_2S concentration and first-year corrosion rate of zinc (December 2014 to December 2015) – (a) linear fitting and (b) power fitting.

As discussed in section 4.6, atmospheric corrosion zinc is unlikely to be accelerated significantly in geothermal environments with low concentrations of sulphur-containing species. For example, its corrosion rates measured in the west and east areas of Rotorua were even lower than that measured at Judgeford where H_2S was extremely low. High corrosion rates were commonly obtained at sites with high H_2S concentrations, such as the wastewater treatment plant, Ngapuna and 22 Malfroy Road. Therefore, a lower concentration limit may exist, below which airborne H_2S will not exert significant influences on atmospheric corrosion of zinc.

A two-stage fitting was then trialled with the data used in Figure 50. A linear trendline with an R^2 value of 0.9789 was obtained with H_2S concentration less than 4 ppb and another linear trendline was obtained with H_2S concentration larger than 3 ppb (Figure 51). This gave a better way to interpret data.

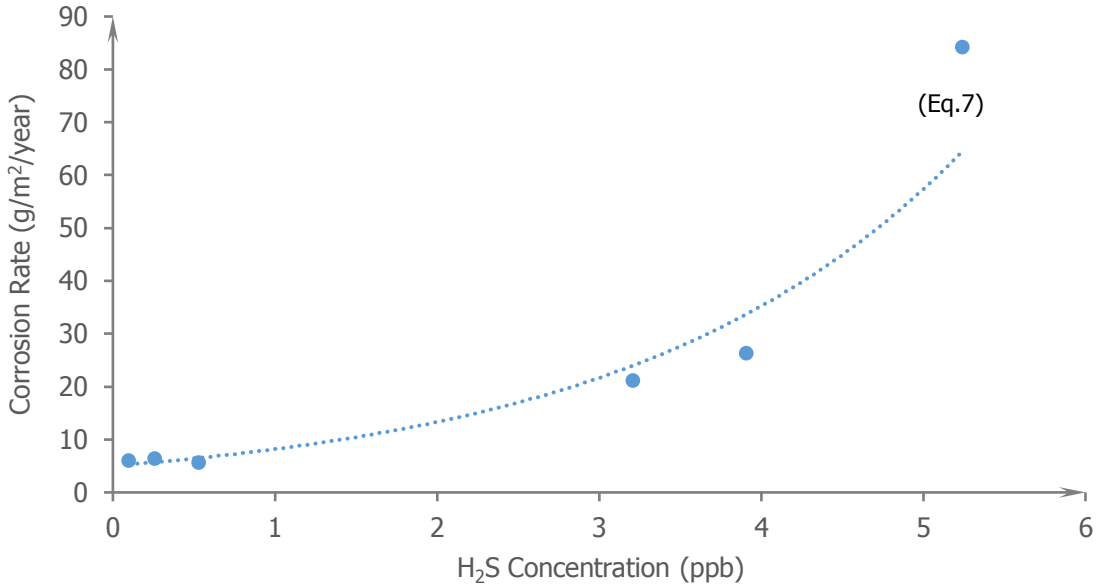

Figure 50. Correlation between H_2S concentration and first-year corrosion rate of zinc (June 2015 to June 2016).

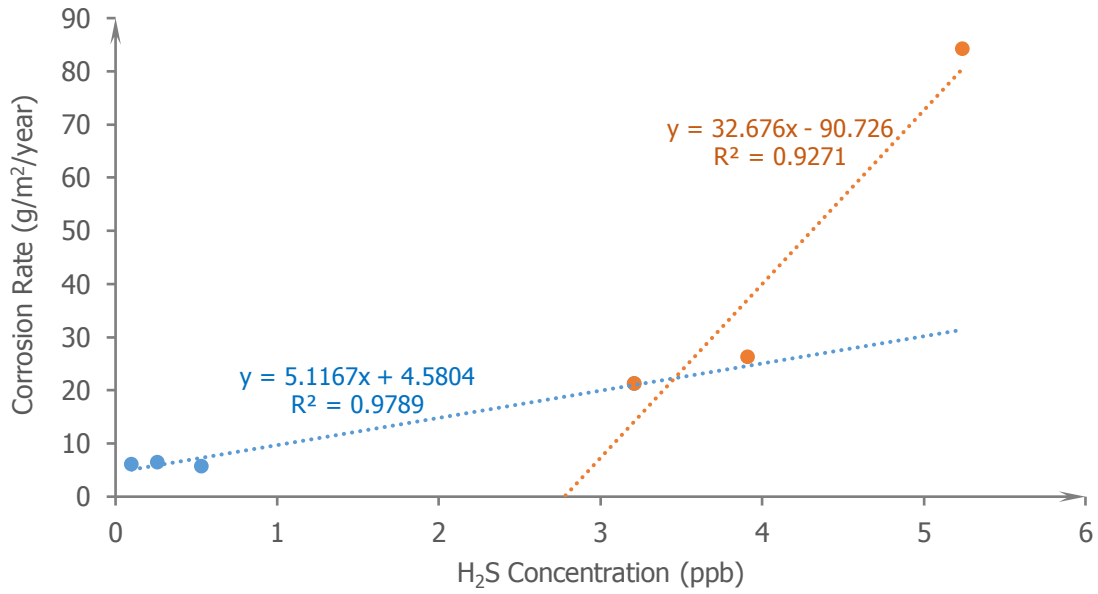

Figure 51. Two-stage fitting of H_2S concentration and first-year zinc corrosion rate data (June 2015 to June 2016).

Another fitting was trialled with those data points where H_2S concentration is higher than 1 ppb (Figure 52). This included two strong geothermal environments, i.e. a fumarole and a geothermal spring within Scion campus.

An equation could be produced as:

$$y = 10.213x^{0.586} \text{ (Eq.8)}$$

with an R^2 value of 0.7641.

A large scatter was observed with data points of high H_2S concentrations (>5 ppb) and high zinc corrosion rates. These data points correspond to three geothermal features – fumarole, spring and Sulphur Bay (wastewater treatment plant).

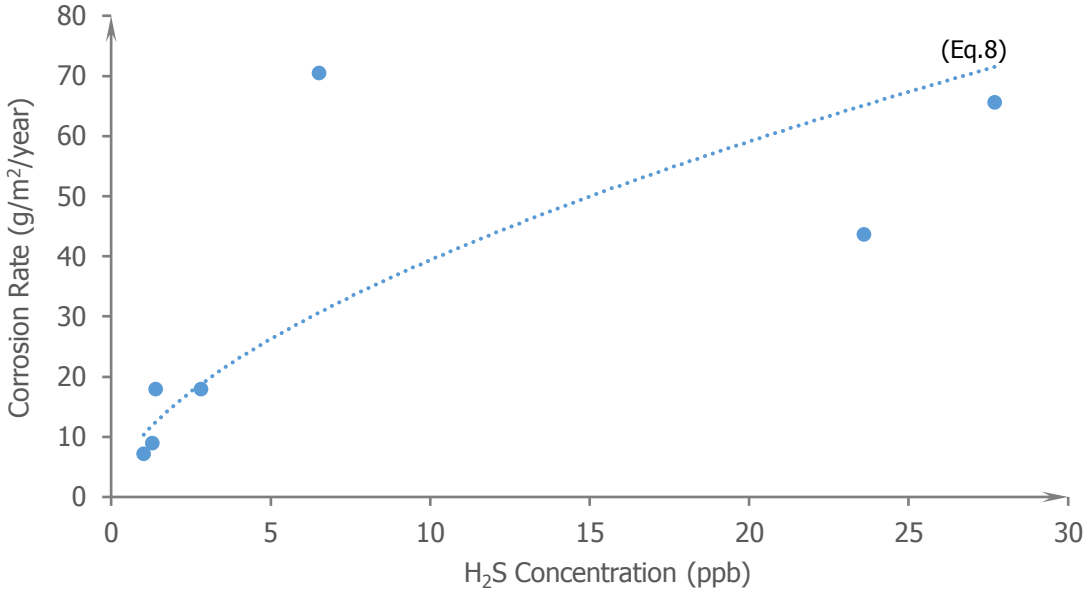

Figure 52. Power fitting of H_2S concentration and first-year zinc corrosion rate (only sites with H_2S concentrations higher than 1 ppb included).

This provides further evidence that geothermal features have some influences on metal corrosion, as discussed in Section 4.4.

5.3 Copper

As discussed in previous sections, copper has a low atmospheric corrosion resistance when exposed to geothermal environments. It also has a high sensitivity to the presence of (very) low concentrations of H_2S in the atmosphere. This sensitivity would be quite useful to explore correlations between airborne H_2S concentration and copper corrosion rate.

In Figure 53, the H_2S concentration measured during the period December 2014 to January 2015 was plotted against the first-year corrosion rate of copper (December 2014 to December 2015). Data collected from exposure sites within Scion campus were excluded to minimise potential influences of geothermal features on metal corrosion kinetics.

Two types of trendline – logarithmic and power – were produced with reasonably high R^2 values.

Logarithmic fitting:

$$y = 90.095 \ln(x) + 149.62 \text{ (Eq.9)}$$

$R^2 = 0.9268$

Power fitting:

$$y = 92.96x^{0.5533} \text{ (Eq.10)}$$

$$R^2 = 0.9216$$

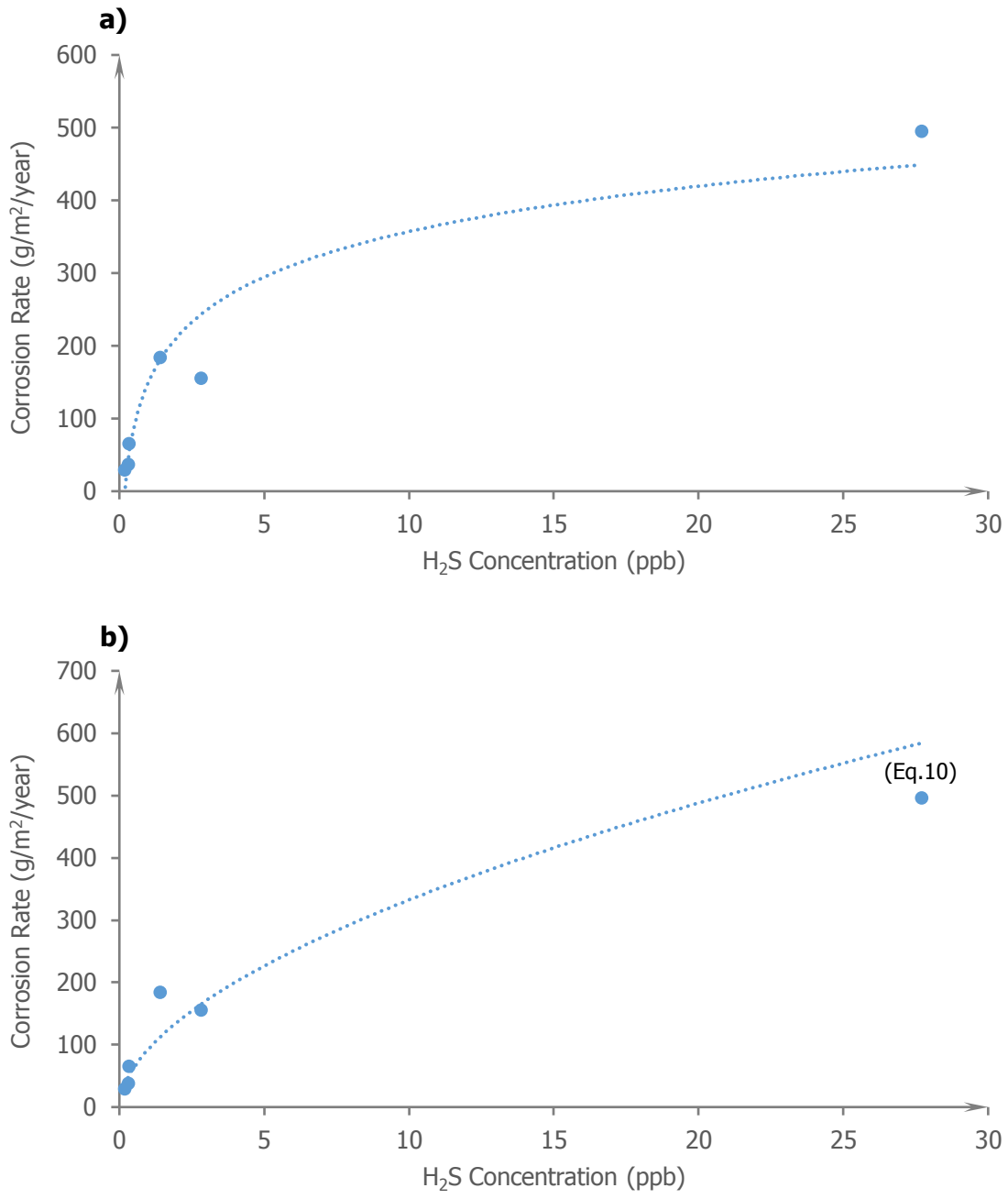

Figure 53. Logarithmic (a) and power (b) fitting of H_2S concentration and first-year corrosion rate of copper (December 2014 to December 2015).

At the 22 Malfroy Road exposure site, although the H_2S concentration was higher than that of Ngapuna, a lower copper corrosion rate was obtained – 154.7 g/m^2/year versus 183.2 g/m^2/year. This gave an unusual data point on the fitting curve.

Copper corrosion in areas with high concentrations of H_2S showed heavy and frequent breaking, cracking and spalling of corrosion products from its surface. However, the

sample exposed at the 22 Malfroy Road site did not show severe physical damage to the growing corrosion product layer, indicating that other unknown factors were contributing and should be explored for corrosion rate data fitting.

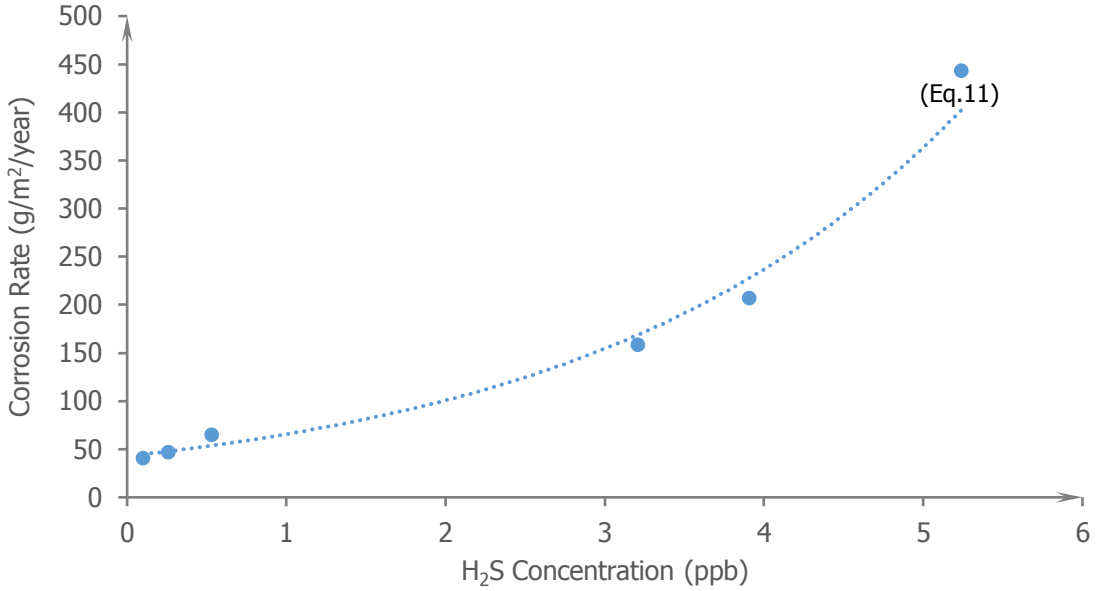

Figure 54. Exponential fitting of H_2S concentration and first-year corrosion rate of copper (June 2015 to June 2016).

The correlation between H_2S concentration and first-year corrosion rate of copper for the period starting from June 2015 was different from those shown in Figure 53 and an exponential fitting might be best for this dataset (Figure 54).

Exponential fitting:

$$y = 42.812e^{0.4277x} \text{ (Eq.11)}$$

$$R^2 = 0.9853$$

These fitting results with mild steel, zinc and copper then showed that short-term airborne H_2S concentration could be correlated with first-year metal corrosion rate. However, the influences of starting season and geothermal feature must be considered before any appropriate correlation can be established and verified.

5.4 Copper surface colour change

Another correlation was found between surface colour of copper and airborne H_2S concentration, in addition to the above discussed correlation between copper corrosion rate and H_2S concentration. The colour of the corrosion products remaining on copper surface changed with the increase of airborne H_2S concentration and corrosion rate, from pink to brown to a mixture of brown and blue and to dark blue (Figure 55).

This surface colour change could be related to changes in phase structure of corrosion products remaining on the surface and surface morphological features.

In areas without airborne H_2S concentrations – for example, Judgeford – Cu_2O was detected as the main corrosion product. In areas with low H_2S concentrations – for example, 216 Malfroy Road – a limited amount of copper sulphide (possibly Cu_2S or

CuS) was formed and mixed with the main corrosion product, Cu_2O. In areas with high H_2S concentrations, the corrosion products were identified as a mixture of copper oxides, sulphides and/or sulphates.

These copper-based corrosion products have different colours. Cu_2O can appear yellow, red or brown depending on preparation method and particle size. Cu_2S is dark-gray to black with a metallic. CuS occurs in nature as the dark indigo blue mineral covellite and its fine powder is black. Hydrated copper sulphate, $CuSO_4 \cdot 5H_2O$ is blue. With a change in the phase composition of these mixed corrosion products, a colour change could be expected.

The morphology of corrosion products, including particle/cluster size, distribution density and surface roughness, can change visual textures and consequently colour appearance and colour (Kinoshita & Yoshioka, 2005). With an increase of airborne H_2S concentration and then corrosion rate, copper surface became rougher with the formation of larger particles and/or clusters and higher porosity (Figure 56). This could result in structural colour change.

Overall, copper, with its high sensitivity to sulphur-containing species, could be developed as a corrosion risk indicator for geothermal environments.

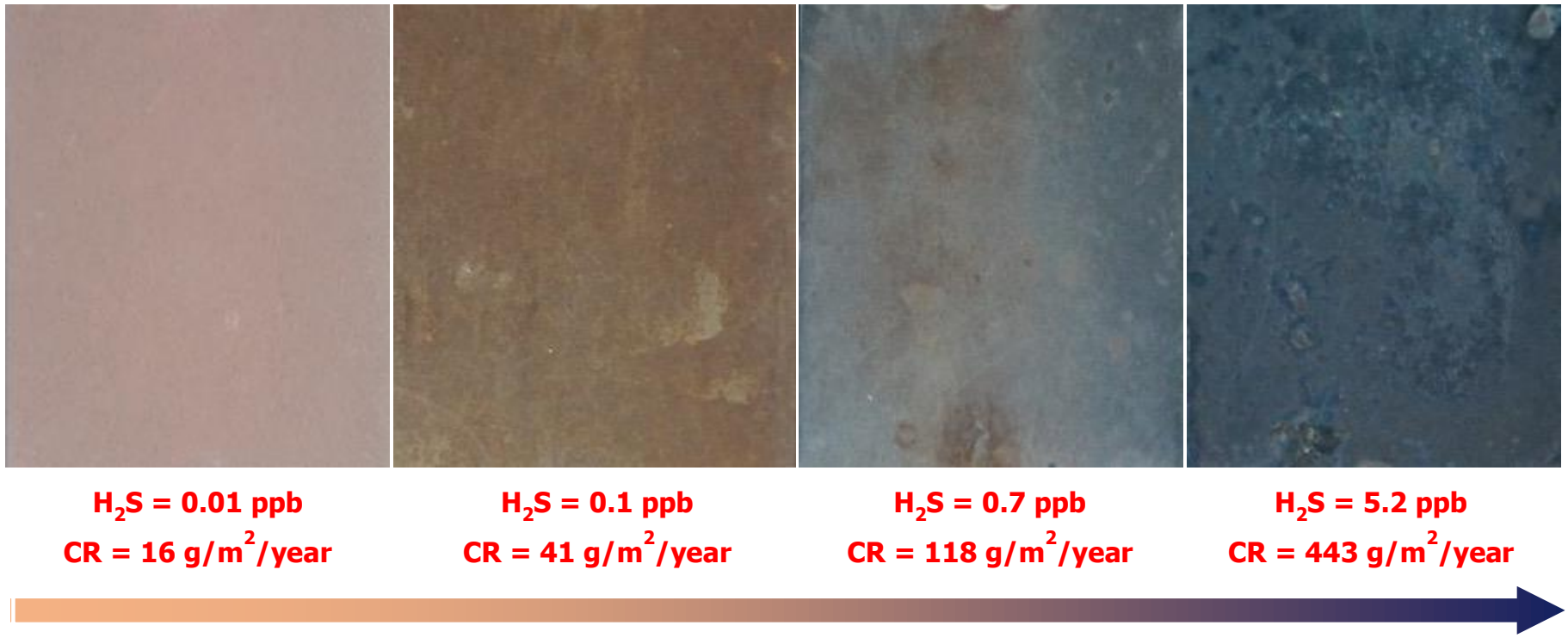

Figure 55. Surface colour variation of copper samples exposed in areas with different airborne H_2S concentrations (exposure period: June 2015 to June 2016; H_2S concentration monitoring: June–July 2015).

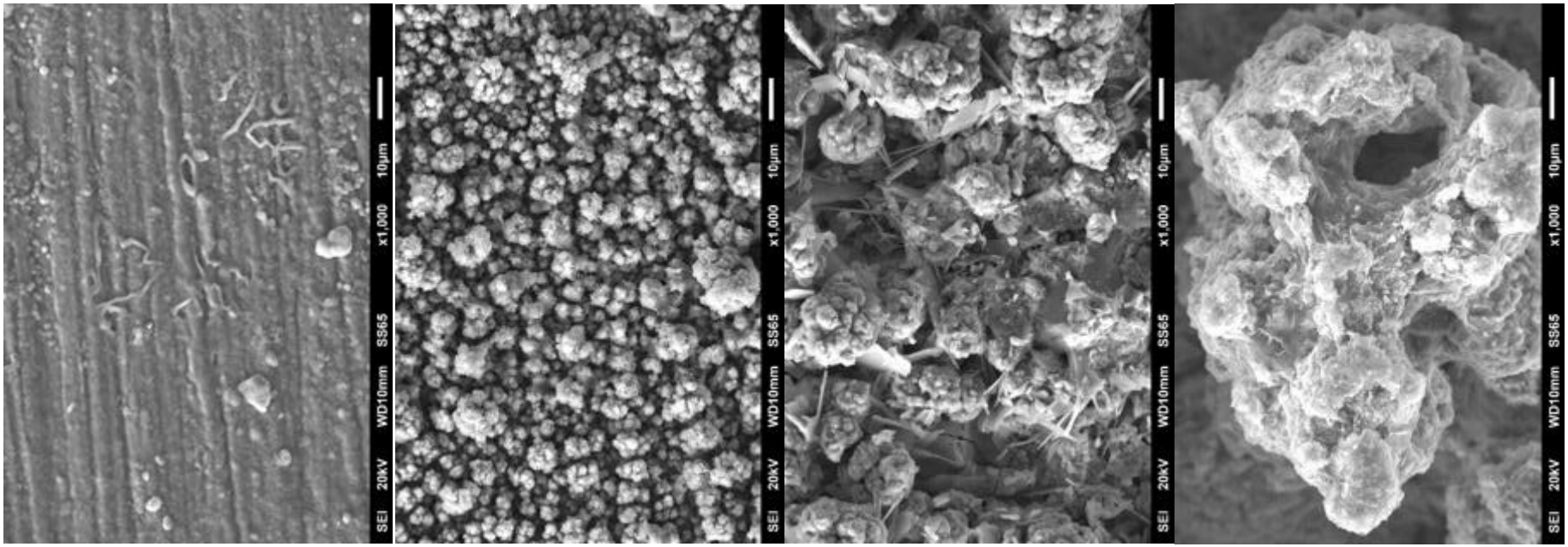

H_2S = 0.01 ppb
CR = 16 g/m^2/year

H_2S = 0.1 ppb
CR = 41 g/m^2/year

H_2S = 0.7 ppb
CR = 118 g/m^2/year

H_2S = 5.2 ppb
CR = 443 g/m^2/year

Figure 56. Surface morphology variation of copper samples exposed in areas with different airborne H_2S concentrations (exposure period: June 2015 to June 2016; H_2S concentration monitoring: June–July 2015).

6. Performance of other materials

The performance of pure aluminium (Al), AISI 304 austenitic stainless steel (SS) and 55%Al-Zn alloy coating was evaluated with a 2-year field exposure in areas with three geothermal features – fumarole, spring and Sulphur Bay (a large, mixed geothermal system; wastewater treatment plant). For comparison, coupons of these materials were also exposed at Oteranga Bay, a severe marine environment on the west coast of Wellington.

6.1 Aluminium and stainless steel

6.1.1 Corrosion rate

Table 4 presents atmopsheric corrosion rates of aluminium and AISI 304 stainless steel derived from this 2-year exposure. The corrosion rate of 55%Al-Zn alloy coating was not measured since it is practically difficult to completely remove corrosion products without damaging the alloy coating.

Table 4. Corrosion rates of aluminium and stainless steel.

Geothermal environment	Atmopsheric corrosion rate (g/m^2/year)	
	Aluminium	AISI 304 stainless steel
Sulphur Bay (mixed geothemal system, WWTP)	0.22	0.03
Fumarole (Scion)	0.18	0.03
Spring (Scion)	0.13	0.03
Severe marine (Oteranga Bay)	1.0	0.90

Atmospheric corrosion of aluminium and stainless steel was very limited, even in areas with very strong geothermal influences. However, these two materials had higher mass losses when exposed to the severe marine environment, indicating that chloride-containing sea salt particles were more corrosive.

6.1.2 Morphology

Visual surface characterisation showed that deterioration of aluminium and stainless steel was limited in strong geothermal environments, evidenced by the absence of any thick corrosion product layers or localised attack (Figure 57). Only some small, black spots were observed on their surfaces and they could be cleaned chemically. No severe attack to the metal substrate was revealed underneath these black spots by optical and electron microscopy characterisation.

Consistent with corrosion rate measurements, morphological characterisation found that these two materials suffered slightly more deterioration when exposed to the severe marine environment. Deterioration of aluminium was shown as a synergistic result of corrosive attack induced by airborne chloride-containing salt particles and/or mechanical impingement (erosion) of sand particles carried by strong winds (Figure 58a). Severe corrosion, either uniform or localised, was not revealed on the skyward surface of AISI 304 stainless steel coupons. The major deterioration mode found on this surface was light tea staining together with signs of mechanical impingement.

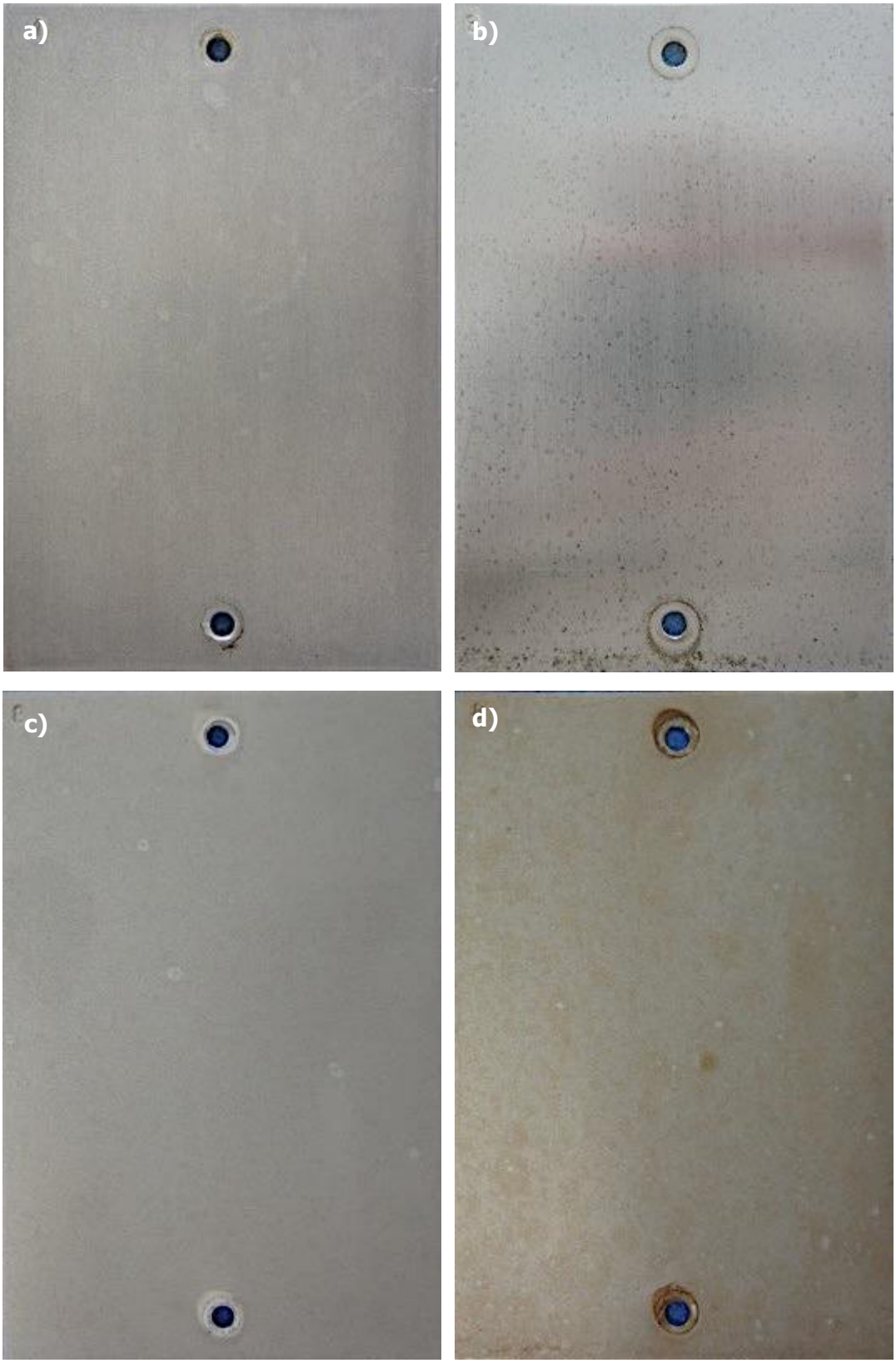

Figure 57. Surface morphology of aluminium and AISI 304 stainless steel after a 2-year exposure – (a) aluminium at the wastewater treatment plant site (south of Sulphur Bay, a large, mixed geothermal system), (b) stainless steel at a geothermal spring (Scion campus), (c) aluminium and (d) stainless steel at Oteranga Bay (severe marine).

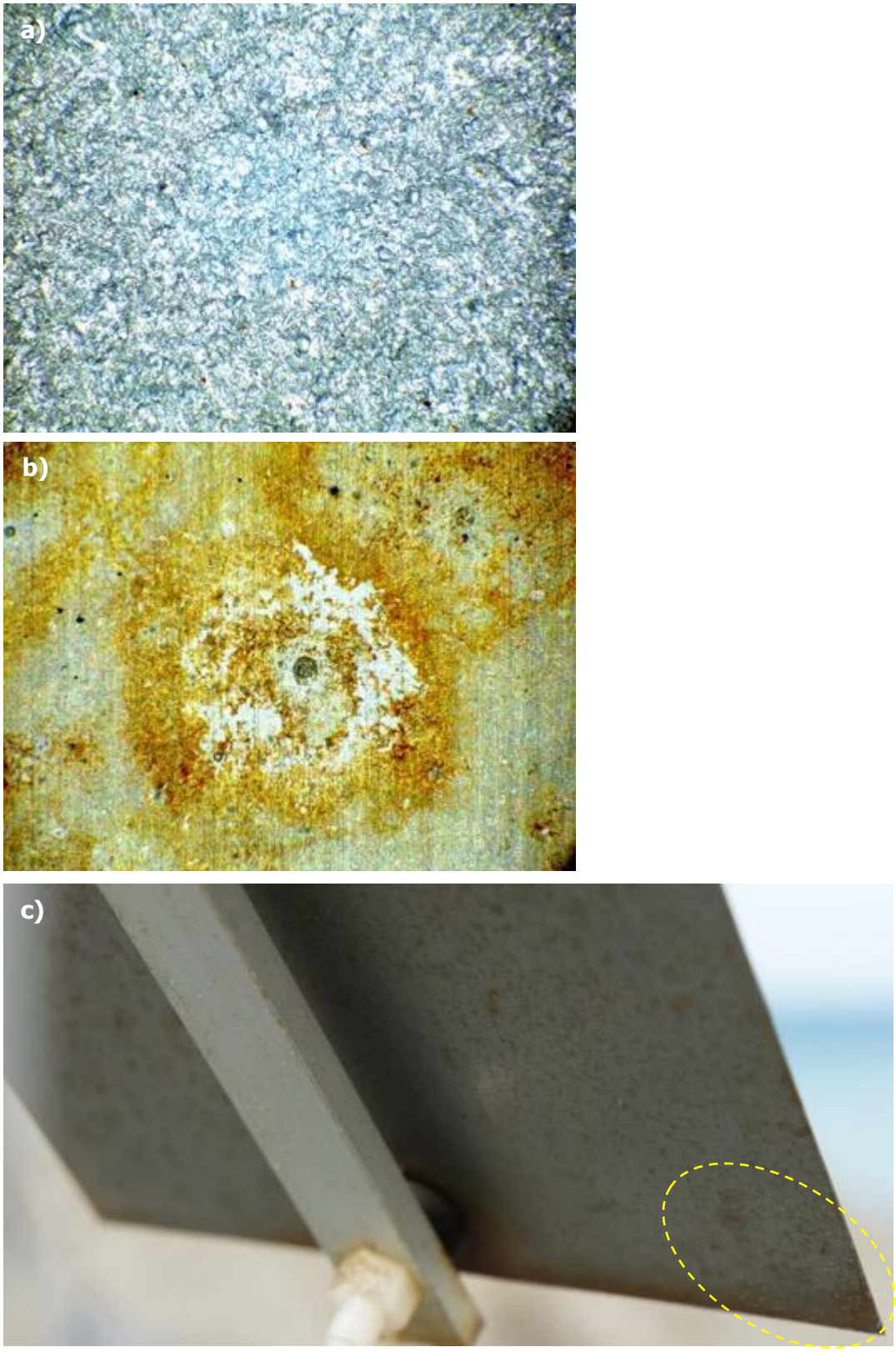

Figure 58. Surface morphology (32×) of aluminium and AISI 304 stainless steel after a 2-year exposure at Oteranga Bay (severe marine) – (a) aluminium surface with mechanical impingement feature, (b) pitting on the groundward surface of stainless steel and (c) salt deposition on the groundward surface of stainless steel.

Relatively severe corrosion and rusting were observed on aluminium and stainless steel in areas under or close to nylon fasteners where crevices could be formed and sea salt particles could be kept for long periods. Pitting corrosion was also observed on the groundward surface of AISI 304 stainless steel where deposition and accumulation of sea salt particles was observed (Figure 58b & c).

Though chemically active, aluminium and its alloys are naturally passive in many environments since it can react rapidly with oxygen or water in the atmosphere to form a thin and stable oxide film on its surface. This passive film, growing slowly with environmental humidity, can slow down the reactions between a corrosive environment and the underlying substrate, particularly in slightly acidic or almost neutral media.

However, this film can dissolve under acidic (low pH) or caustic (high pH) conditions (Burleigh, 2003; de la Fuente et al., 2007). External factors, such as salts and corrosive gases in the atmosphere, may contribute to the loss of this passivation, initialising localised corrosion such as pits (Lashermes et al., 1982; Blucher et al., 2006). In general, pitting would occur preferentially in regions of this passive oxide film where there are defects, such as lower thickness, partial damage, vacancies, dislocations, impurities or second phase particles.

When exposed to the atmosphere, stainless steel can develop a complex, thin chromium-rich passive film on its surface (Jin & Atrens, 1990). The formation and growth of this film is dependent on the composition and surface finish of the stainless steel and also the environmental factors such as presence of chlorides or sulphates, pH and temperature (Strehblow, 1984; Olefjord & Wegrelius, 1990; Mitrovic-Scepanovic et al., 1987; Schmutz & Landolt, 1999). Some studies indicate that the presence of sulphur-containing species, such as H_2S, HS^- and S^{2-} in chloride solutions can transform the passive films on stainless steels into less protective sulphide films such as $Fe(Cr)S_x$, therefore promoting pitting corrosion by chloride ions (Ding et al., 2013). Degradation of this passivation will significantly influence the corrosion performance of stainless steels (Lee et al., 2015).

It is postulated that a limited number of environmental factors can contribute to the partial damage of passive films naturally grown on aluminium and AISI 304 stainless steel and to initialise localised corrosion in geothermal environments. Thus, these two materials can be sufficiently resistant to atmospheric geothermal attack, at least within short-term exposures.

6.2 Al-Zn alloy coating

Heavy rusting was not observed on 55%Al-Zn alloy coating samples in geothermal environments after this 2-year exposure. Instead, a number of small, randomly distributed rust spots were formed (Figure 59a). This indicated that deterioration of this coating was localised, partially exposing steel substrate to the highly aggressive environment. Heavy rusting was observed close to the cutting edges, indicating that the unprotected steel cannot be effectively protected by the cathodic protection effect commonly lent by zinc coating in natural environments (Figure 59b).

Spot rusting was observed only occasionally on the samples exposed to the severe marine environment together with some grey/white patches (Figure 59c). Rusting was limited to small areas close to the bottom cutting edge. Relatively severe damage to the coating was observed in small areas on the skyward surface and identified to be related to mechanical impacts from sand and/or salt particles carried by strong winds.

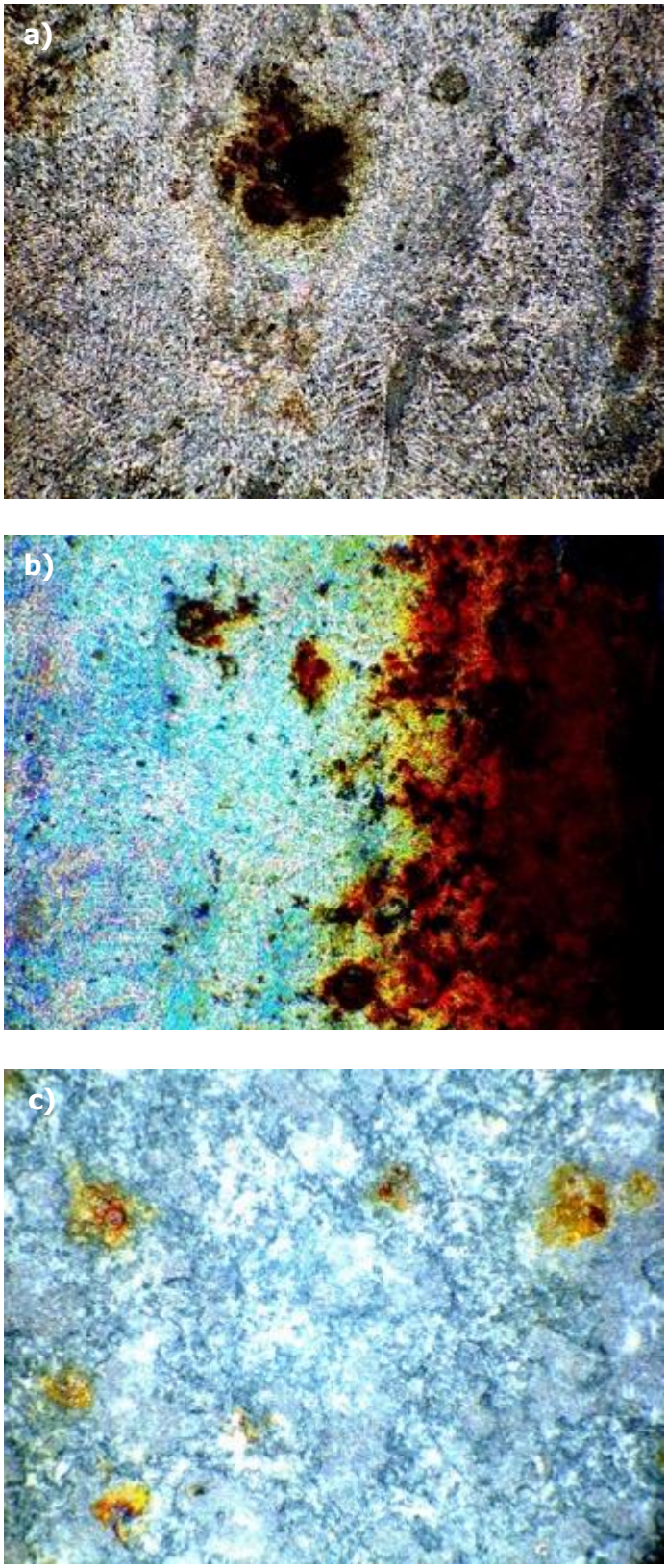

Figure 59. Surface morphology (32×) of 55%Al-Zn alloy coating after a 2-year exposure at (a) a fumarole (Scion campus), (b) the wastewater treatment plant (south of Sulphur Bay – a large, mixed geothermal system) and (c) Oteranga Bay (severe marine).

The 55%Al-Zn alloy coating tested in this study has a nominal elemental composition of 55% aluminium, 43.5% zinc and 1.5% silicon (wt.%). This formulation was initially developed in the United States by the Bethlehem Steel Company (Iezzi, 1981; Townsend et al., 1986; Townsend, 1999). Since the introduction of commercial production in 1972, the use of this formulation has increased dramatically. It was introduced to Australia as Zincalume® in approximately 1973. Production of Zincalume® at the BHP New Zealand Steel Glenbrook plant was started in 1994. This material is widely used within New Zealand building and construction industry as roof and wall claddings, spoutings, downpipes and other rainwater goods.

The 55%Al-Zn alloy coating has a complex microstructure with an aluminium-rich phase and a zinc-rich phase. The aluminium-rich phase forms into the dendrite, while the zinc-rich phase occupies the regions between the dendrites, therefore normally termed as the interdendritic phase (Figures 60-61). The dendrite constitutes ~80% of the coating volume (Shastry, 2005). An intermetallic layer made up of two sublayers – a quaternary Fe-Al-Si-Zn and a ternary Fe-Al-Si – is normally formed to metallurgically bond the coating to the steel substrate (O'Donnell, 1990). Silicon can also present in the microstructure as needle-like particles in the interdendritic regions.

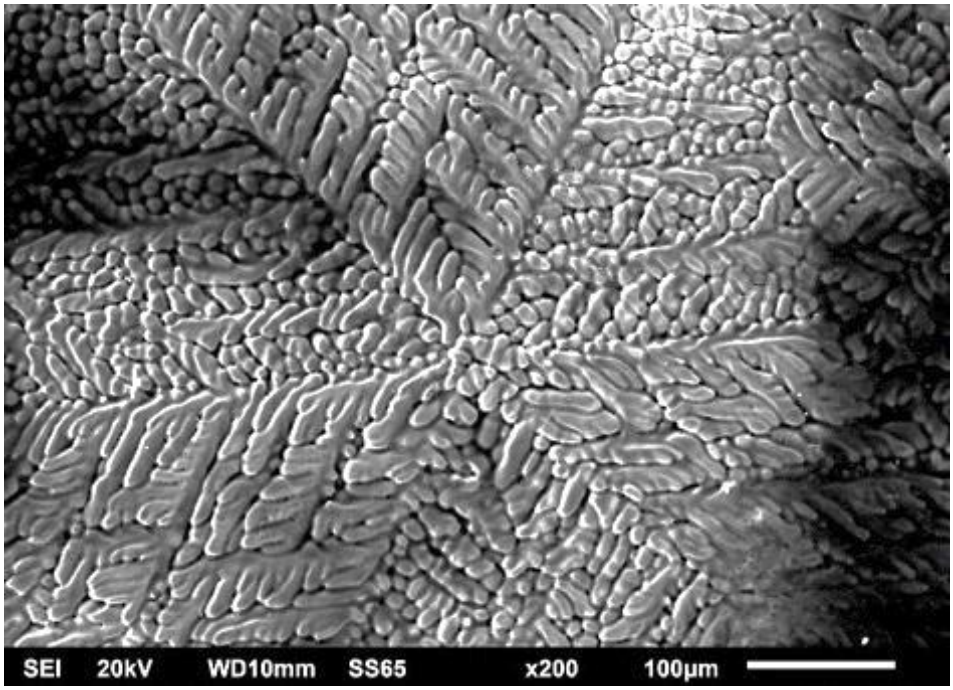

Figure 60. Typical surface morphology of 55%Al-Zn alloy coating.

The 55%Al-Zn alloy coating combines some features of hot-dip galvanised (zinc) and aluminium-based coatings. When exposed to the atmosphere, corrosion takes place in the zinc-rich region at the outer surface of the coating preferentially. The corrosion products mechanically lock into the interdendritic spaces, creating a barrier against further attack. As a result, the corrosion rate normally decreases with time. This type of corrosion can provide sacrificial protection to cut edges in many atmospheric environments, though it might not be as effective as a pure zinc coating.

Aluminium in this alloy coating can provide protection only when activated such as in marine or industrial environments. After extended exposures, corrosion may extend to the dendritic region and change gradually from active, zinc-like behaviour to passive,

aluminium-like behaviour. The attack can reach the steel substrate without all of the aluminium-rich regions being totally consumed (Palma et al., 1998; Schweitzer, 2007). Overall, the 55%Al-Zn alloy coatings show enhanced corrosion resistance when compared with the conventional hot-dip galvanised zinc coatings.

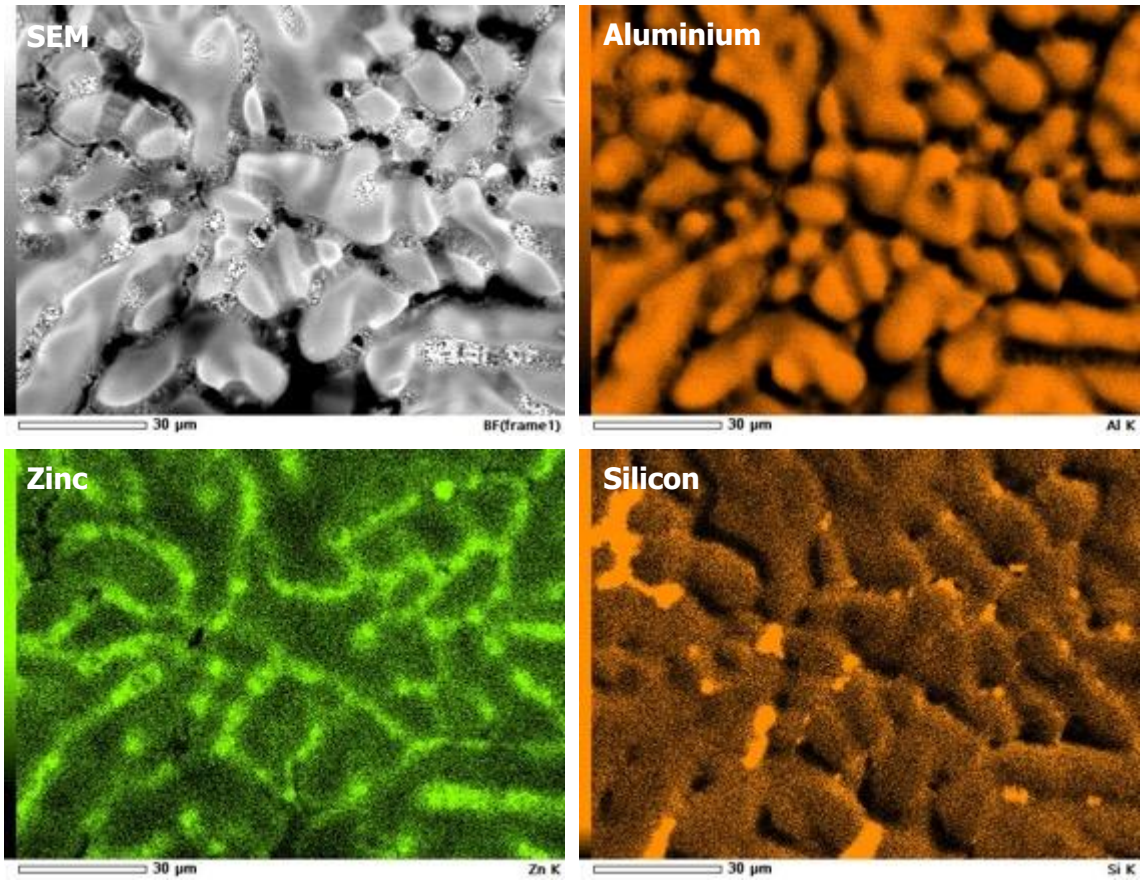

Figure 61. EDS elemental mapping of 55%Al-Zn alloy coating surface.

Degradation of 55%Al-Zn alloy coatings followed this pattern when exposed to geothermal environments though with some differences. As shown in Figure 62, the enrichment of sulphur and oxygen was obvious in the surface areas where zinc-rich phase was detected. As discussed in previous sections, zinc has a low corrosion resistance when exposed to strong geothermal environments since those loose and non-adherent corrosion products rich with zinc sulphide were not able to provide good protection to the underlying substrate. Consequently, zinc-rich interdendritic regions were attacked and consumed quickly, evidenced by the detection of sulphur and oxygen at the deep section of the coating (Figure 62).

Sulphur-containing gaseous species (H_2S or SO_2), in comparison with solid chloride-containing sea salt particles from marine environments, have a higher capability of attacking the metal substrate protected by surface coatings. These gaseous species could enter into the inner part of the coating and/or reach the coating-steel substrate interface more easily through those fast channels introduced by corrosion processes such as pores and cracks.

As discussed in previous sections, mild steel has an extremely poor resistance to the attack of sulphur-containing species, such as H_2S. Once reaching the coating-substrate interface, these gaseous species can react rapidly with mild steel to produce iron-based

sulphides and/or oxides that have very limited protection capability (Figure 63). This will lead to an extremely large volume expansion and huge stresses within confined spaces, producing even more physical defects in the coating such as bubbles and/or cracks (Figure 64).

During extended exposure, severe and localised attack to the steel substrate will continue along the interface, leading to larger volume expansion and more damaged areas. Eventually, the coating will fail, shown as the formation of iron-rich rust on large surface areas.

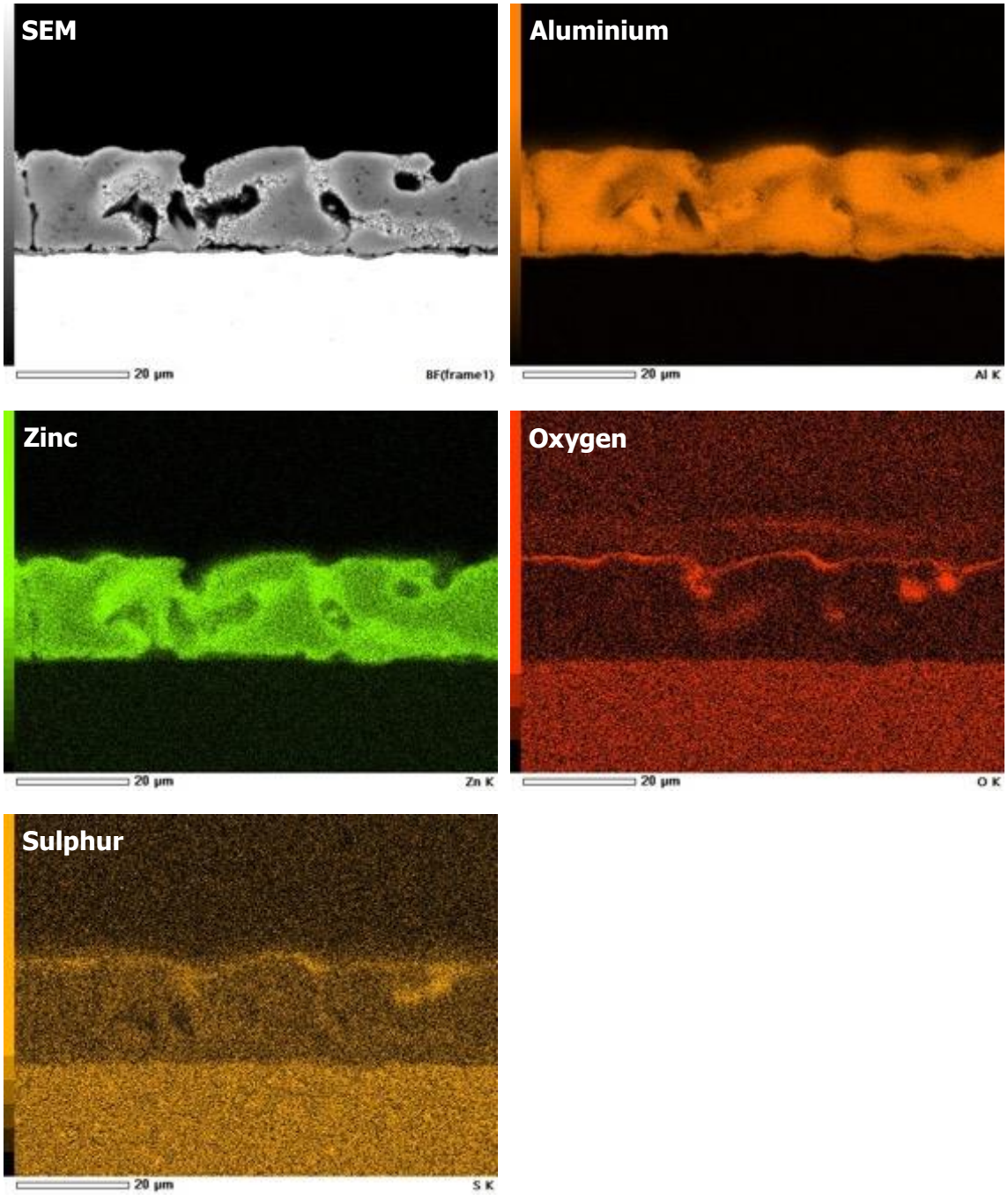

Figure 62. EDS elemental mapping on the cross-section of a 55%Al-Zn alloy coating after a 2-year exposure to a strong geothermal environment. This part of coating was not suffering from severe corrosive attack.

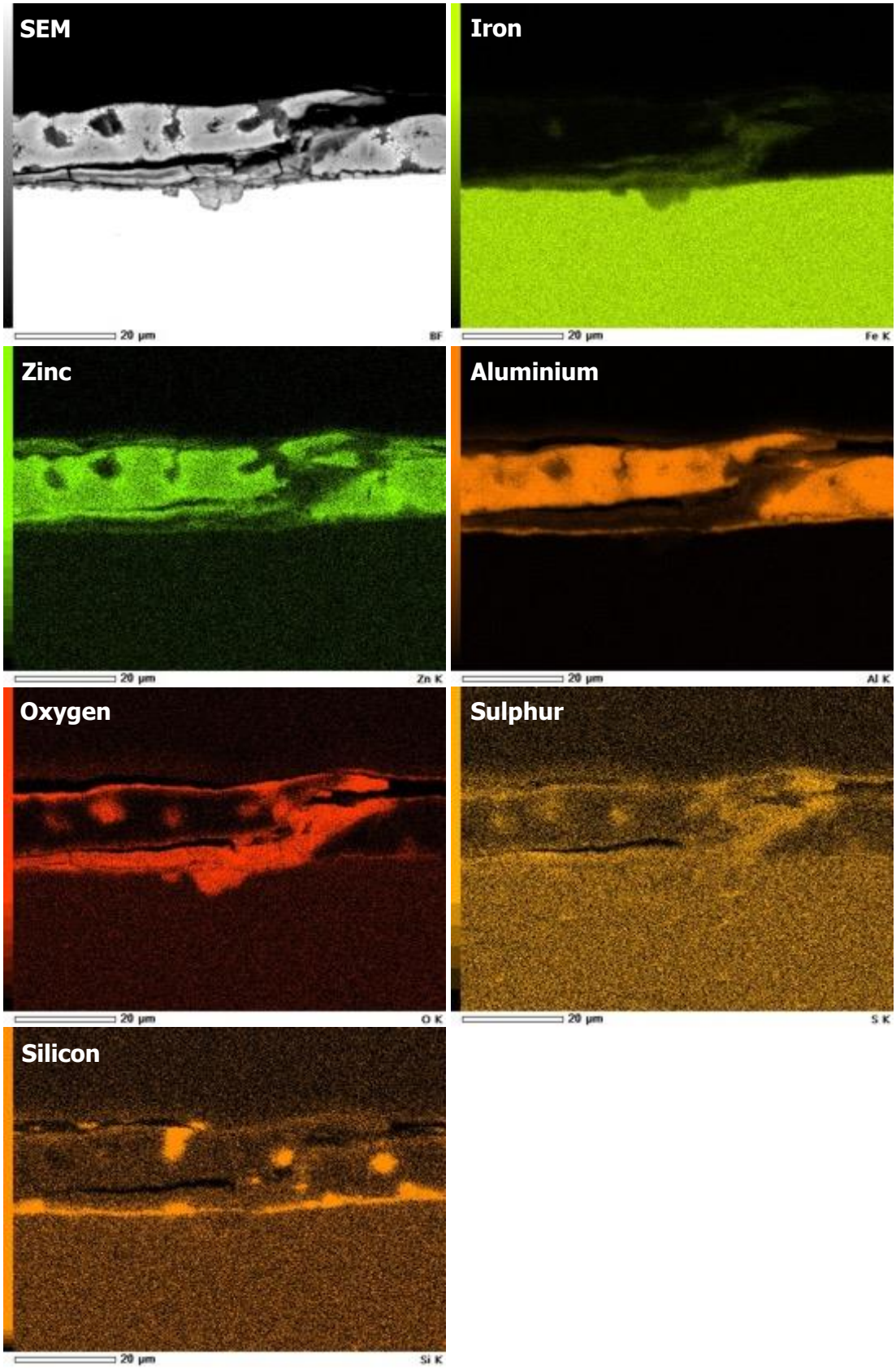

Figure 63. EDS elemental mapping on the cross-section of a 55%Al-Zn alloy coating after a 2-year exposure to a strong geothermal environment. This part of coating was suffering from severe corrosive attack.

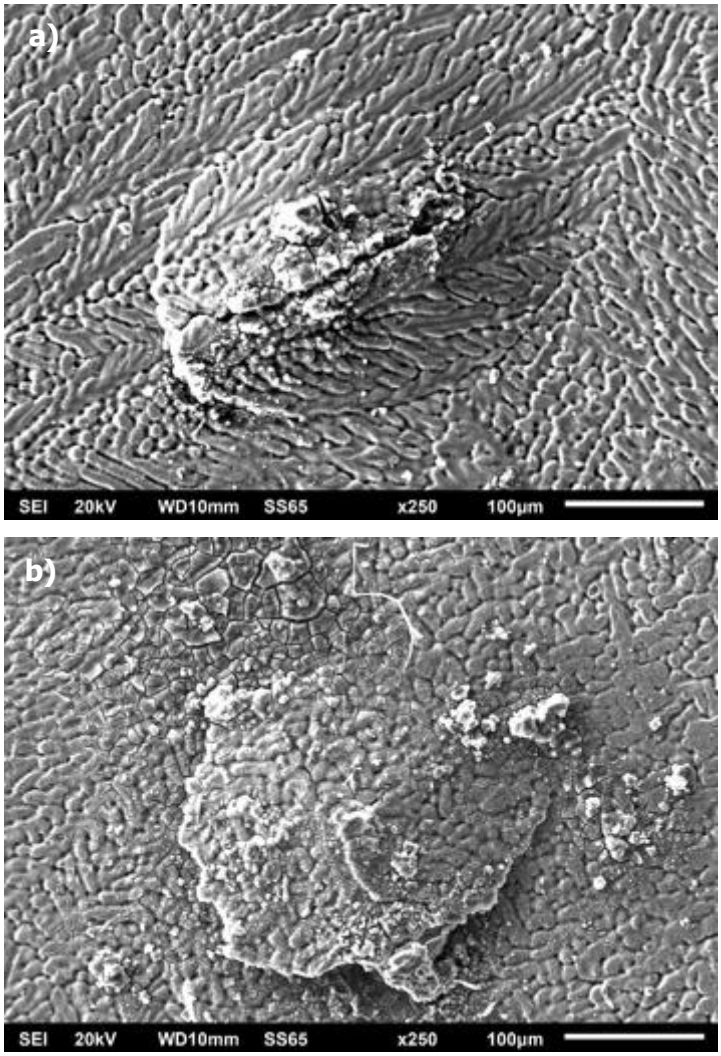

Figure 64. Failures observed on 55%Al-Zn alloy coatings exposed to an environment with strong geothermal influences – (a) bubbling/cracking and (b) lifting up.

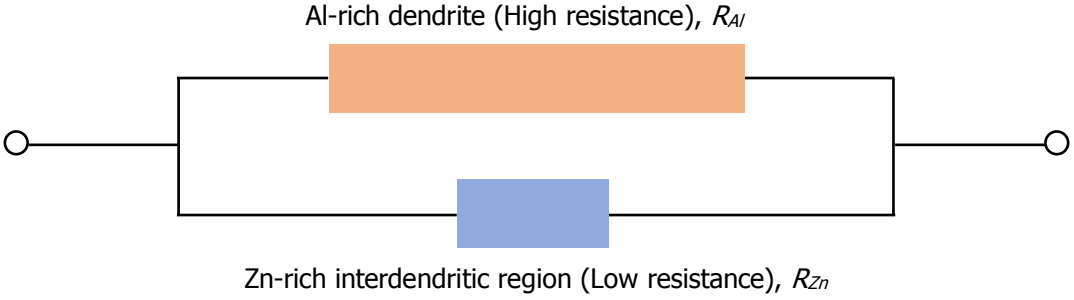

$$\frac{1}{R_{Total}} = \frac{1}{R_{Al}} + \frac{1}{R_{Zn}}$$

$$R_{Total} = \frac{R_{Al} \times R_{Zn}}{R_{Al} + R_{Zn}}$$

Figure 65. Similarity between an Al-Zn alloy coating system and a parallel circuit.

Within this deterioration, the aluminium-rich dendrites showed no or very limited corrosion, due mainly to their extremely high resistance to the attack of sulphur-containing gaseous species (discussed in section 6.1).

The resistance of an Al-Zn alloy coating can then be roughly treated as a parallel circuit, as shown in Figure 65. Its resistance to environmental attack, R_{Total}, is governed by that of the component that has the lowest corrosion resistance, i.e. Zn-rich interdendritic region, R_{Zn}.

Overall, this type of coating deterioration process and failure mode in geothermal environments happened more quickly when compared with that in other environments such as marine. 55%Al-Zn alloy coatings have typical service lives of ~10–15 years in severe marine environments, before significant rusting was observed on their surface (Townsend, 1993, 1998; Townsend & Borzillo, 1987, 1996). This is much longer than current observation in geothermal environments.

6.3 Wood

Discolouration of wood is commonly seen as a deep or shallow change in colour that diverges from its natural colour (Uzunovic et al., 2008). It can develop in both hardwoods and softwoods, but light-coloured woods are particularly prone to this problem. It also occurs in both sapwood and heartwood and can happen at any stage in the wood processing chain – standing trees, green logs, green or kiln-dried timber and wood products in service (Kreber, 1994).

In general, wood discolouration can be classified into two major types – microbial and non-microbial. Microbial discolouration is mainly caused by micro-organisms, particularly blue stain fungi, mould or bacteria. Non-microbial discolouration commonly occurs under specific conditions and can be chemical, biochemical, mechanical or photochemical. With the increasing adoption of engineered wood products, discolouration is less tolerable and has been recognised as an important topic of wood research, in terms of mechanism and prevention.

Discolouration mainly causes cosmetic damage to the wood surface. However, significant reduction of structural properties can happen in some situations.

6.3.1 Visual inspection

Discolouration of wood and its products was frequently observed in geothermal environments. For example, in areas close to Sulphur Bay with a number of active geothermal sources, preservative treated woods could turn uniformly blue quickly (Figure 66). This discolouration appears to be somewhat different from the discolouration mentioned above.

Field exposure of untreated and treated *Pinus radiata* wood samples was carried out at two strong geothermal environments for 1 year – a small fumarole in Scion campus and a large, mixed geothermal system, Sulphur Bay (wastewater treatment plant).

After this 1-year exposure, all wood samples, except the untreated, showed surface discolouration and turned blue (Figure 67). The cross-sectional observation also showed that this colour change could affect areas of up to ~1 mm deep from the top, directly exposed surface (Figure 68).

Figure 66. An example of wood discolouration noticed in an area with strong geothermal influences (south of Sulphur Bay).

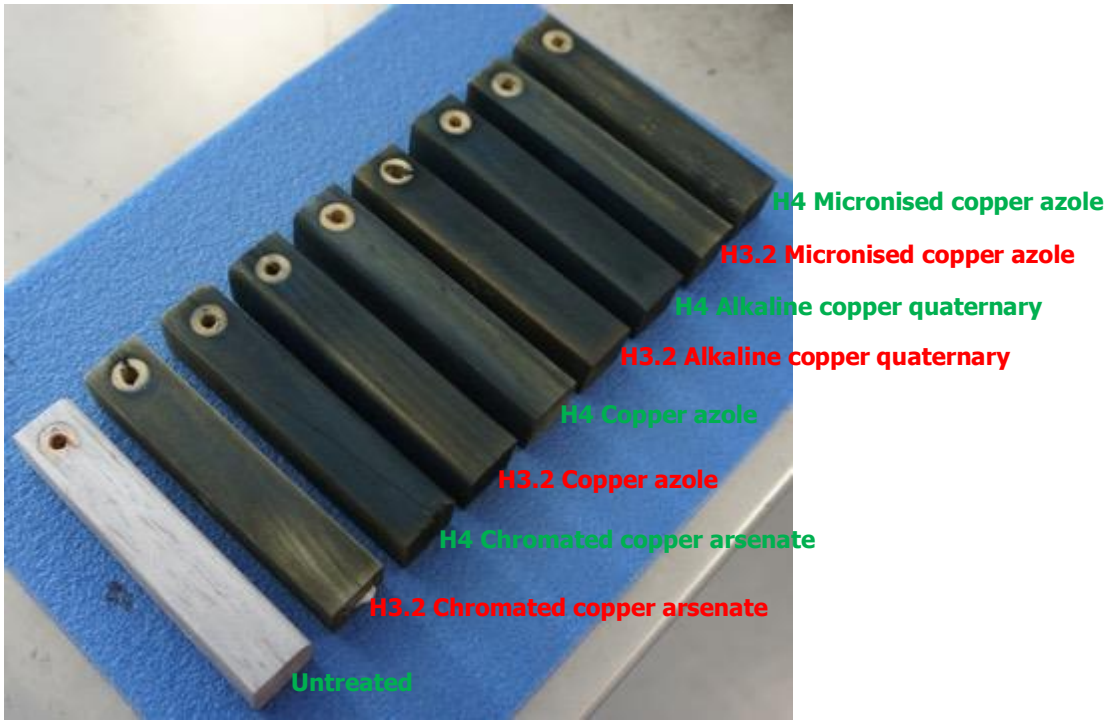

Figure 67. Discolouration of untreated and treated wood samples exposed at a location ~5 m away from a fumarole.

This discolouration was relevant to the presence of preservation chemicals in the wood since the untreated wood showed no discolouration. The common species in those four treatment chemicals is copper ion. As discussed in section 5.4, the copper surface showed a regular colour change with airborne H_2S concentration and its atmospheric corrosion rate. The corrosion products formed on the copper samples exposed to strong geothermal environments had a typical blue colour, sometimes brown which

was quite similar to this wood discolouration (Figure 55). These corrosion products were identified as a mixture of sulphide, sulphate and/or oxide of copper.

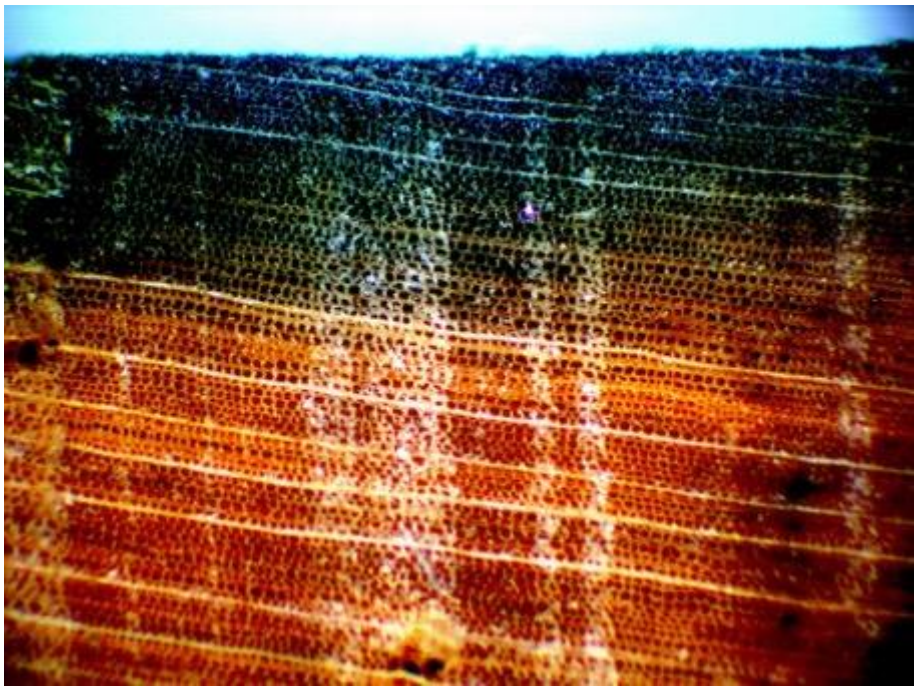

Figure 68. Optical microscopic view (32×) of the cross-section of an H4 micronised copper azole treated wood block showing discolouration after 1-year exposure at a location ~5 m away from a fumarole.

Based on these results, this type of wood discolouration is postulated to be caused by the formation of copper sulphide and/or sulphate through interactions between copper-containing species within the preservative chemicals and geothermal sulphur-containing gaseous species diffusing into wood structures.

What other evidences do we have to support this?

6.3.2 SEM/EDS analysis

Some randomly distributed particles were observed on the top surface of treated wood samples. Most of them were rich with both copper and sulphur, although oxygen was also detected by EDS analysis (Figure 69). The co-presence of these elements implied the formation of copper sulphides, sulphates and/or oxides.

Small particles and/or clusters of particles were also observed on the exposed surface of the untreated wood sample (Figure 70). These particles were quite diverse in their compositions and could be rich either with sulphur, silicon or aluminium, but not with copper. Sulphur was mainly sourced from geothermal discharges, while silicon and aluminium were possibly from dust or minerals. Meanwhile, these untreated wood samples showed no discolouration.

Morphological observations were also performed with cross-sectional wood samples prepared by microtome. This was complemented by EDS elemental mapping which can produce informative coloured images to view the distribution of specific elements in a specimen of interest.

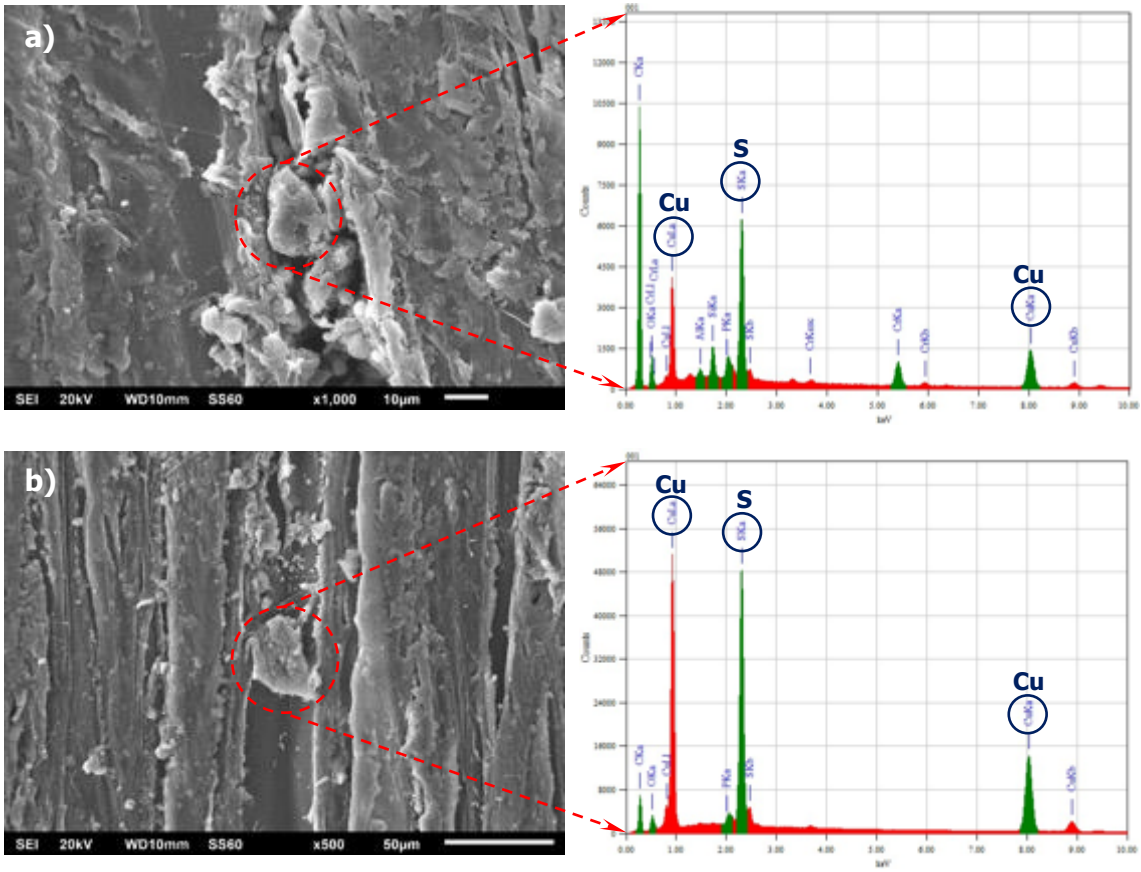

Figure 69. Particles rich with copper and sulphur identified on the top surface of (a) H4 chromated copper arsenate and (b) H4 alkaline copper quaternary treated wood samples after a 1-year exposure at a location ~5 m away from a fumarole.

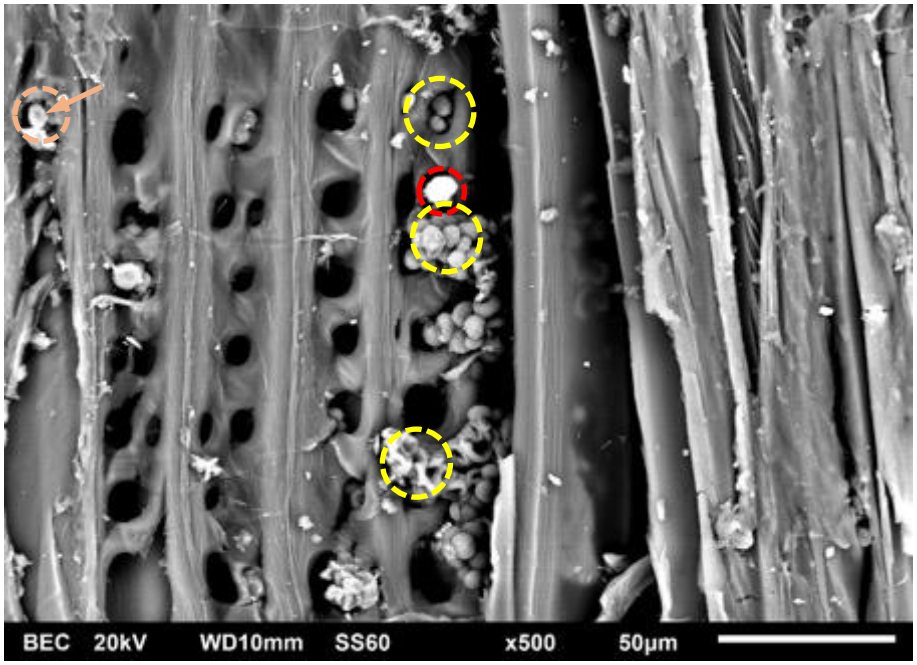

Figure 70. Particles rich with either sulphur (yellow circle), silicon (red circle) or aluminium (orange circle + arrow) identified on the top surface of an untreated wood sample after a 1-year exposure at a location ~5 m away from a fumarole.

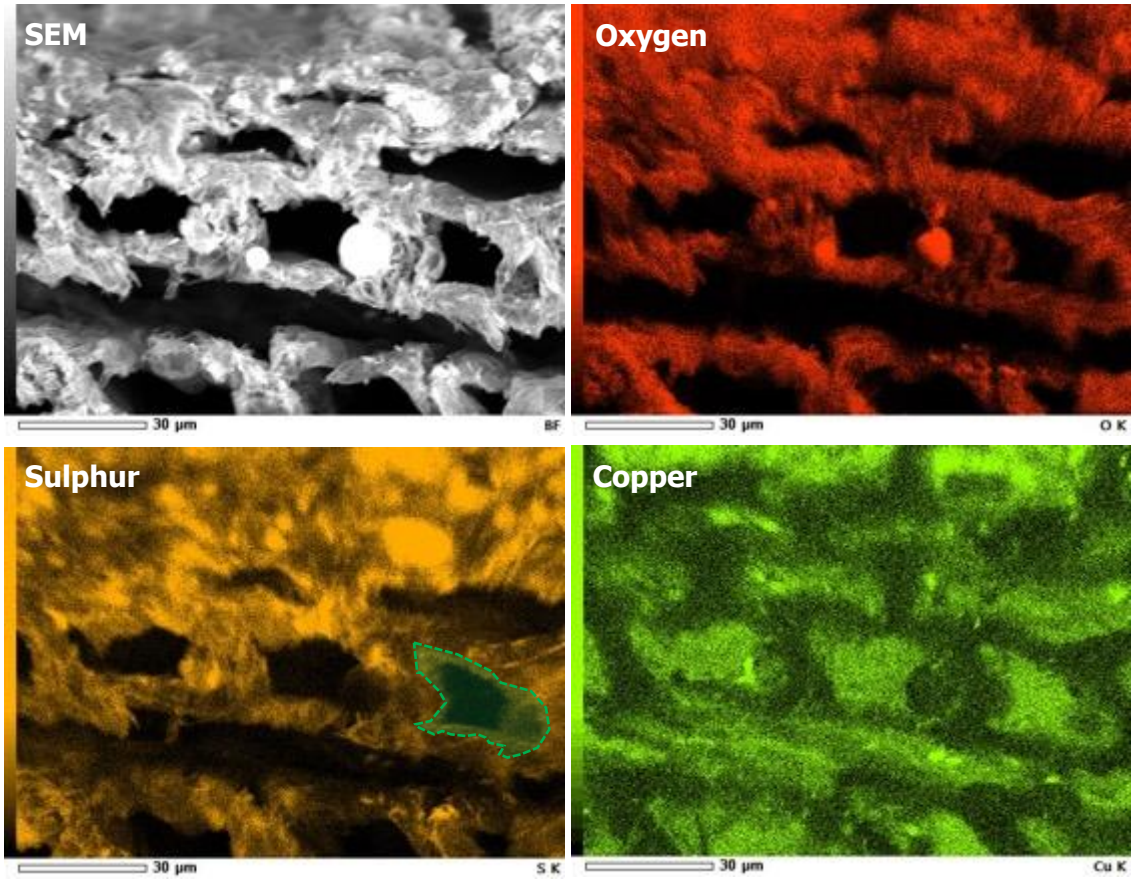

Figure 71. EDS elemental mapping over a cross-section of an H4 micronised copper azole treated wood sample. Overlapping of copper and sulphur was observed in the cell wall areas and also the areas close to the top surface.

As shown in Figure 71, a layer with obvious overlapping of copper and sulphur was observed in areas very close to the top surface. In deeper sections, the distribution of sulphur was more concentrated in the cell wall, while copper was more concentrated in the cell cavity. However, a closer look of their distribution revealed that sulphur and copper were overlapping in the cell wall area. See the green patch in the sulphur map for an example. The co-presence of these two elements indicated that they might be combined chemically to form copper sulphide or sulphates in cell wall areas.

6.3.3 XRD analysis

EDS analysis in the above section gave useful information to identify potential element(s) and to show their distributions in samples through both quantatitaive and qualitative ways. However, this technique does not have the capability to identify the phase structure of the unknown material that has the elements detected. For example, the chemical combination of copper and sulphur may form CuS, Cu_2S, CuS_2, or non-stoichiometric $Cu_{2-x}S$. Determination of unknown crystalline materials is critical to reveal the interactions between treated woods and goethermal environment in this discolouration study.

X-ray diffraction (XRD) was used to investigate the phase structure of any new products formed within wood samples after a 1-year exposure. Several new peaks were found with the diffraction pattern collected from the wood samples treated with copper-containing preservation chemicals (Figure 72). These new peaks were identified

as copper sulphide, CuS. This result was consistent with EDS analysis, which showed the enrichment of copper and sulphur within most small particles on the exposed top surface and overlapping within the cell wall region.

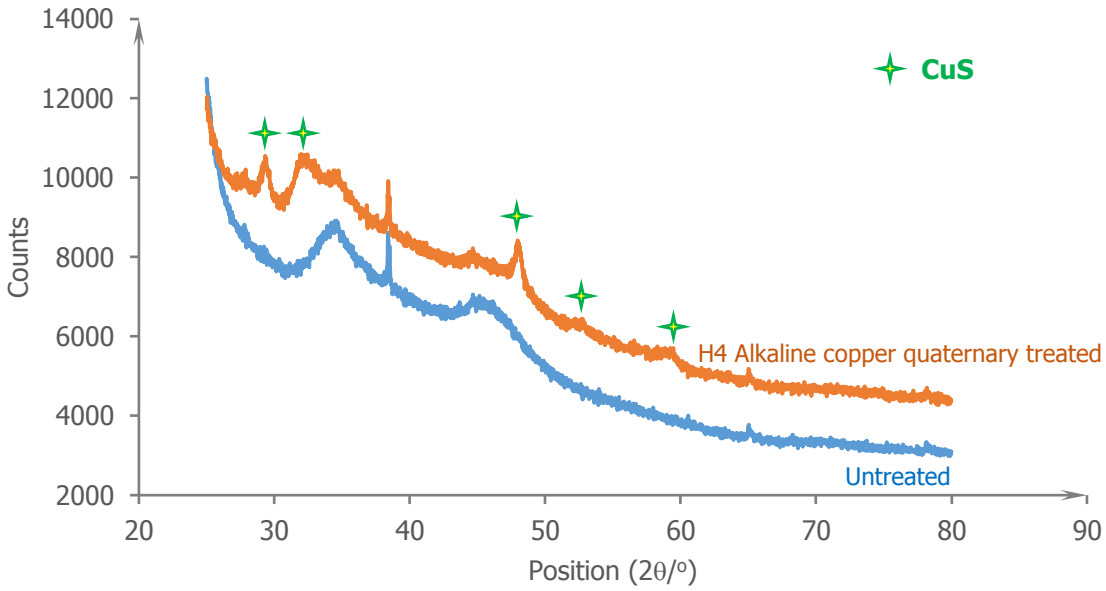

Figure 72. XRD patterns of untreated and H4 alkaline copper quaternary treated wood samples after a 1-year exposure at a location ~5 m away from a fumarole.

Based on SEM, EDS and XRD analysis, discolouration of wood treated with copper-bearing preservatives in strong geothermal environments is likely to be the result of the formation of copper sulphide on the surface and within the structure.

Colours other than blue and/or dark blue, such as brown or dark brown, have also been observed with treated woods exposed to geothermal environments. By carrying out more tests in extended exposures and/or in areas with different exposure conditions it would be possible to investigate the mechanisms behind and also the influences of discolouration on wood durability.

7. Galvanic corrosion

When two dissimilar conducting materials are in electrical contact and exposed to a corrosive environment, galvanic corrosion can occur and the anodic or active material will be corroded preferentially. This corrosion may become extreme or otherwise differ from the normal corrosion taking place in the absence of an electrical connection between these two materials (Zhang, 2011). Galvanic corrosion frequently causes many performance issues on buildings when there is a direct contact between or water run-off from different construction materials.

Galvanic corrosion series derived from immersion in sea water is commonly used to determine galvanic corrosion risks. However, metals with a potential difference of only 50 mV have shown galvanic corrosion problems, while other metals with a potential difference of ~800 mV have been used together safely (Francis, 2000). The relative position of a metal in the galvanic corrosion series may also change with the corrosive environment.

Many factors can affect galvanic corrosion in addition to the potential difference. These typically include surface condition, geometry and exposure environment. Therefore, galvanic corrosion is more complicated than other corrosion types because it is an interaction between material and environment with additional involvement of geometric factors.

Table 5. First-year corrosion rate (g/m^2/year) derived from galvanic pairs.

Galvanic pair	Dec 2014 – Dec 2015		Jun 2015 – Jun 2016	
	Fumarole	Mixed geothermal system (WWTP)	Fumarole	Mixed geothermal system (WWTP)
Al – Al	0.6	0.27 – 0.53	0	0 – 0.24
Cu – Cu	252.5	316.6 – 400	214 – 221	294 – 309
SS – SS	0 – 0.3	0.3	0	0 – 0.28
Zn – Zn	37.0	46.2 – 61.3	34.8 – 40.4	42.4 – 67.9
Al – SS	Al: 1.4	Al: 1.6	Al: 0	Al: 2.0
	SS: 0.3	SS: 0.3	SS: 0.3	SS: 0
Al – Zn	Al: 1.1	Al: 0.6	Al: 0	Al: 0
	Zn: 48.0	Zn: 63.1	Zn: 36.7	Zn: 44.6
Cu – SS	Cu: 383.7	Cu: 548.8	Cu: 375	Cu: 568
	SS: 0.3	SS: 0	SS: 0.3	SS: 0
SS – Al/Zn	SS: 0.6	SS: 1.2	SS: 0	SS: 0
	Al/Zn: ×	Al/Zn: ×	Al/Zn: ×	Al/Zn: ×

Note: Mass loss of 55%Al-Zn alloy coating not measured.

Avoiding electrical contacts between certain metals is recommended in Table 21 (Compatibility of materials in contact) of New Zealand Building Code Acceptable Solution (E2/AS1).

This study assessed the galvanic corrosion risks of some of these metallic pairs when exposed to two geothermal environments – Sulphur Bay (a large, mixed geothermal system; wastewater treatment plant) and a small fumarole in Scion campus.

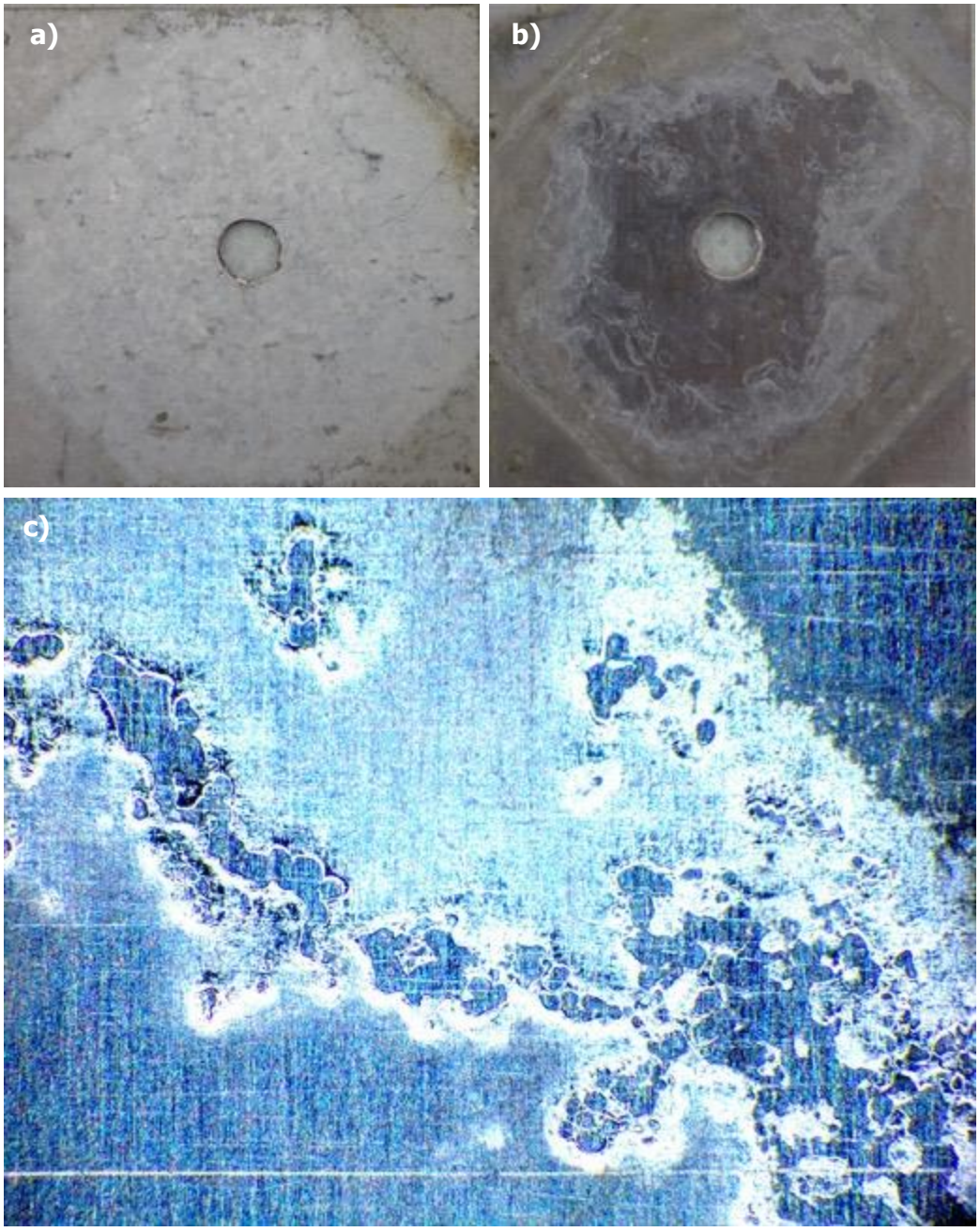

Figure 73. Surface morphology of (a) 55%Al-Zn alloy coating and (b) AISI 304 stainless steel disassembled from a galvanic pair exposed at the wastewater treatment plant site for 1 year (December 2014 to December 2015). (c) After cleaning, localised damage to the stainless steel surface directly contacting with the Al-Zn alloy coating was observed (25×).

The atmospheric corrosion rates derived from these pairs after a 1-year exposure are given in Table 5. Together with surface morphological observations, the following observations could be made.

- The direct contact between aluminium and stainless steel increased the corrosion rate of aluminium. This was similar to the observations in other environments, such as urban and marine (Kucera & Mattsson, 1982). However, the atmospheric corrosion rate of aluminium within this galvanic pair was still very low.
- The direct contact between copper and stainless steel increased the corrosion rate of copper up to ~1.9 times. In the galvanic corrosion series, copper is more active than AISI 304 stainless steel (approximately 200 mV difference). E2/AS1 Table 21 recommends that the direct contact of these two materials should be avoided in the sea spray zone or Zone D (NZS 3604:2011) where the deposition of sea salt particles might be severe.
- The direct contact between aluminium and zinc did not consistently increase the deterioration of one specific metal. The potential difference between aluminium and zinc is about 200 mV, and zinc is slightly more active. The test started from December 2014 showed that corrosion rates of both aluminium and zinc were slightly increased. When the exposure was started from June 2015, an increase of corrosion rate was not observed with aluminium or zinc. This indicated that the potential difference measured in seawater for these two metals might not always serve as a reliable indicator of galvanic corrosion risks. However, the mechanisms behind this unusual change in corrosion rates of these two electrically connected metals was not clearly understood with this short-term testing.
- Within most galvanic pairs, AISI 304 stainless steel did not show obvious degradation after this exposure. However, mass losses and surface damage were observed with stainless steel paired with 55%Al-Zn alloy coating after a 1-year exposure started from December 2014 (Figure 73). Although some changes were noticeable, severe deterioration of the Al-Zn alloy coating was not revealed.
- This phenomenon is unusual. According to E2/AS1 Table 21, direct contact between stainless steel and Al-Zn alloy coating should only be avoided in the sea spray zone or Zone D (NZS 3604:2011) where there is a high chance of salt deposition. Meanwhile, Al-Zn alloy coating would be the material under accelerated attack. In this study, corrosion of stainless steel was found within the contacting area, indicating that a crevice corrosion mechanism might be contributing. Compared with the fully exposed sample top surface, this contacting area was able to retain moisture or contaminants within long periods, providing an ideal area for localised corrosion on stainless steel. As shown in Figure 73c, pits were developing under the white corrosion products revealed in Figure 73b.

These observations in geothermal environments supported most recommendations in E2/AS1 Table 21, though some unusual deterioration behaviours were revealed and should be better understood with appropriate tests.

8. Summary

Sulphur-containing species (H_2S and/or SO_2) were detected with an obvious concentration profile across Rotorua city. They were high in areas close to or in the central city and low in the west and east areas. This was a direct result of more active geothermal features in the central city area and prevailing wind conditions.

Mild steel, zinc and copper had extremely high corrosion rates in strong geothermal environments. Mild steel and zinc were found to exhibit an accelerating and/or oscillating corrosion behaviour in a 2-year exposure. This behaviour was different from the corrosion kinetics commonly observed in other New Zealand natural environments. This unusual behaviour can be partly explained:

- Corrosion products formed on mild steel had a large number of physical defects (cracks and pores), acting as effective collectors and reservoirs for moisture, sulphur-containing gaseous species or particulate matters and promoting corrosion.
- Discrete particles rich with sulphides were formed on zinc surface. A thin layer rich with oxide was developed at the interface between corrosion products and metal substrate. Those sulphide particles could be washed away by rainwater, partially exposing underlying oxide layer or metal to the aggressive environment and disrupting their environmental stability and protection capability.

However, the specific scientific mechanisms behind this unusual corrosion behaviour are not fully understood based on the results derived from this short-term test and further study is needed.

Mild steel corrosion rate could be reduced by approximately 4 times with a separation of ~50 m from a small fumarole. However, low concentrations of geothermal sulphur-containing species can still affect morphology and microstructure of corrosion products growing on mild steel, zinc and copper, therefore their protection capability in extended exposures is unknown.

A 50 m separation from a geothermal spot has been recommended by NZS 3604:2011 *Timber-framed buildings* as a boundary for safe building practice. This separation is not always sufficient to decrease local atmospheric corrosivity.

- Mild steel exposed at a location ~60 m southwest of an active, small fumarole had its first-year corrosion rates ranging typically from 443 g/m^2/year to 551 g/m^2/year, based on which a ISO 9223:2012 C4 (High) corrosivity category can be defined.
- Mild steel exposed at a location ~200 m south of Sulphur Bay (a large, mixed geothermal system) had its first-year corrosion rates ranging typically from 3,044 g/m^2/year to 3,443 g/m^2/year. At a location ~400 m southwest, the first-year corrosion rate was ~2,293 g/m^2/year. The atmospheric corrosivity can be classified into CX (Extreme) – the highest corrosivity category defined by ISO 9223:2012.

In areas approximately 500 m of an active geothermal source, the atmospheric corrosivity is strongly influenced by many factors including size, emission capability and chemistry of the geothermal feature and weather conditions. The atmospheric corrosivity category could range up to ISO 9223:2012 CX (Extreme) with considerable variations. This study suggested that the atmospheric corrosivity of these areas should be assessed with first-year corrosion rates of relevant metals and climatic monitoring.

Mild steel, zinc and copper respond to geothermal sulphur-containing species induced attack differently and copper was most prone to geothermal attack. Even in areas with (very) low concentrations of sulphur-containing species, copper still showed corrosion rates approximately 2–5 times higher than in areas without geothermal influences. Consequently, atmospheric corrosivity classification according to ISO 9223:2012 may have significant differences if different model metals were used, such as mild steel, zinc and copper. If only one specific model metal was used to characterise a specific geothermal environment, either overestimation or underestimation of its corrosivity category could happen, leading to overprotection or underprotection, i.e. higher materials costs or faster premature failure.

This study showed that first-year corrosion rates of mild steel, zinc and copper could be correlated with H_2S concentrations measured in the first 3 weeks of exposure. However, mathematical fitting functions showed relatively large deviations, particularly with data points of low and high H_2S concentrations. They were also strongly dependent on the starting season of exposure, i.e. a different function might be derived for the same metal if the exposure was started in a different season. The following should be considered to improve these mathematical fitting functions:

- The environmental conditions in the initial stage of exposure are critical to atmospheric corrosion kinetics in extended exposure. However, H_2S concentration showed large variations in seasonal scales. It would be more sensible to investigate the influences of this concentration variation on corrosion process and find out more representative concentration data for fitting.
- Airborne SO_2 may contribute to atmospheric corrosion of mild steel, zinc and copper in geothermal environments tested in this study. The source of SO_2 should be identified, i.e. a direct emission from geothermal feature or a product of H_2S oxidation in air, and the separate and/or synergistic effects of H_2S and SO_2 on metal atmospheric corrosion should be investigated.
- In areas with (very) low concentration of H_2S, corrosion rates of mild steel and zinc were low and comparable with those in areas without geothermal influences. Climatic parameters such as ambient temperature, relative humidity and/or rainfall may then play more important roles in atmospheric corrosion and should be quantified and included into fitting functions properly.

9. Recommendation

This study revealed that material deterioration in geothermal environments was different and unique when compared with that in other New Zealand natural environments. Further studies are needed to answer the following:

- Why and how unusual material deterioration behaviours happen.
- How to better characterise geothermal environments and classify their corrosivity.

This study revealed that performance data derived from short-term tests cannot be confidently extrapolated to assess long-term durability and to estimate service life of building materials and components in geothermal environments. Further studies with well defined research components and experimental procedures are needed to:

- Evaluate long-term deterioration and durability of more representative materials and protective coatings.
- Establish a comprehensive comparative material performance database for service life modelling and prediction in geothermal environments.

These studies, together with BRANZ's long-standing atmospheric corrosion research, can help performance evaluation, service life estimation and material specification in geothermal environments as well as delivery of a more complete profile of material performance within New Zealand environments.

References

Arzola, S. and Genesca, J. (2005). The effect of H_2S concentration on the corrosion behaviour of API 5L X-70 steel. *Journal of Solid State Electrochemistry,* 9(4), 197–200.

Blücher, D. B., Svensson, J. E. and Johansson, L. G. (2005). Influence of ppb levels of SO_2 on the atmospheric corrosion of aluminium in the presence of NaCl. *Journal of the Electrochemical Society*, 152(10), B397–404.

Blücher, D. B., Svensson, J. E. and Johansson, L. G. (2006). The influence of CO_2, $AlCl_3 \cdot 6H_2O$, $MgCl_2 \cdot 6H_2O$, Na_2SO_4 and NaCl on the atmospheric corrosion of aluminium. *Corrosion Science*, 48(7), 1848–1866.

Burleigh, T. D. (2003). Corrosion of aluminium and its alloys. In G. E. Totten and D. Scott MacKenzie (Eds.), *Handbook of Aluminium, Vol.2, Alloy Production and Materials Manufacturing*. New York and Basel: Marcel Dekker.

Cole, I. S. and Ganther, W. D. (2006). Experimental determination of time taken for openly exposed metal surfaces to dry. *Corrosion Engineering, Science and Technology*, 41(2), 161–167.

Cole, I. S. and Paterson, D. A. (2007). Holistic model for atmospheric corrosion, Part 7 - Cleaning of salt from metal surfaces. *Corrosion Engineering, Science and Technology*, 42(2), 106–111.

Cox, R. A. and Sandalls, F. J. (1974). The photo-oxidation of hydrogen sulphide and dimethyl sulphide in air. *Atmospheric Environment* (1967), 8(12), 1269–1281.

de la Fuente, D., Castaño, J. G. and Morcillo, M. (2007). Long-term atmospheric corrosion of zinc. *Corrosion Science*, 49(3), 1420–1436.

de la Fuente, D., Otero-Huerta, E. and Morcillo, M. (2007). Studies of long-term weathering of aluminium in the atmosphere. *Corrosion Science*, 49(7), 3134–3148.

de la Fuente, D., Diaz, I., Simancas, J., Chico, B. and Morcillo, M. (2011). Long-term Atmospheric Corrosion of Mild Steel. *Corrosion Science*, 53(2), 604–617.

Ding, J., Zhang, L., Yu, Y., Li, D. and Lu, M. (2013). Stress corrosion cracking mechanism of UNS S31803 duplex stainless steel under high H_2S-CO_2 pressure with high Cl^- content. CORROSION 2013, 17–21 March 2013. Orlando, Florida, USA. NACE International, Paper 2531.

Duncan, J. R. and Cordner, R. J. (1991). Atmospheric corrosion rates over two years exposure at 156 sites in New Zealand. *IPENZ Transactions*, 18(1)/GEN, 37–49.

Francis, R. (2000). *Bimetallic Corrosion. Guides to Good Practice in Corrosion Control*. National Physical Laboratory, Queens Road, Teddington, Middlesex TW11 0LW. www.npl.co.uk.

Friel, J. J. (1986). Atmospheric corrosion products on Al, Zn, and Al-Zn metallic coatings. *Corrosion*, 42(7), 422–426.

Gao, W., Gifford, D. and Liu Z. Y. (1997). Corrosion behaviour of Zincalume and galvanised coatings in a sulphur-containing atmosphere. *IPENZ Transactions*, 24(1)/EMCh, 51–60.

Gordon, D. A., Scott, B. J. and Mroczek, E. K. (2005). *Rotorua Geothermal Field Management Monitoring Update: 2005*. Environment Bay of Plenty, Environmental Publication 2005/12, June 2005. 5 Quay Street, P O Box 364, Whakatane, New Zealand. ISSN 1175 – 9372.

Guttman, H. (1968). Effects of atmospheric factors on the corrosion of rolled zinc. In W.H. Ailor and S.K. Cobum (Eds.), *Metal Corrosion in the Atmosphere*, STP 435, ASTM. pp.223–239.

Haberecht, P. W. and Kane, C. D. (1999). Determining the chloride deposition rate, chloride aerosol flux and the corrosion rates in subfloor building conditions in a severe marine environment. *Proceedings of the 14th International Corrosion Congress*. 26 September – 01 October 1999. Cape Town, South Africa.

Hawthorn, G. A., Nullet, M. A., Srinivasan, R. and Hihara, L. H. (2007). Corrosion testing and atmospheric monitoring in an active volcanic environment. *Proceedings of the 2007 Tri-Service Corrosion Conference*. 3–7 December 2007. Denver, USA.

Hinz, R. (2011). *Hydrogen Sulphide in Rotorua, New Zealand: Personal Exposure Assessment and Health Effects*. Master of Science Thesis. Massey University, Palmerston North, New Zealand.

Holcroft, G. (1998). Ventilation, salt ingress, timber moisture and corrosion rates in model coastal subfloor spaces. *Corrosion and Materials*, 23(2-3), 7–11.

Horwell, C. J., Patterson, J. E., Gamble, J. A. and Allen, A. G. (2005). Monitoring and mapping of hydrogen sulphide emissions across an active geothermal field: Rotorua, New Zealand. *Journal of Volcanology and Geothermal Research*, 139(3-4), 259–269.

Iezzi, R. A. (1981). Prepainted galvalume - U.S. perspective. *Steel Times International*. September 1981. presented at the European Coil Coaters Association Annual Meeting, Stockholm, Sweden. pp130–137.

Iremonger, S. (2012). *A Review of Odour Properties of H_2S – Odour Threshold Investigation 2012*. Environmental Publication 2012/06. Bay of Plenty Regional Council, 5 Quay Street, PO Box 364, Whakatane 3158, New Zealand.

Jin, S. and Atrens, A. (1990). Passive films on stainless steels in aqueous media. *Applied Physics A*, 50(3), 287–300.

Kane, C. (1996). Atmospheric corrosion survey of New Zealand – Six year exposure results. *Transactions of the Institute of Professional Engineers New Zealand: Electrical/Mechanical/Chemical Engineering Section*, 23(1), 29–39.

Kinoshita, S. and Yoshioka, S. (2005). Structural colors in nature: The role of regularity and irregularity in the structure. *ChemPhysChem*, 6(8), 1442–1459. doi:10.1002/cphc.200500007.

Kreber, B. (1994). *Understanding Wood Discolouration Helps Maximise Wood Profits*. Western Dry Kiln Association, Corvallis, OR. Forintek Canada Corp.

Kucera, V. and Mattsson, E. (1982). Atmospheric corrosion of bimetallic structures. In W.H. Ailor (Ed.), *Atmospheric Corrosion*. John Wiley & Sons, Inc. New York. pp561–574.

Kurata, Y., Sanada, N., Nanjo, H., Ikeuchi, J. and Lichti, K. A. (1995). Material damage in a volcanic environment. Proceedings of World Geothermal Congress. Milan, Italy. pp2409–2414.

Landolfo, R., Cascini, L. and Portioli, F. (2010). Modelling of metal structure corrosion damage: A state of the art report. *Sustainability*, 2, 2163–2175.

Lashermes, M., Guilhaudis, A., Reboul, M. and Trentelivers, G. (1982). Thirty-year atmospheric corrosion of aluminium alloys in France. In W.H. Ailor (Ed.), *Atmospheric Corrosion*. John Wiley & Sons, Inc., New York. pp353-364.

Lee, H. F., Yang, T. F., Lan, T. F., Song, S. R. and Tsao, S. J. (2005). Fumarolic gas composition of the Tatun volcano group, northern Taiwan, *TAO*, 16(4), 843–864.

Lee, J. S., Kitagawa, Y., Nakanishi, T., Hasegawa, Y. and Fushimi, K. (2015). Effect of hydrogen sulfide ions on the passive behavior of type 316L stainless steel. *Journal of The Electrochemical Society*, 162(14), C685–C692.

Lichti, K. A., Gilman, N. A., Sanada, N., Kurata, Y., Nanjo, H., Ikeuchi, J. and Christenson, B. W. (1996). Corrosion chemistry of some volcanic environments, *Proceedings of 18th New Zealand Geothermal Workshop*. 6–8 November 1996. University of Auckland, Auckland, New Zealand. pp21–28.

Luketina, K. M. (2007). *Regional Geothermal Geochemistry Monitoring Programme (REGEMP II)*. Document No: 1115830. Environment Waikato, PO Box 4010, Hamilton East, New Zealand.

Ma, Y. T., Li, Y. and Wang, F. H. (2010). The atmospheric corrosion kinetics of low carbon steel in a tropical marine environment. *Corrosion Science*, 52(5), 1796–1800.

Manning, M. (1988). Corrosion of building materials due to atmospheric pollution in the United Kingdom. In K. Mellan (Ed.), *Air Pollution, Acid Rain and the Environment*. Elsevier Science Publishers Ltd. England.

Mitrovic-Scepanovic, V., Macdougall, B. R. and Graham, M. J. (1987). The effect of Cl^- ions on the passivation of Fe-26Cr alloy. *Corrosion Science*, 27(3), 239–247.

Morcillo, M., de la Fuente, D., Diaz, I. and Cano, H. (2011). Atmospheric corrosion of mild steel. *Revista de Metalurgia*, 47(5), 426–444.

New Zealand Geothermal Association. (2016). NZ Geothermal Fields, Retrieved from http://nzgeothermal.org.nz/nz_geo_fields/.

Ochieng, L., Kipng'ok, J., Kanda, I., Igunza, G. and Wanjie, C. (2012). Geochemistry of fumarole discharges and borehole waters of Korosi-Chepchuk geothermal prospect, Kenya. *GRC Transactions*, 36, 17–21.

O'Donnell, A. J. (1990). *An Evaluation of the Sacrificial Protection Afforded by Continuous Galvanized Coatings*. PhD Thesis, University of Pretoria. South Africa.

Oesch, S. and Heimgartner, P. (1996). Environmental effects on metallic materials – Results of an outdoor exposure programme running in Switzerland. *Materials and Corrosion*, 47(8), 425–438.

Olafsdottir, S., Gardarsson, S. M. and Andradottir, H. O. (2014). Spatial distribution of hydrogen sulphide from two geothermal power plants in complex terrain. *Atmospheric Environment*, 82, 60–70.

Olefjord, I. and Wegrelius, L. (1990). Surface analysis of passive state, *Corrosion Science*, 31, 89–98.

Palma, E., Puente, J. M. and Morcillo, M. (1998). The atmospheric corrosion mechanism of 55% Al-Zn coating on steel. *Corrosion Science*, 40(1), 61–68.

Parekh, S. P., Pandya, A. V. and Kadiya, H. K. (2012). Progressive atmospheric corrosion study of metals like mild steel, zinc and aluminium in urban station of Ahmedabad district. *International Journal of ChemTech Research*, 4(4), 1770–1774.

Ratouis, T. M. P., O'Sullivan, M. and O'Sullivan, J. (2014). An updated numerical model of Rotorua geothermal field. *Proceedings of 39th Workshop on Geothermal Reservoir Engineering*. 24–26 February 2014. Stanford University, Stanford, California, USA.

Rebak, R. B. and Perz, T. E. (2017). Effect of carbon dioxide and hydrogen sulfide on the localized corrosion of carbon steels and corrosion resistant alloys. Corrosion 2017. 26–30 March 2017. New Orleans, USA. NACE International. Paper No.8933.

Salas, B. V., Wiener, M. S., Badilla, G. L., Beltran, M. C., Zlatev, R., Stoycheva, M., de Dios Ocampo Diaz, J., Osuna, L. V. and Gaynor, J. T. (2012). H_2S pollution and its effect on corrosion of electronic components, In G. Badilla, B. Valdez, and M. Schorr (Eds.), *Air Quality – New Perspective*. InTech. pp263–286.

Schmutz, P. and Landolt, D. (1999). In-situ microgravimetric studies of passive alloys: Potential sweep and potential step experiments with Fe-25Cr and Fe-17Cr-33Mo in acid and alkaline solution. *Corrosion Science*, 41(11), 2143–2163.

Schweitzer, P. A. (2007). *Corrosion of Linings & Coatings: Cathodic and inhibitor protection and corrosion monitoring*, 2nd edition. Taylor & Francis LLC, Boca Raton.

Scott, S. W. (2011). *Gas Chemistry of the Hellisheidi Geothermal Field*. Master Thesis. University of Iceland, Reykjavik, Iceland.

Shastry, C. R. (2005). Corrosion of metallic coated steels. In S.D. Cramer and B.S. Covino, Jr (Eds.), *ASM Handbook: Vol.13B: Corrosion: Materials*. ASM International. pp35-39. www.asminternational.org.

Spedding, D. J. and Cope, D. M. (1984). Field measurements of hydrogen sulphide oxidation. *Atmospheric Environment* (1967), 18(9), 1791–1795.

Strehblow, H. H. (1984). Breakdown of passivity and localized corrosion: Theoretical concepts and fundamental experimental results. *Werkstoffe und Korrosion*, 35(10), 437–448.

Syed, S. (2006). Atmospheric corrosion of materials. *Emirates Journal for Engineering Research*, 11(1), 1–24.

Teschner, M., Vougioukalakis, G. E., Faber, E., Poggenburg, J. and Hatziyannis, G. (2005). Real time monitoring of gas-geochemical parameters in Nisyros fumaroles, *Developments in Volcanology*, 7, 247–254.

Total Materia. (2002). Corrosion of zinc. Retrieved from http://www.totalmateria.com/Article40.htm.

Townsend, H. E., Allegra, L., Dutton, R. J. and Kriner, S. A. (1986). Hot-dip coated sheet steels – A review. *Materials Performance*, 25(8), 36–46.

Townsend, H. E. and Borzillo, A. R. (1987). Twenty-year atmospheric corrosion tests of hot-dip coated sheet steel. *Materials Performance*, 26(7), 37–41.

Townsend, H. E. (1993). Twenty-five-year corrosion tests of 55%Al-Zn alloy coated steel sheet. *Materials Performance*, 32(4), 68–71.

Townsend, H. E. and Borzillo, A. R. (1996). Thirty-year atmospheric corrosion performance of 55% aluminum-zinc alloy-coated sheet steel. *Materials Performance*, 35(4), 30–36.

Townsend, H. E. (1998). Atmospheric corrosion resistance of skyward- and groundward-exposed surfaces of zinc- and 55% Al-Zn alloy-coated steel sheet. *Corrosion*, 54(7), 561–565.

Townsend, H. E. (1999). Extending the limits of growth through development of corrosion-resistant steel products. *Corrosion*, 55(6), 547–553.

Tran, T. T. M., Fiaud, C., Sutter, E. M. M. and Villanova, A. (2003). The atmospheric corrosion of copper by hydrogen sulphide in underground conditions. *Corrosion Science*, 45(12), 2787-2802.

Uzunovic, A., Byrne, T., Gignac, M. and Yang, D. Q. (2008). *Wood Discolouration and Their Prevention – With an Emphasis on Bluestain*. Special Publication SP-50, ISSN #1916-4238. FPInnovations Forintek, Montreal, Canada.

Wohlers, H. C., and Feldstein, M. (1966). Hydrogen sulphide darkening of exterior paint. *Journal of the Air Pollution Control Association*, 16(1), 19–21.

Yamashita, M., Miyuki, H., Matsuda, Y., Nagano, H. and Misawa, T. (1994). The long term growth of the protective rust layer formed on weathering steel by atmospheric corrosion during a quarter of a century. *Corrosion Science*, 36(2), 283–299.

Zhang, X. G. (2011). Galvanic corrosion. In R. W. Revie (Ed.), *Uhlig's Corrosion Handbook*, 3rd edition. John Wiley & Sons, Inc. pp123–143.